Fermi National Accelerator Laboratory

An Improved 8 GeV Beam Transport System
for the Fermi National Accelerator Laboratory

Michael J. Syphers

Fermi National Accelerator Laboratory
P.O. Box 500
Batavia, IL 60510 USA

June 1987

AN IMPROVED 8 GEV BEAM TRANSPORT SYSTEM
FOR THE FERMI NATIONAL ACCELERATOR LABORATORY

BY

Michael James Syphers
B.S. Indiana University
M.S. De Paul University

THESIS

Submitted in Partial Fulfillment of the Requirements
for the Degree of Doctor of Philosophy in Physics
in the Graduate College of the
University of Illinois at Chicago, 1987

Chicago, Illinois

ACKNOWLEDGMENT

The author wishes to sincerely thank James S. Kouvel, Antonio Pagnamenta, and in particular Clive Halliwell of the University of Illinois at Chicago for their continued support throughout the course of this project. In addition, the author wishes to thank the members of the PhD in Accelerator Physics Committee of the Fermi National Accelerator Laboratory for allowing him the opportunity to participate in their program.

A project the magnitude of the 8 GeV Line requires the help and cooperation of many. For their assistance with the development and implementation of the 8 GeV Line the author would like to thank the following members of the Fermilab staff: Rich Orr, John Peoples, Fred Mills, Dixon Bogert, Dick Andrews, Gerry Tool, Bob Mau, and members of the Accelerator Division Controls, Mechanical Support, Electrical Engineering, and Operations Groups. For many useful conversations concerning the original 8 GeV transport system, the new design, magnet design and measurements, and general beam dynamics issues, the author wishes to thank Jim Lackey, Craig Moore, Rol Johnson, Dave Finley, Mike Harrison, Bruce Brown (all of Fermilab), and Lyn Evans (CERN). A special thanks must go to Al Garren (LBL) for introducing the author to the art of accelerator design and to Ardith Kenney (LBL) for her assistance.

Above all the author wishes to thank Ellen Syphers for her help and encouragement and Donald A. Edwards of Fermilab and the University of Illinois at Chicago for his teachings, guidance, and support throughout the entire project. Without them, the completion of this work would not have been possible.

ABSTRACT

A new 8 GeV beam transport system between the Booster and Main Ring synchrotrons at the Fermi National Accelerator Laboratory is presented. The system was developed in an effort to improve the transverse phase space area occupied by the proton beam upon injection into the Main Ring accelerator. Problems with the original system are described and general methods of beamline design are formulated. Errors in the transverse properties of a beamline at the injection point of the second synchrotron and their effects on the region in transverse phase space occupied by a beam of particles are discussed. Results from the commissioning phase of the project are presented as well as measurements of the degree of phase space dilution generated by the transfer of 8 GeV protons from the Booster synchrotron to the Main Ring synchrotron.

TABLE OF CONTENTS

LIST OF FIGURES

I.   Introduction

The Synchrotron

The primary instrument used in High Energy Physics (HEP) research today is the alternating gradient synchrotron. The beams of high energy particles (generally electrons or protons) produced by synchrotrons may be used to study sub-nuclear structure in one of two modes. In one mode (the "fixed target" mode) particles are extracted from the synchrotron and transported to a stationary target. The energy available to create new particles is proportional to the square root of the energy of the incident beam. In many instances the particles created from these primary collisions will be used to form secondary beams.

In the other mode of operation (the "colliding beams" mode), two separate beams of particles in the synchrotron are directed toward one another and are made to collide. Some synchrotrons accelerate and store the two beams in separate intersecting rings. Others have one beam of particles and a beam of antiparticles occupying the same ring. These two beams are accelerated to the desired energy simultaneously and then made to collide at a specific point in the synchrotron. As opposed to the fixed target mode, the energy available to create new particle states in the colliding beams mode is proportional to the beam energy. For example, in an electron colliding beams accelerator the available energy is twice the beam energy; in a proton collider the available energy typically is a fraction of

twice the beam energy. This is because hadrons are composed of more fundamental particles. The type of HEP interactions studied using colliding beams is much more limited compared with those of a fixed target experiment. In a collider, the particles must be stable (such as protons, antiprotons, electrons, or positrons) as they must live long enough to be stored for extended periods of time (typically several hours).

Just as important a parameter as the beam energy in HEP experiments is the reaction rate. The rate at which a particular event can be observed is a product of the probability that the event can occur and a collection of other parameters which describe the particle beam and its environment. Collectively these parameters define the luminosity, the product of the number of target particles and the number of incident particles per second divided by the cross sectional area(s) of the beam(s). For fixed target mode the luminosity depends upon the rate at which particles from the accelerator reach the target and the density and length of the target. For colliding beams mode the luminosity is proportional to the number of particles in each beam, the frequency at which the beams interact, and also is inversely proportional to the cross sectional area of the two colliding beams. Although the colliding beams accelerators can acquire much higher center of mass energies, the luminosities achieved so far in these machines are typically orders of magnitude below those of fixed target experiments.

In addition to its effect on the luminosity of a colliding beams accelerator, there are other reasons why small transverse

beam size is beneficial in a synchrotron. The size of the
magnets which make up the accelerator and therefore the cost of
the machine depend very naturally on the beam diameter. In
addition, the process of extracting the beam from the accelerator
during fixed target operation is made much more efficient if the
beam size is small. The transverse size of the particle beam at
a specific point in the synchrotron depends upon the focusing
properties of the synchrotron at that point as well as the area
in transverse phase space occupied by the beam. This phase space
area is referred to as the beam emittance. The preservation of
the emittance throughout the entire acceleration process is a
major concern of accelerator physics.

The particular concern of this thesis is the control of the
transverse emittance of the beam during transfer from one
synchrotron to another. If the beam transport system connecting
the two synchrotrons does not provide a proper match of the
focusing properties, beam trajectory, or dispersive properties of
the two machines, the result will be an increase in the beam
emittance, ultimately resulting in a degradation of the
luminosity of the accelerator. The transport system between the
output of the 8 GeV Booster proton synchrotron and the input of
the 150 GeV Main Ring synchrotron at the Fermi National
Accelerator Laboratory is investigated. Before discussing this
investigation and its results, a brief overview of the Fermilab
accelerator system is in order.

The Fermilab Accelerator System

The dynamical ranges of accelerators are limited due to technological reasons. Therefore, several machines operating in series are required to accelerate particles to a kinetic energy of several hundred GeV. Figure I-1 shows the layout of the Fermilab accelerator system. The process begins in a Cockcroft-Walton[1] style accelerator. Negative hydrogen ions are extracted from a plasma inside the dome of the accelerator. The ions then travel through an evacuated cylinder connecting the charged dome to one of the metal walls of the room containing the accelerator. With the dome being charged to a potential of 750,000 volts, the kinetic energy of the ions leaving the accelerator is 750 keV.

The beam immediately enters the second accelerator, a 145 m linear accelerator, or Linac. This device consists of resonant radio-frequency cavities which operate at a frequency of 200 MHz. By using a resonant cavity just at the entrance of the Linac, the continuous beam of particles arriving from the Cockcroft-Walton are formed into small groups of particles called "bunches." Within the cavities, quadrupole magnets of alternating gradient focus the beam. The kinetic energy of the particles leaving the Linac is 200 MeV. Once the beam exits the Linac, another resonant cavity is used to initialize a debunching of the beam.

Next in line is the first of three synchrotrons, the 8 GeV Booster. At the injection point of the Booster, the negative hydrogen ions pass through a thin carbon foil which strips the ions of their electrons, creating a beam of positively charged protons. (The use of a negative ion injection scheme provides a

Figure I-1

General Layout

of FNAL Accelerators

Fixed Target
Experiments

Main Ring,
Tevatron

B0

Colliding Beams
Experiments

D0

Cockcroft—
Walton

Linac

Booster

8 GeV Line

Antiproton
Source

(Not to Scale)
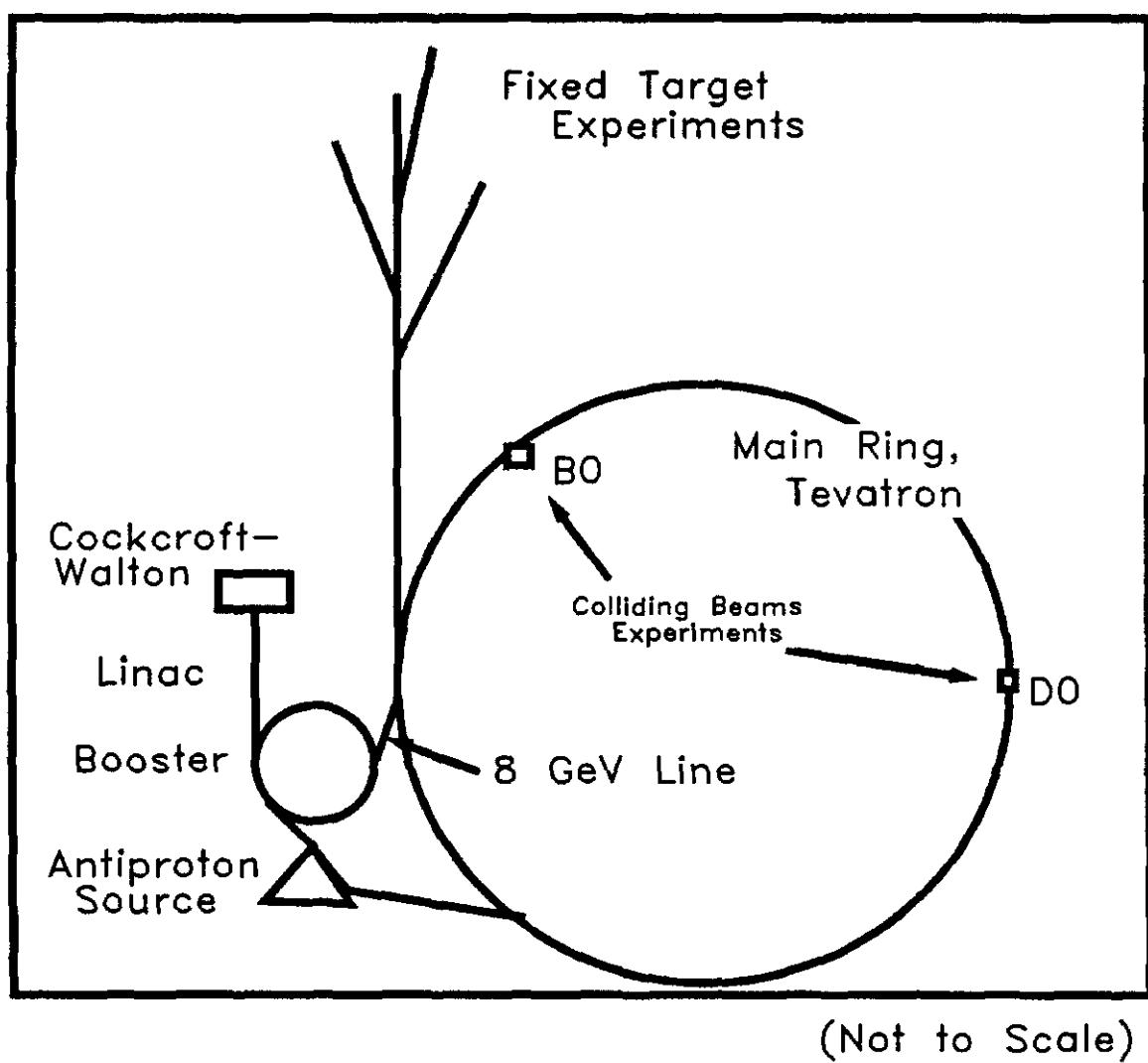
higher injection efficiency for the Booster accelerator when higher intensity beams are requested.) Once the beam is injected, 18 radio-frequency (RF) cavities located around the 474 m circumference of the Booster group the particles into bunches again. The operating frequency of a synchrotron RF system is a multiple of the the revolution frequency. This "multiple" is referred to as the harmonic number of the synchrotron. For the Booster accelerator, the harmonic number was chosen to be 84, hence 84 bunches are formed in the Booster. Due to the increase in speed of the particles during the acceleration process, the RF frequency changes from 30.2 MHz at injection to roughly 52.8 MHz at extraction.

The major magnetic elements of the Booster synchrotron are gradient magnets, combining a radially inward bending force and a focusing force. The magnets are arranged such that elements which focus in the vertical plane and defocus in the horizontal plane alternate with elements which focus in the horizontal plane and defocus in the vertical plane, thus the name "alternating gradient synchrotron." The gradient magnets are part of a resonant circuit which allows the Booster to accelerate particles from .200 GeV to 8 GeV kinetic energy at a 15 Hz rate.

Once extracted from the Booster, the beam is transported to the Main Ring synchrotron. This is the original Fermilab 400 GeV accelerator which is currently used as a 150 GeV injector for the Tevatron accelerator. The mean radius of the Main Ring is 1000 meters, exactly 13.25 times the mean radius of the Booster accelerator, so that up to 13 batches of Booster beam may be

injected into the Main Ring. The RF systems of the Booster and Main Ring are phase-locked during the transfer so that debunching and rebunching of the particles are not required. The RF frequency of the Main Ring is 84 x 13.25 = 1113 times the revolution frequency and changes by less than one percent during the acceleration process.

Focusing and steering of the particle beam is provided by separate magnetic elements in the Main Ring synchrotron. Most of the four-mile circumference is occupied by dipole magnets and quadrupole magnets. At six equally spaced intervals around the ring, long (50 meters) straight sections break the normal lattice to allow room for such necessary equipment as RF cavities, injection and extraction devices, and a beam abort system.

The Main Ring accelerator is also used for the production of antiprotons for use in the colliding beams program. Protons may be extracted from the Main Ring at an energy of 120 GeV and sent toward the antiproton storage rings. (See Figure I-1.) Upon striking a tungsten target, 8 GeV antiprotons are produced which are subsequently gathered and stored in the antiproton accumulator ring. This process is repeated many times until the accumulator ring has acquired a high density of antiprotons. A beam of antiprotons may then be reverse injected into the Main Ring, accelerated to an energy of 150 GeV, and then reverse injected into the Tevatron for colliding beams experiments.

Located 25.5 inches directly below the Main Ring is the Tevatron, the world's first superconducting proton synchrotron. The Tevatron accepts 150 GeV protons and/or antiprotons from the

Main Ring and accelerates them to 900 GeV. In many respects, this machine is very similar to the Main Ring synchrotron. The arrangement of bending and focusing magnets that comprise the Tevatron is essentially the same as that in the Main Ring. The RF frequency of the Tevatron's accelerating cavities is locked to the Main Ring frequency during transfer and the RF harmonic number is the same for both of these systems. However, the cryogenics system, which cools the Tevatron magnets to 4.5°K, and the accelerator physics issues inherent in large storage rings consisting of superconducting magnets greatly add to the complexity of the Tevatron.

To finish the overview of the Fermilab accelerators, one detail needs to be mentioned which will be of importance in later discussions. Two of the long straight sections of the Tevatron are dedicated to large multipurpose particle detectors for use in the colliding beams program. To help prevent possible interference from Main Ring antiproton production during colliding beams experiments, modifications were made to the Main Ring synchrotron geometry to guide the beam up and over the detectors. These "overpasses," produce a significant effect on the characteristics of the circulating Main Ring beam. As will be seen in the next section, the old injection system could not provide a proper match to these new characteristics, leading to inefficiencies in the beam transfer.

References

1. Cockcroft, J. D., and E. T. S. Walton, _Proceedings of the Royal Society_ (London), Vol. A136, 1932, p. 619.

II. Original Booster to Main Ring Beam Transport System

General Description

The original Booster to Main Ring transport line, (8 GeV
Line) was developed using preproduction Main Ring quadrupole
magnets, short versions of Main Ring dipole magnets with modified
coil packages, and a minimum number of power supplies. The
resulting design[1] consisted of 18 quadrupole magnets powered in
series and seven dipole magnets powered by three separate
supplies. The geometry of the beamline is shown in Figure II-1.
The beam was extracted vertically from the Booster synchrotron
and injected vertically into the Main Ring. The horizontal kink
in the beamline provided a change in the dispersive properties of
the line necessary to match the horizontal trajectories of
particles with various momenta to their desired trajectories in
the Main Ring.

Vertical extraction from the Booster is accomplished using
four 1 meter transmission-line kicker magnets with rise times of
roughly 25-30 nsec, almost fast enough to achieve full current
during the time between successive bunches. (One Booster bunch
is sacrificed during the extraction process.) These kickers,
located 20 meters in front of the extraction point, provide the
beam with a 1 milliradian vertical kick which translates to about
a 20 mm vertical displacement at the extraction point. There,
the beam enters another pulsed magnetic device, the first of a
pair of pulsed septum magnets.[2] The first septum magnet is
located at the beginning of a Booster long straight section. The

Figure II-1

Original 8 GeV Beamline Layout
(Horizontal Plane)
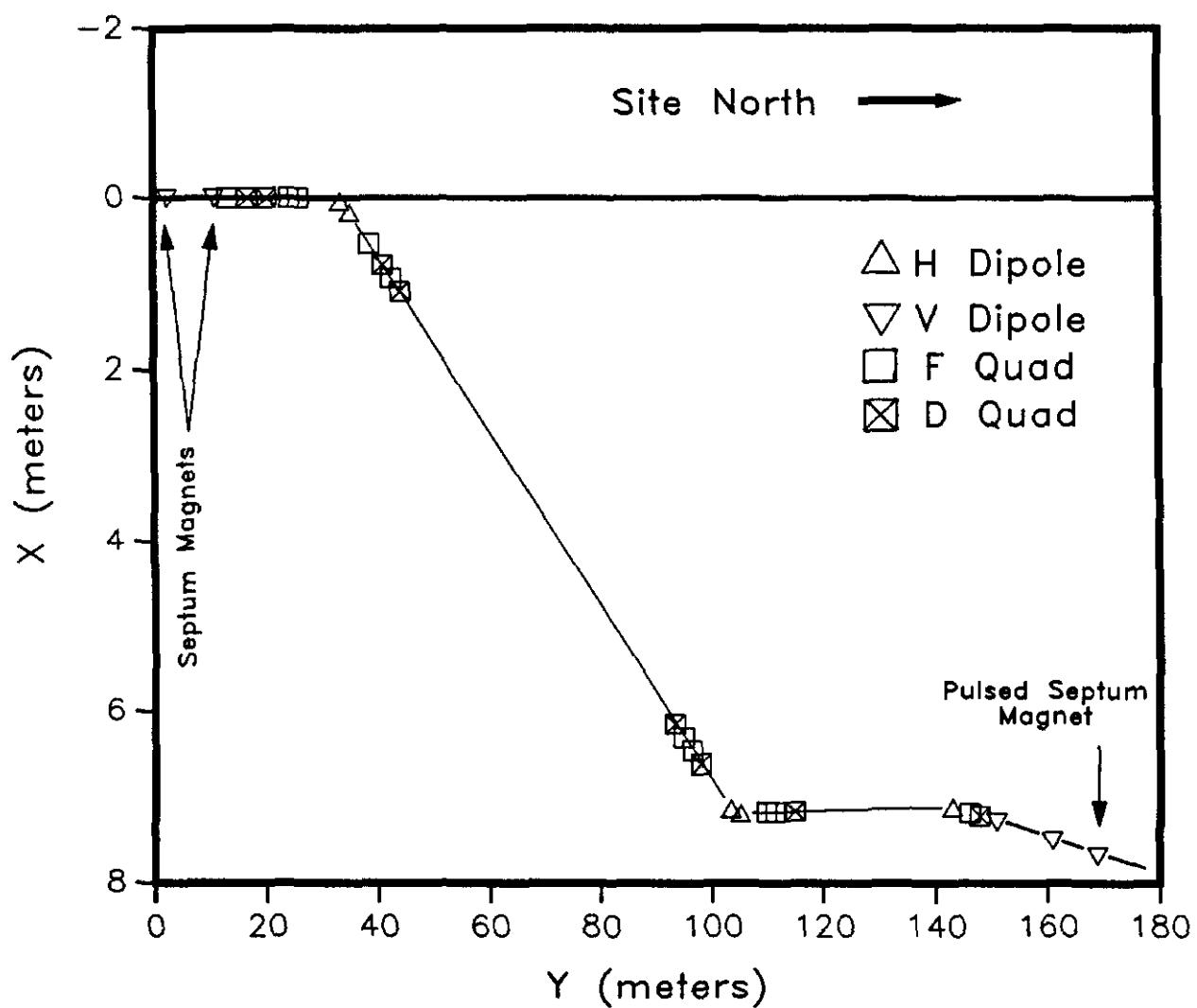
actual "septum" of this magnet separates a strong field region
from a relatively "field-free" region. Normally, the circulating
Booster beam passes through the field-free region. At
extraction, the "kicked" beam enters the field region of the
septum magnet. This magnet delivers an upward 44 mrad kick to
the displaced beam, enough to send it over the next Booster
gradient magnet at the end of the long straight section. (See
Figure II-2.)   The second of the septum magnets bends the beam
down by 44 mrad, the beam being 45.7 cm above the Booster closed
orbit at this point. The beam was then steered toward the Main
Ring injection point roughly 170 m away, eventually being aligned
horizontally with the Main Ring closed orbit and displaced
vertically by 50 cm. (The plane of the Main Ring lies 30.5 cm
below the plane of the Booster. Thus, the old beamline contained
a net 1.6 mrad downward pitch for about 140 m.)

To inject onto the closed orbit of the Main Ring
accelerator, the old 8 GeV Line employed two vertically bending
dipole magnets (to bring the beam to within a few centimeters of
the orbit), another pulsed septum magnet, and two pulsed vertical
kicker magnets. (See Figure II-3.) The beam left the two
dipoles with about an 11 mrad downward angle with respect to the
Main Ring closed orbit and the pulsed septum reduced this pitch
to just under 1 mrad. The kickers, located just downstream of
the first set of Main Ring quadrupoles, completed the injection
process with a total upward kick of 0.7 mrad.

To understand the focusing properties of a synchrotron or
beamline, the equation of motion for a particle in one transverse

Figure II-2

Booster Extraction Region
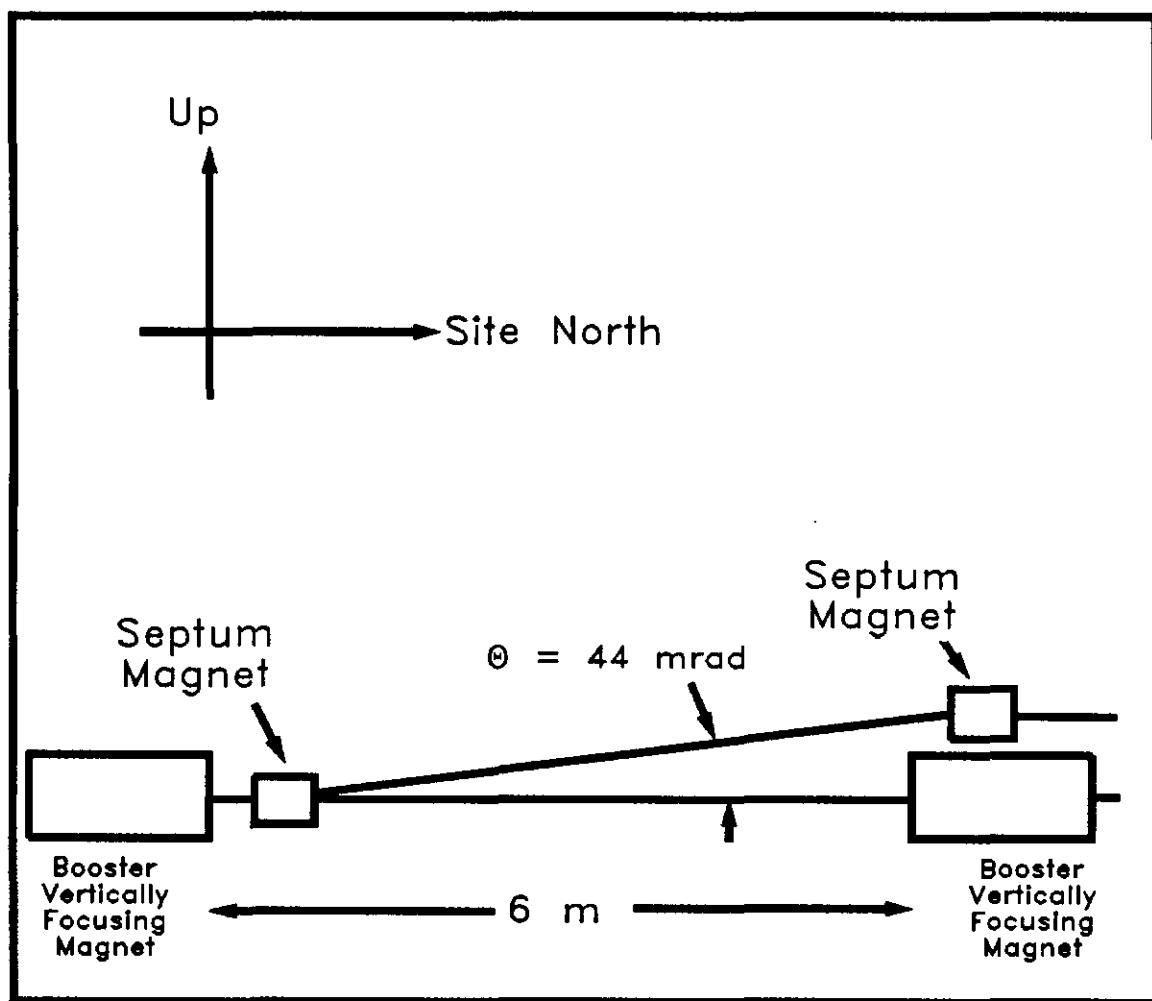
Figure II-3

Original Main Ring Injection Region Layout
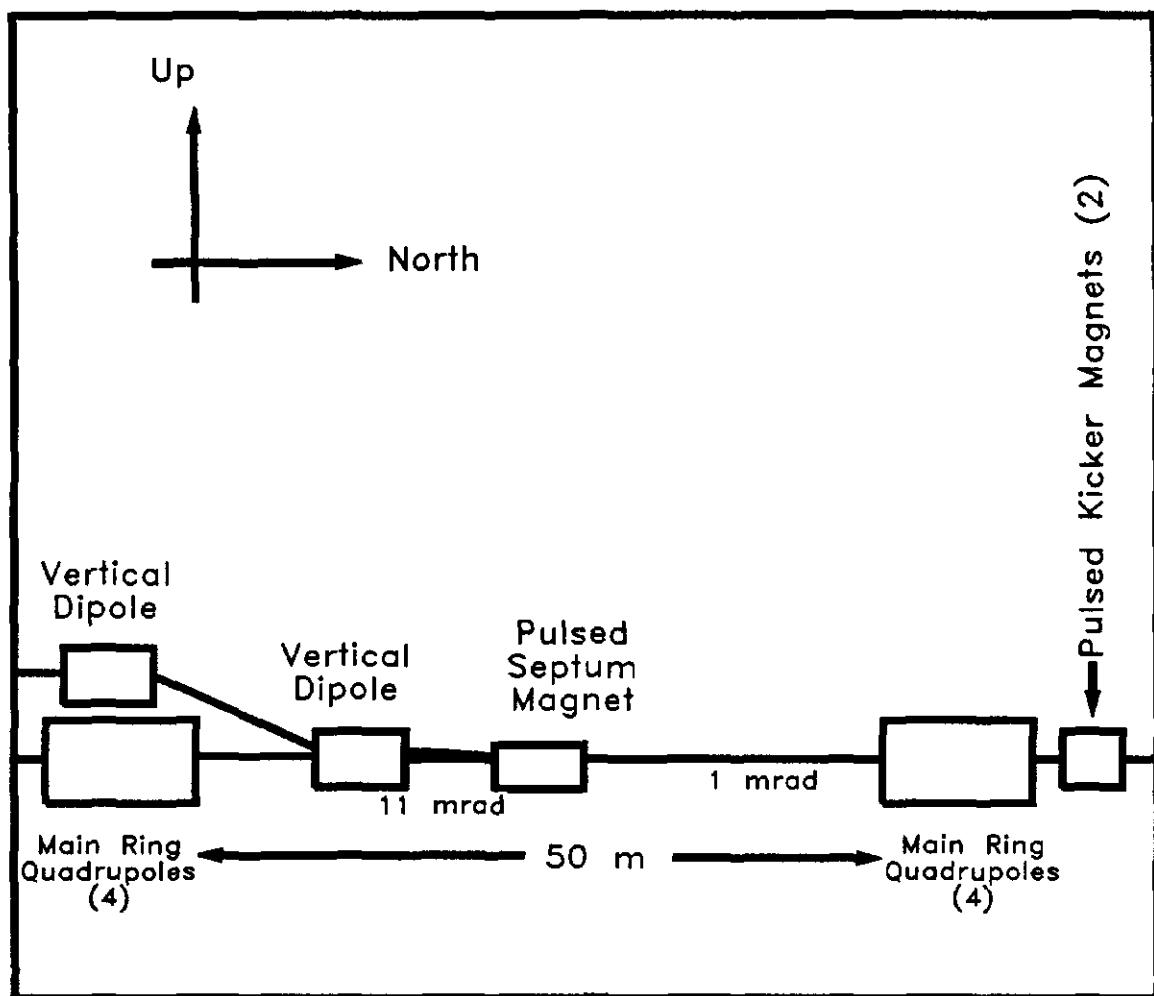
degree of freedom may be written in the form of Hill's Equation,[3]

$$x''(s) + K(s)x = 0 \ ,$$

where s = the particle's longitudinal position within the machine, x(s) is the transverse displacement of the particle from the ideal closed orbit, and $x'' \equiv d^2x/ds^2$. The modified "spring constant," $K(s) \equiv (e/p)(\partial B_y/\partial x)$ where p is the particle momentum, is determined by the focusing elements within the machine. The solution to Hill's Equation may be written as[4]

$$x(s) = A \sqrt{\beta(s)} \sin(\psi(s) + \delta)$$

where A and δ are constants. The parameter $\beta(s)$ is referred to as the betatron amplitude function, or beta function, and the betatron phase advance ψ is given by $d\psi/ds = 1/\beta(s)$. For a beam of particles, the beam size varies with $\beta^{1/2}(s)$.

Since x(s) represents the horizontal displacement of a particle of design momentum p from the design trajectory along the path length s, the ideal closed orbit for this particle is simply given by x(s) = 0. However, a particle of momentum p+Δp will have a different ideal closed orbit defined by

$$x_{\Delta p}(s) = D_x(s,\Delta p/p)\frac{\Delta p}{p} \ .$$

The quantity D_x is referred to as the horizontal dispersion function of the accelerator. For most large synchrotrons such as the Booster, Main Ring, and Tevatron, the dispersion functions themselves are essentially independent of $\Delta p/p$. (Dispersion is discussed in more detail in Chapter III.)

The arrangement of quadrupoles in the old line shown in Figure II-1 provided focusing of the beam as well as additional

steering for the off-momentum particles. The beamline contained a dispersion-free region in the middle, the purpose of which was to allow for the adjustment of the betatron amplitude functions (by tuning quadrupole currents) without fear of changing the dispersion functions.[5] Figures II-4 and II-5 show the amplitude and dispersion functions for the old beamline. Indeed the horizontal dispersion is approximately zero in the middle region (although the vertical dispersion function is not). However, to obtain this condition using a limited number of power supplies the maximum values of the amplitude functions had to approach 300-400 meters. (For comparison, the maximum values in the Booster and Main Ring accelerators are 34 meters and 120 meters, respectively.) Since there were no aperture restrictions in these regions of high beta, performance was not expected to be hindered.

Problems With the Original Design

In an effort to improve the quality and reliability of the beam being delivered to the experimental areas and in preparation for the luminosity demands of the Tevatron I colliding beams program, an accelerator emittance improvement program was initiated within the FNAL Accelerator Division during the spring of 1985. Discussions began which were concerned with possible upgrades to existing accelerator systems. Many systems which were installed in the laboratory's infancy were built to meet much lesser demands than are required to meet today's goals. One such system which received attention was the 15-year-old 8 GeV Line.

Figure II-4

Design Amplitude Functions
of Original 8 GeV Beamline

Figure II-5

Dispersion Functions
of Original 8 GeV Beamline
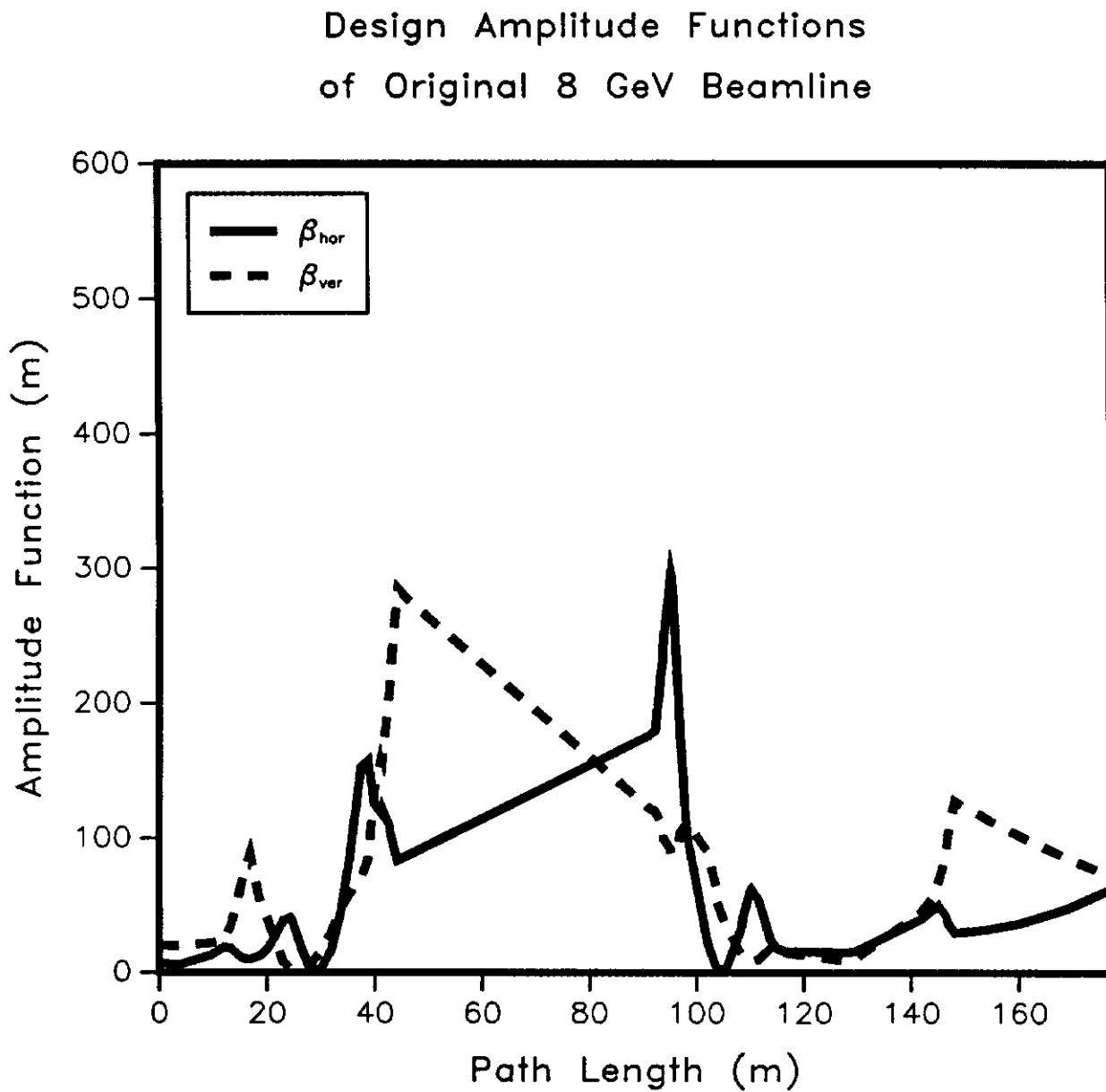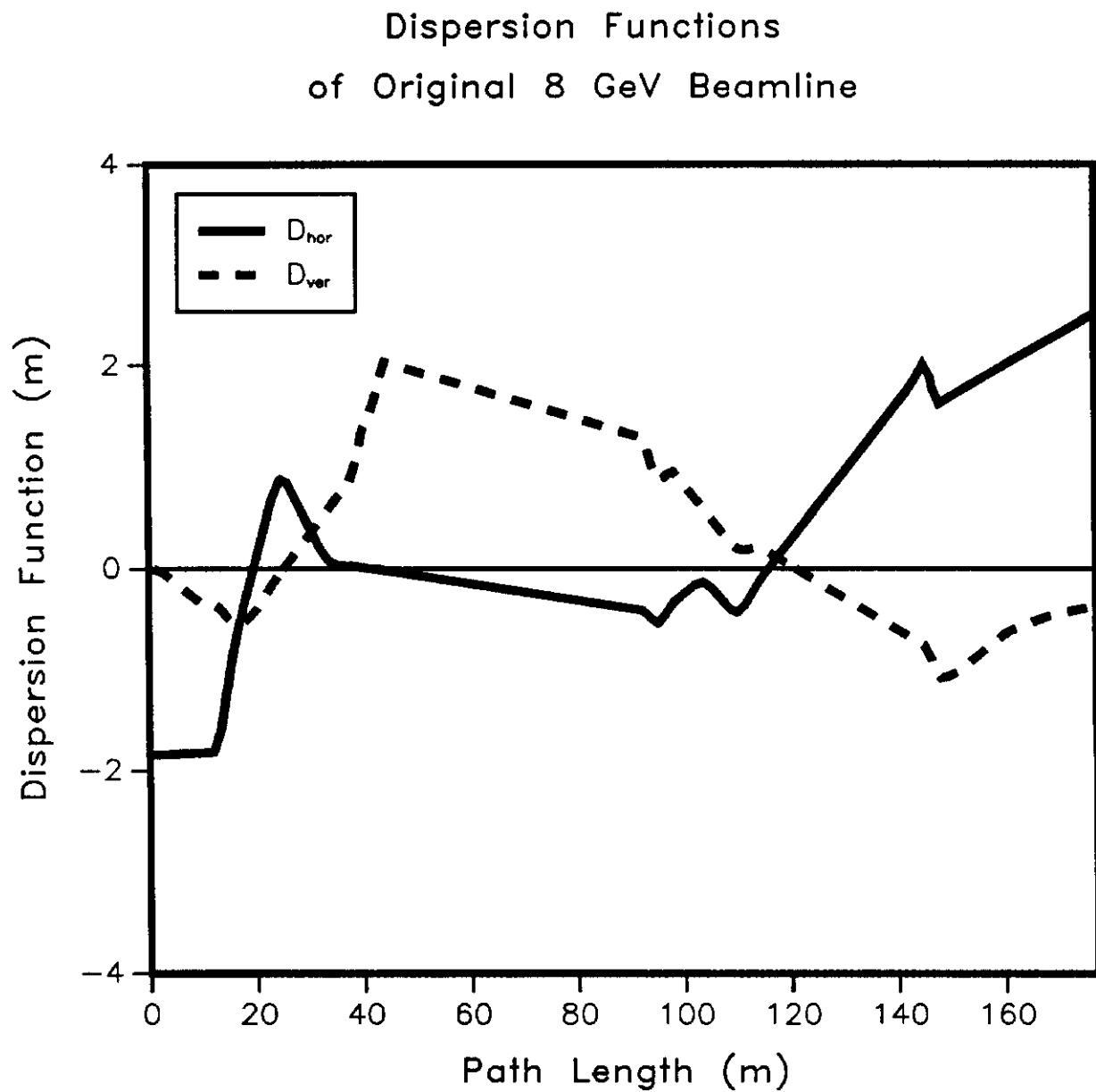
In late June, 1985 some effort was put into understanding the present conditions of the beam being transported through the 8 GeV Line. At that time, the beamline's diagnostic equipment consisted solely of 12 beam profile monitors placed throughout the line. These monitors were horizontal and vertical planes of wires (or, in many instances, foils) which could be inserted into the path of the beam using the control system. As the foil planes generated an appreciable amount of multiple scattering, only one monitor could be placed in the beam at a time to obtain useful results. A serious study of the beam arriving from Booster required a significant block of time dedicated to this task. The signals from these wires were processed by an applications program run from the Fermilab Main Control Room and provided the operator with beam position and distribution information. Using data gathered by these monitors, an analysis of the beam characteristics through the line was performed.[6],[7] The results of the study are shown in Figure II-6. The maximum beam sizes observed corresponded to maximum amplitude functions with values on the order of 600 meters in the vertical plane. Although the overall character of the beamline optics resembled the original design, large deviations from the design were apparent.

Meanwhile, one of the quadrupole magnets in the beamline developed a mechanical problem and had to be replaced. When the magnet was removed from the beamline, it was transported to the FNAL Magnet Test Facility where a number of measurements were performed.[8] This was the first (and only) magnet in the 8 GeV

Figure II-6

Measured Amplitude Functions
of Original 8 GeV Beamline
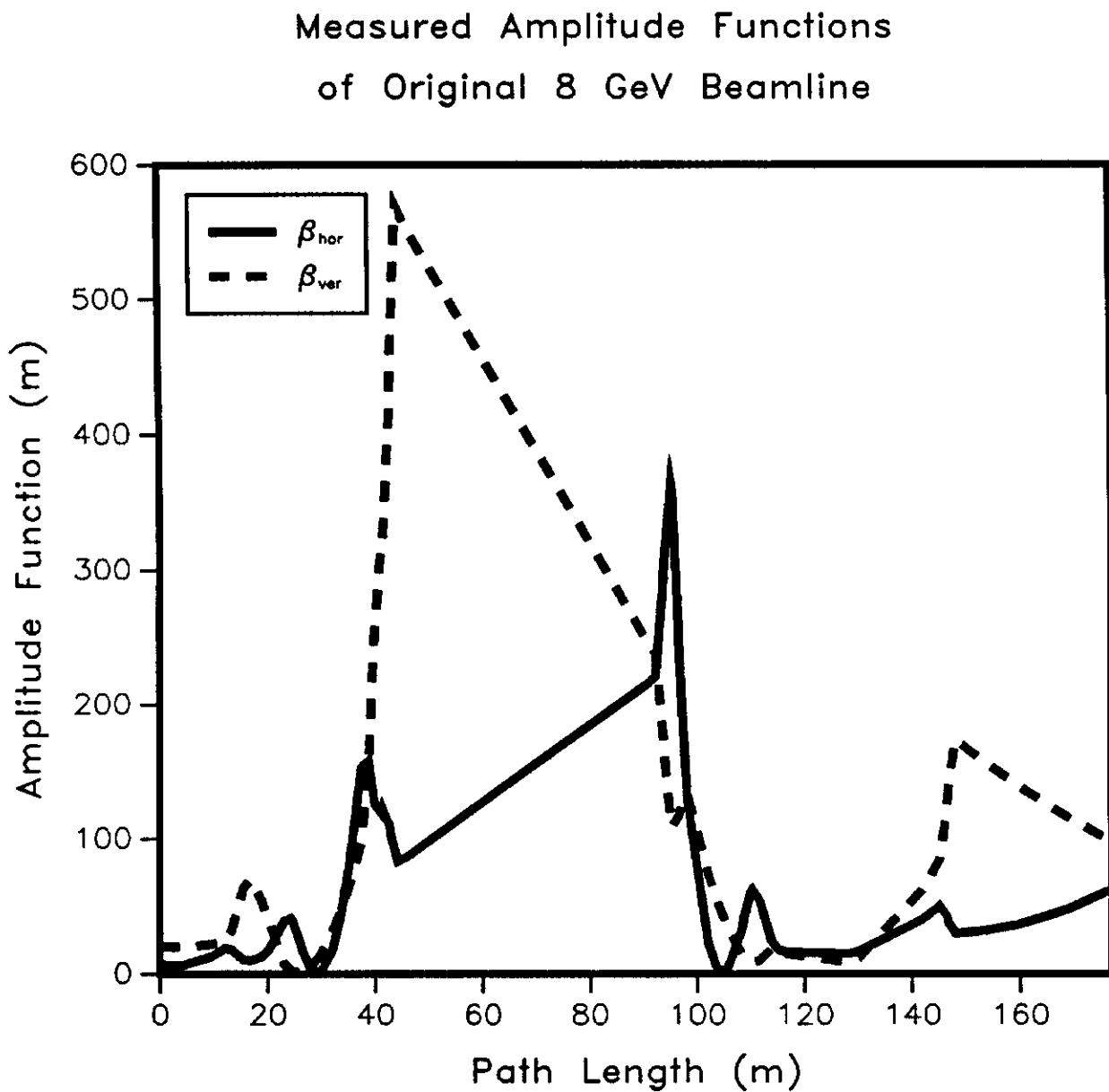
Line ever to have been magnetically measured. The quadrupole magnets used in the line, being Main Ring style magnets, were designed to run at currents of over 4000 Amperes. The gradient provided by these magnets at this current is 220 kG/m. For use in the 8 GeV Line, the quadrupoles operated at a typical current of 700 Amperes, or 40 kG/m. The remnant field gradients in the quadrupole, as determined from the measurements, were significant (0.2 kG/m) and the effects of hysteresis were quite large. Depending upon the exact method used to bring the quadrupole up to nominal current, the final field gradient in the magnet could differ by as much as 0.2-1.0 kG/m. Changes of this magnitude were enough to alter the values of the amplitude function throughout the beamline significantly, especially when its values were large initially.

Large betatron amplitude functions correspond to large beam size at those locations, but more importantly they increase the sensitivity of the match of the beamline to the downstream accelerator. A gradient error $\Delta B'$ at a location of high beta will affect the values of the amplitude function at locations downstream of the error. Using the techniques discussed in Chapter III, if $\Delta q \equiv \Delta B'L/(B\rho)$, where L is the length of the magnet producing the error and $B\rho$ is the magnetic rigidity, then

$$\Delta\beta/\beta = -(\Delta q \beta_0)\sin 2\psi_0 + (\Delta q \beta_0)^2(1 - \cos 2\psi_0)/2$$

where $\Delta\beta/\beta$ is the relative change in the amplitude function downstream of the gradient error, β_0 is the amplitude function at the location of the error and ψ_0 is the original phase advance measured from the location of the error to the downstream

location. If the amplitude function delivered by the beamline is not well matched to the natural amplitude function of the synchrotron at the injection point, then the beam will undergo larger than necessary betatron oscillations once in the new machine. Thus, the particles will occupy more area in transverse phase space and the beam size will grow. This process is known as phase space dilution, or emittance dilution. The details of the analysis of dilution are found in Chapter V.

Figure II-7 shows how an increase in transverse emittance can be caused by errors in the fields of the quadrupoles in the old 8 GeV Line. (The details of this calculation are presented in Chapter V.) As can be seen, due to the large amplitude function at the locations of certain quadrupoles, errors in the gradients of those magnets can produce significant dilution.

As well as affecting the beam size, large amplitude functions in the beamline also increase the beam's sensitivity to steering errors. These steering errors may be due to a misalignment of a quadrupole magnet, for instance. The displacement of a particle downstream of a steering error of magnitude θ is given by

$$\Delta x(s) = \theta \sqrt{\beta(s_0)\beta(s)} \sin\left[\psi(s) - \psi(s_0)\right] .$$

Hence, larger values of the amplitude function β will necessitate more sensitive position correction schemes. If the injection positions are too far from the closed orbit of the synchrotron, the particles will undergo larger than normal betatron oscillations and will occupy more phase space than necessary. Again, a form of dilution will take place.

Figure II-7

Transverse Emittance Dilution

Due to Gradient Error of $\Delta B'/B' = 4\%$

Quadrupole Magnet of the Original 8 GeV Line
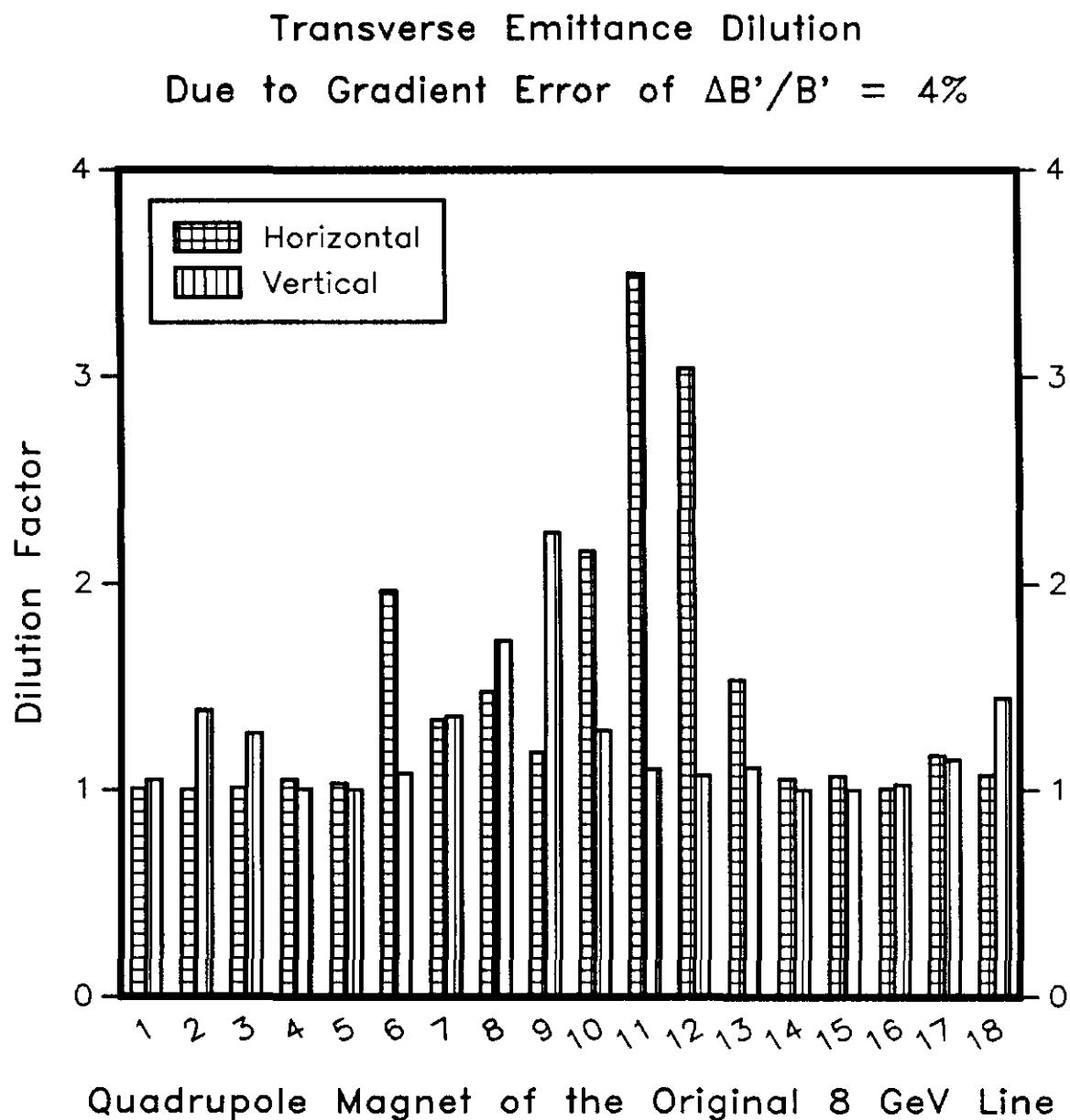
An additional problem separate from those described above existed. It really was not the "fault" of the beamline, but needed to be corrected by the beamline system. The problem involved the Main Ring overpasses. In most circular machines the ideal trajectory of the particles is confined to the horizontal plane. However, once the overpass at the DO experimental region (see Figure I-1) was installed, the new closed trajectories for off-momentum particles in the Main Ring included motion in the vertical degree of freedom. The vertical dispersion at the Main Ring injection point became significantly large after this modification. As shown in Figure II-8, beam losses were observed at regions of large vertical dispersion in the Main Ring due to the momentum spread of the beam coming from the Booster.[9] Since the vertical dispersion function at the injection point in the Main Ring no longer matched the vertical dispersion function of the 8 GeV Line, the trajectories of off-momentum particles arriving from the Booster would not lie on their desired orbits once in the Main Ring. The result would be larger than necessary betatron oscillations during successive revolutions around the Main Ring for these particles. This motion would have contributed to the dilution of the transverse emittance. A lack of flexibility of the 8 GeV Line power supply system prevented any correction of this problem short of redesigning the end of the beamline -- either its magnetic elements, its power supply circuits, or both.

Another improvement which could have been made to the 8 GeV Line was to the pulsed injection system. Because the

Figure II-8

Main Ring Beam Losses
at Regions of Large Vertical Dispersion
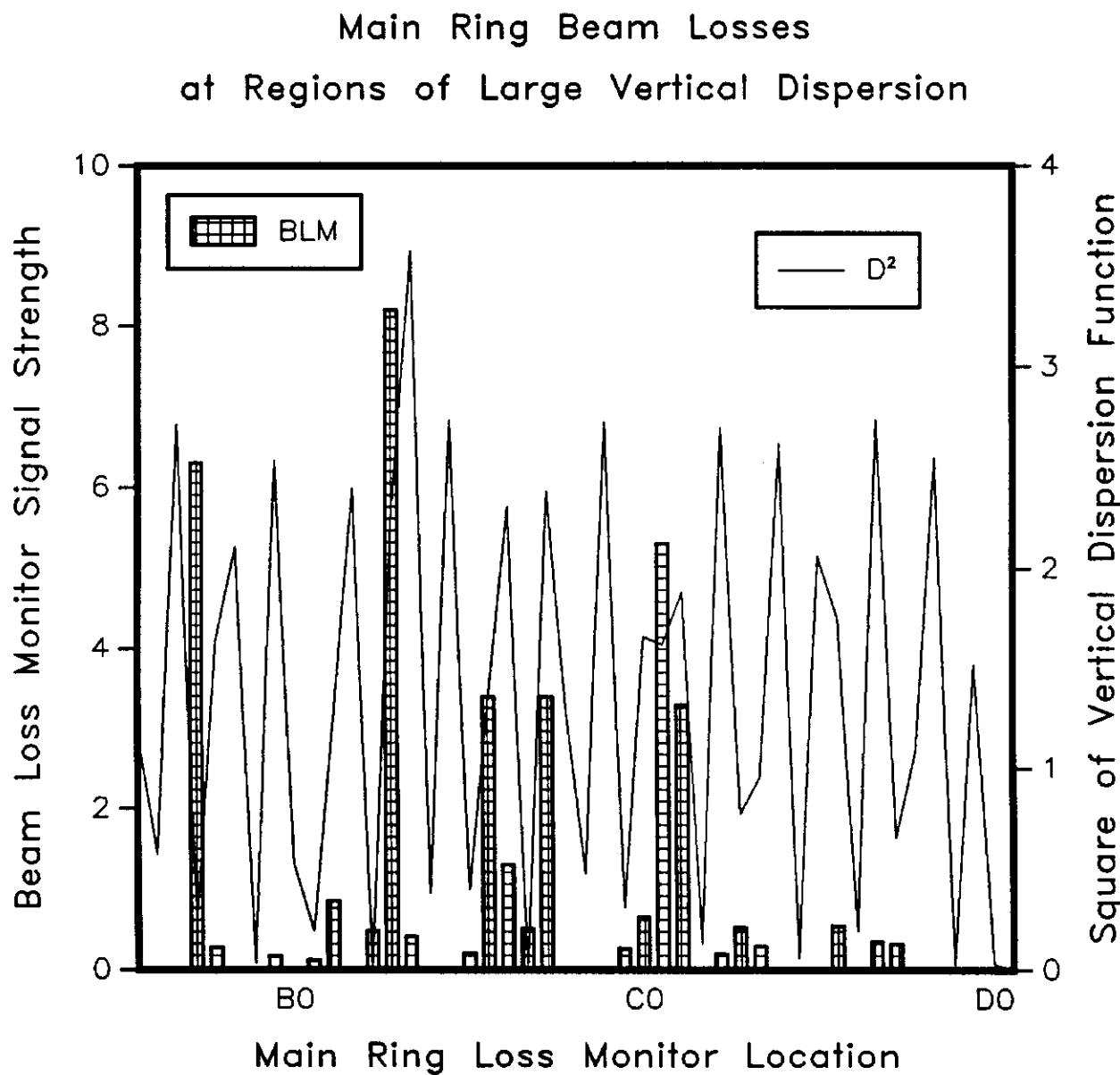
circumference of the Booster synchrotron is roughly one thirteenth the circumference of the Main Ring, the Booster can be filled 13 times and each "batch" of Booster beam can be delivered to the Main Ring one batch directly behind another. During the 66.6 msec between Booster cycles, the previously injected batches will circulate the Main Ring 3000 times. Due to the finite rise time (~200 μsec) of the pulsed septum magnet at the injection point (see Figure II-3), the circulating beam would be subjected to a vertical orbit distortion created by this device whenever another batch was about to be transfered between the two rings. Although the circulating beam passed through the "field-free-region" of the septum, the true fields in this region were strong enough to displace the vertical closed orbit by as much as 5 mm.

It became apparent that major improvements could be made to the 8 GeV beam transport system. The vertical dispersion was mismatched and was blamed for causing beam loss throughout the Main Ring accelerator. The sensitivity of the amplitude function match to gradient errors had been evident for some time as is shown in Figure II-9.[10] The diagnostics system needed improvement and expansion. At the same time, improvements could be made to the injection system, power supply system, and to the magnetic elements. By July of 1985 a new line was being designed by the author.

Figure II-9

Measured Dilution Factors
2/21/79 to 3/7/82
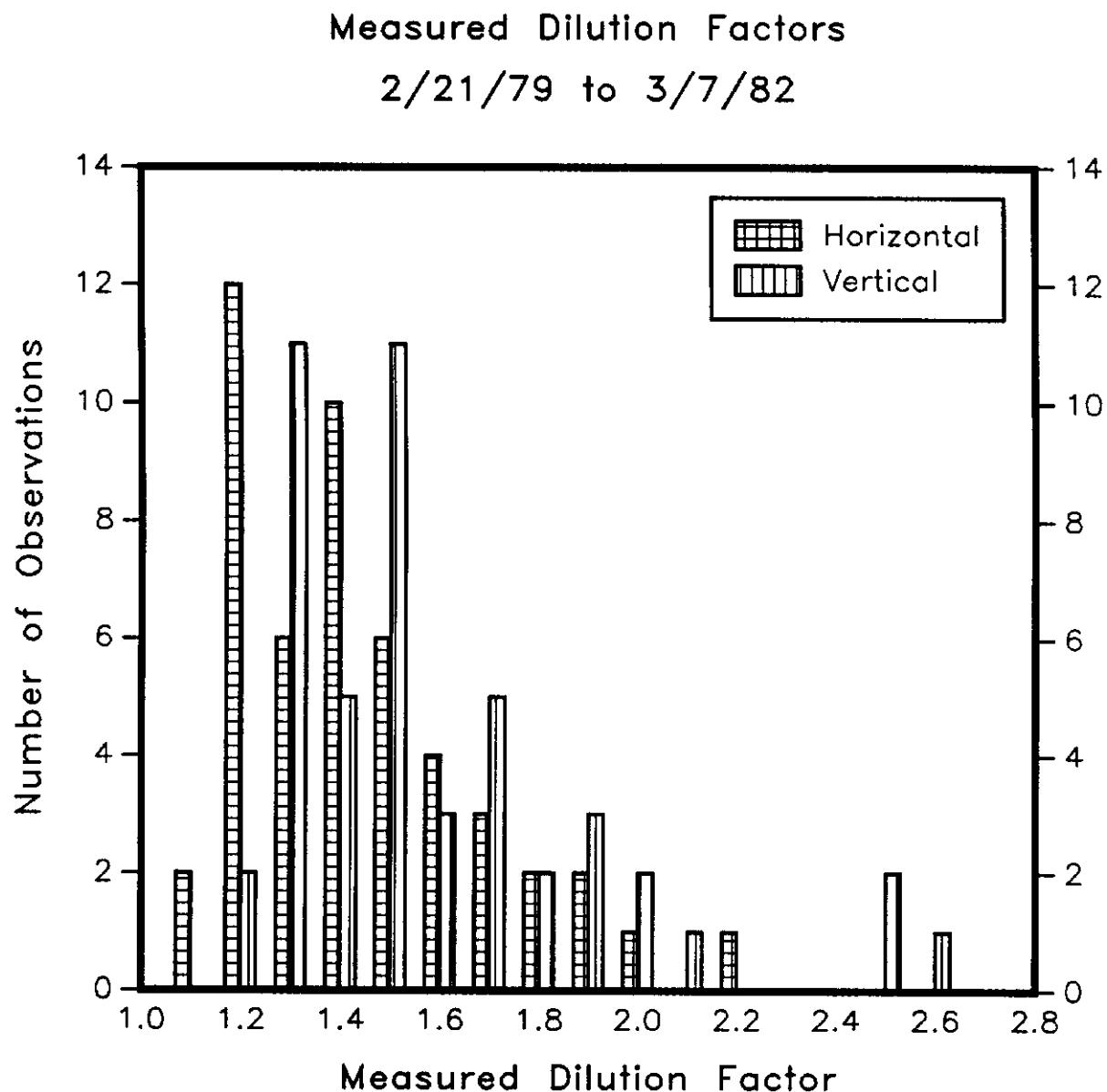
Criteria for a New System

To aid in the design of a new 8 GeV transport system, the following set of criteria was developed:

Firstly, the charged particle beam was to be steered from the extraction point of the Booster to the injection point of the Main Ring. The system needed to be able to accept various Booster extraction trajectories and, at the other end of the line, be able to make proper adjustments to the position and direction of the beam leading into the Main Ring. Correction elements were needed to provide additional steering capabilities of the beam through the middle of the line.

Secondly, focusing elements were needed to transport the transverse amplitude functions and dispersion functions delivered by the Booster synchrotron to the Main Ring synchrotron and produce a proper match of these functions to the Main Ring lattice. The beam size should be small throughout the line to reduce its sensitivity to magnet errors. Also, the power supply system should be flexible enough to allow adjustments for changes in the characteristics of the Booster beam.

Thirdly, the optical properties of the beamline should easily accommodate useful measurements of transverse emittances and momentum spread as well as beam positions. The diagnostics system must be upgraded to allow simultaneous collection of profile and position data from all monitors without generating significant beam loss.

Fourthly, if possible, a new injection scheme should be developed using magnetic elements which would have less effect on the already circulating beam (or at least affect it in a way which may be easily compensated by other means).

Fifthly, all elements (in particular, quadrupoles and devices which will reside within the Main Ring beampipe) should be magnetically measured.

References

1. Maschke, A. W., and L. W. Oleksiuk, "The NAL Booster-to-Main Ring Beam Transfer System," IEEE Transactions on Nuclear Science, Vol. NS-18, No. 3; June, 1971.

2. Cosgrove, D. F., R. P. Johnson, and S. C. Snowdon, "A Pulsed Septum Magnet for Extraction From the Fermilab Booster," IEEE Transactions on Nuclear Science, Vol. NS-24, No. 3, June, 1977.

3. Courant, E. D. and H. S. Snyder. "Theory of the Alternating Gradient Synchrotron," Annals of Physics, Vol. 3, No. 1 (January, 1958), p. 3.

4. Courant, E. D. and H. S. Snyder. "Theory of the Alternating Gradient Synchrotron," Annals of Physics, Vol. 3, No. 1 (January, 1958), p. 11.

5. Ibid.

6. Syphers, M. J., "8 GeV Emittance Measurements," FNAL Accelerator Experiment #125, Fermi National Accelerator Laboratory, Accelerator Division internal report, July 18, 1985.

7. Syphers, M. J., "An Analysis of 8 GeV Multiwire Data Using SYNCH," FNAL Accelerator Experiment #126, Fermi National Accelerator Laboratory, Accelerator Division internal report, July 23, 1985.

8. Schmidt, C., "Hysteresis Measurements of a Main-Ring Type Quadrupole," FNAL Accelerator Experiment #127, Fermi National Accelerator Laboratory, Accelerator Division internal report, July 25, 1985.

9. Data shown in the figure are from FNAL Main Control Room logbook, June 5, 1985, as recorded by C. Ankenbrandt.

10. These particular measurements of dilution factors were made at random. Data courtesy of C. Moore, FNAL.

III.   Transportation of Charged Particle Beam

From One Synchrotron to Another

Reduction of the Problem

To describe the trajectory of a single particle in a
synchrotron, the motion may be referenced to an ideal closed
path, the design orbit of the synchrotron. In transporting
particles from one synchrotron to another, the primary function
of the interconnecting beamline is to provide a path from the
extraction point of the first synchrotron to the injection point
of the second synchrotron. Not only must the extraction and
injection points be connected, but the slopes of the trajectory
at each point must be correct. This amounts to 12 constraints
which must be satisfied by the bending elements of the beamline.

The motion of a group of particles about the ideal
trajectory is now considered. The longitudinal behavior of the
particles may be treated independently from their transverse
motion. Usually, no longitudinal acceleration takes place in the
beamline connecting the two accelerators; such is the case for
the 8 GeV Line. The matching of the longitudinal phase space is
performed by the separate RF systems of the two synchrotrons by
making proper adjustments to the RF accelerating voltage output
and the relative phase between the two systems. Hence, during
the design of the beamline, longitudinal behavior of the
particles may be ignored.

As mentioned previously, the particles in a synchrotron
circulate the machine in groups, or "bunches." Typically the

length of a bunch of particles is many times the transverse size of the bunch. For instance, the bunch length of the Booster beam is roughly 1 meter while its diameter is on the order of a centimeter. For many purposes the bunch may be treated as an infinitely long distribution of charge. As an example, the Coulomb force on a particle in a bunch due to the other particles will be examined.

Given a line charge of length L containing N protons with a cylindrically symmetric Gaussian distribution of variance σ^2 in the transverse plane traveling with a speed βc, the total force on a proton a distance r from the axis of symmetry is

$$F(r) \;=\; \frac{N\,e^2}{2\pi\epsilon_o \gamma^2 L\; r}\;\left(1 - e^{-r^2/2\sigma^2}\right)\;.$$

For $r \ll \sigma$, the motion in the transverse plane reduces to

$$x'' \;=\; \frac{N\,r_c}{\gamma^3 \beta^2 L\;\sigma^2}\;x \quad\equiv\quad K\;x$$

where r_c is the classical radius of the proton. To obtain an estimate of K, typical numbers for the output of the Booster are used: $N = 10^{10}$, $\beta = 1$, $\gamma = 9.5$, $L = 1$ m, and $\sigma = .005$ m. Then K = 6 x $10^{-7}/m^2$. The effect of the space charge defocusing is to be compared with the focusing brought about by the elements of the beamline. The effective focal length of a focusing element is given by $1/(Kl)$ where l is the length of the element. Within a focusing element with a typical length of 1 meter and focal length of 10 meters, $K = .1/m^2$. Even over a typical spacing between focusing elements of ten meters, the space charge effect certainly may be neglected when designing the beamline.

Similarly, the size of other self-interactions, such as intrabeam scattering, are also negligible. Hence, the particles are considered to be noninteracting and, along with the fact that longitudinal behavior may be ignored, the number of degrees of freedom important to the problem is reduced from 3N to two.

The two degrees of freedom remaining are those transverse to the ideal particle trajectory which are usually chosen to be the horizontal (x) and vertical (y) directions. This nomenclature can become confusing when the entire synchrotron or beamline does not reside entirely in one plane. However, the beamline geometry will be assumed simple enough that this confusion may be easily overcome.

For each degree of freedom the particle trajectories obey the homogeneous Hill's Equation

$$x'' + K(s)x = 0$$

with solutions which may be written in terms of an amplitude function, $\beta(s)$:

$$x(s) = A\beta^{1/2}\sin(\psi(s)+\delta).$$

The constant A may be solved for in terms of x and $x' \equiv dx/ds$:

$$A^2 = (x^2 + (\beta x' + \alpha x)^2)/\beta$$

$$= \gamma x^2 + 2\alpha xx' + \beta x'^2,$$

where $\alpha \equiv -(d\beta/ds)/2$ and $\gamma \equiv (1 + \alpha^2)/\beta$. Thus, the particle traverses an elliptical path in x–x' phase space. Though the values of α, β, and γ vary with s, the quantity A^2 is independent of s and is referred to as the Courant-Snyder invariant. The area of the phase space ellipse is equal to πA^2.

If the particle distribution in one degree of freedom is assumed to be Gaussian in form with variance σ^2 and stationary in time, then the density of particles in x–x' phase space at a particular longitudinal location s may be written as

$$n(x,x') \ dx \ dx' = \frac{N \ \beta(s) \ dx \ dx'}{2\pi \ \sigma^2} \ e^{-\left[x^2 + (\beta x' + \alpha x)^2 \right]/2\sigma^2} \ .$$

If $\epsilon \equiv$ area of the region in phase space containing 95% of the particles $(1 - e^{-3} = .9502$, to be more precise), then $\epsilon = 6\pi\sigma^2/\beta$. Thus $\sigma^2 = \epsilon\beta/6\pi$, or the beam size varies with $(\epsilon\beta)^{1/2}$. As β is a parameter characteristic of the machine, the quantity ϵ, referred to as the transverse emittance, contains much of the notion of the quality of the beam in the synchrotron. To avoid an increase of the beam emittance during beam transfer between two synchrotrons, the horizontal and vertical amplitude functions β_x and β_y must be properly matched at the injection point.

A Gaussian particle distribution was used in the above discussion. Transverse particle distributions in electron synchrotrons are inherently Gaussian due to the interplay between synchrotron radiation excitation and damping. There is no reason to believe that the distributions should be Gaussian in a proton synchrotron where synchrotron radiation is insignificant, but from experience with these machines the normal distribution provides a reasonably accurate description of actual beams.[1]

The notion that the homogeneous Hill's Equation is obeyed in each degree of freedom separately throughout the beamline is based upon the assumption that linear coupling between the two

degrees of freedom and nonlinear magnetic fields may be ignored. Linear coupling may be introduced by dipole or quadrupole fields rotated about the longitudinal axis. The field of a dipole magnet used for steering of the beam through an angle θ_0 in the horizontal plane has components $B_x=0$, $B_y=B$. If the magnet is rotated about the longitudinal axis by an angle ϕ the field components relative to x and y become $B_x=B\sin\phi$, $B_y=B\cos\phi$. Thus a vertical deflection of the beam through an angle $\theta_0\sin\phi$ is introduced. A typical alignment error of a magnet may result in a rotation of .5 mrad. A typical dipole magnet in a beam line may bend the beam by as much as 50mrad. Thus, steering errors on the order of 25 μrad are easily introduced. These errors will be of significance during the operation of the beamline. Downstream of the steering error, the displacement of the beam is given by

$$\Delta x_{max} = \Delta\theta\sqrt{\beta_0\beta} \sim (25\mu\text{rad})(30\text{m}) \sim 1 \text{ mm} .$$

This is one reason why a beam position correction system must be included as part of the beamline design. However, the placement of correction elements may be left until after the general design of the beamline has been decided. During the first pass through the design, these effects may be ignored.

For a quadrupole magnet, the field components are of the form $B_x = B'y$, $B_y = B'x$, where B' is called the quadrupole gradient. If the magnet is rotated through an angle ϕ, the components in the original coordinate system become

$$B_x = B'(y \cos2\phi - x \sin2\phi) ,$$
$$B_y = B'(x \cos2\phi + y \sin2\phi) .$$

For x ≃ y, this implies a change in both the horizontal and vertical quadrupole strengths of roughly $\Delta B'/B' = 2\phi$. For the typical alignment error of .0005 rad used above, this amounts to a gradient error of 0.1%. This would produce a maximum amplitude function error downstream of the gradient error on the order of $\Delta\beta/\beta \sim (\Delta B'/B')(\beta\Delta q) = (.001)(30m/10m) = 0.3\%$. So, an error in the downstream beam size on the order of $\Delta\sigma/\sigma \sim (\Delta\beta/\beta)/2 = 0.15\%$ would be produced which would go easily unnoticed.

Magnetic elements used in the beamline are assumed to have fields which depend upon transverse position in at most a linear fashion, such as dipoles and quadrupoles. However, in real magnets higher order multipoles will exist due to the finite size of the magnets. In a circular accelerator these imperfections must be compensated to avoid resonant behavior near rational values of the betatron oscillation frequency. In a "single pass" beamline the imperfections may be ignored as long as they are indeed small, as will be assumed in this discussion.

To summarize, the problem of transporting a charged particle beam from the output of one synchrotron to the input of a second synchrotron has been reduced to a problem of matching the trajectory of the beam at the extraction and injection points as well as matching several independent parameters associated with the focusing properties of the second synchrotron in the two transverse degrees of freedom. To be more specific, the ideal trajectory must be matched, requiring 12 parameters (X,Y,Z, and slopes at each end of the line). The trajectories of off-momentum particles must be matched as well. This amounts to

matching the momentum dispersion functions $D_x(s)$, $D_y(s)$ and their slopes. Finally, the betatron amplitude functions β_x, β_y and their slopes given by α_x, α_y must be matched. This yields a total of 20 constraints which must be satisfied by the strengths and locations of magnetic elements in the beamline. Naturally the final product will depend upon other, less fundamental constraints as well such as physical space limitations, engineering limitations, and funding and deadlines.

Method of Solution

Now that the problem has been defined, the general rules for computing ideal trajectories, betatron amplitude functions, and dispersion functions will be described. First, the propagation of the ideal particle trajectory through beamline elements is considered. Cartesian coordinates X, Y, and Z will be used in this discussion, where the X-Y plane is taken to be the horizontal plane and Z is take to be the vertical direction. The beamline is assumed to be made up of dipole magnets and quadrupole magnets. The ideal trajectory is assumed to pass through the centers of the quadrupole magnets where the field is zero and hence the quadrupoles do not enter into the calculation of the trajectory at all.

The angle X' is defined to be the angle between the Y-axis and the projection of the trajectory onto the X-Y plane as shown in Figure III-1. The angle Z' is the vertical pitch of the trajectory. A vertical deflection by a bending magnet is defined as a deflection through an angle $\theta=L/\rho$ where the circle of radius

Figure III-1

Cartesian Coordinate System
for Ideal Trajectory
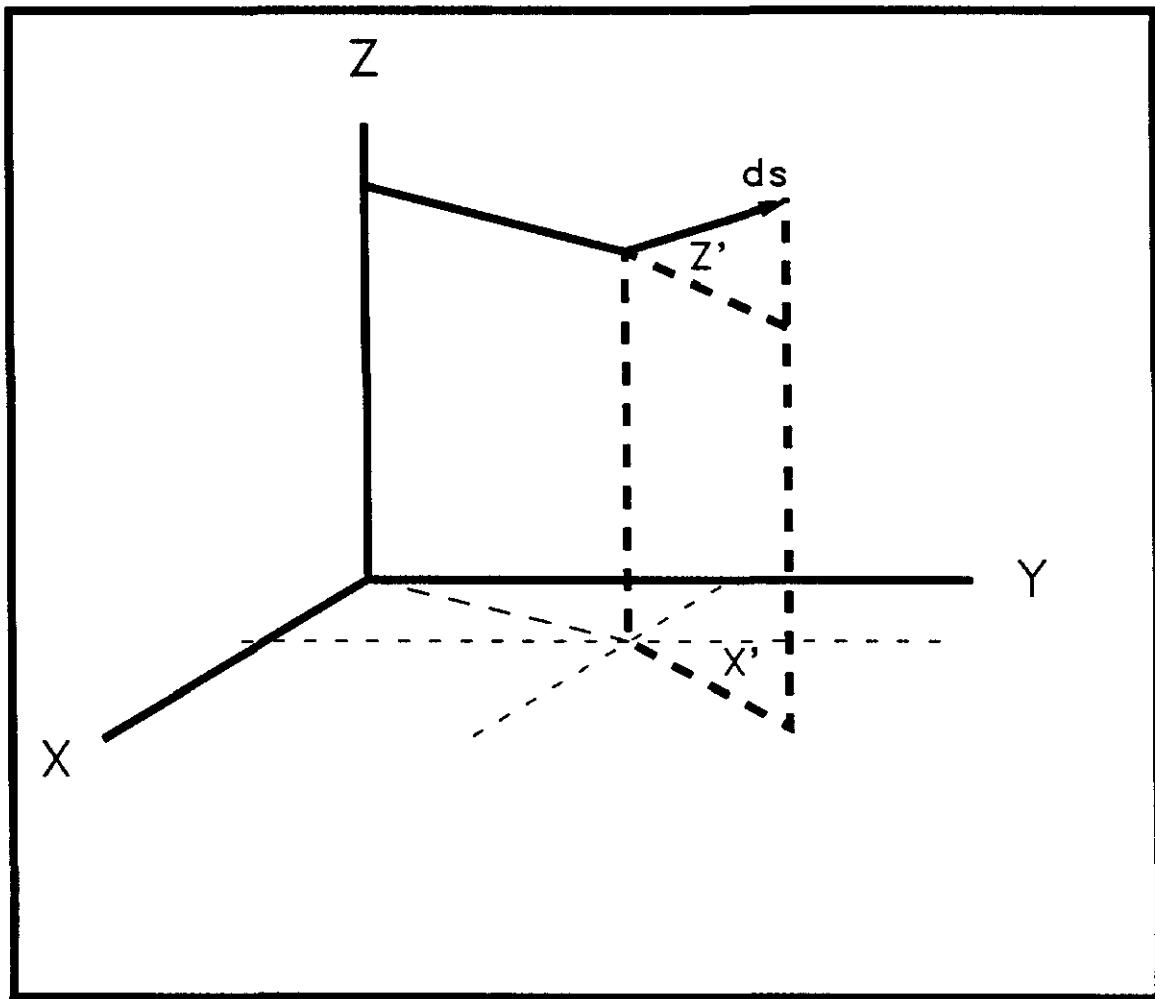
ρ lies entirely in a plane perpendicular to the X-Y plane. The path length through the magnet is L. A horizontal deflection by a bending magnet implies the circle of radius ρ lies entirely in a plane parallel to the X-Y plane. Now, the coordinates (X,Y,Z) of the ideal trajectory at the output of a horizontal bending element, a vertical bending element, or a drift region may be written in terms of the coordinates (X_0,Y_0,Z_0) of the trajectory at the input of the element, the radius of curvature ρ, and the angle of deflection θ. The results are presented below.

Horizontal Bending Element:

$$X = X_0 + \rho(\sin\theta\sin X' + (1-\cos\theta)\cos X')$$

$$Y = Y_0 + \rho(\sin\theta\cos X' - (1-\cos\theta)\sin X')\cos Z'$$

$$Z = Z_0 + \rho(\sin\theta\cos X' - (1-\cos\theta)\sin X')\sin Z'$$

$$X' = X'_0 + \theta$$

$$Z' = Z'_0$$

Vertical Bending Element:

$$X = X_0 + \rho(\sin\theta\cos Z' - (1-\cos\theta)\sin Z')\sin X'$$

$$Y = Y_0 + \rho(\sin\theta\cos Z' - (1-\cos\theta)\sin Z')\cos X'$$

$$Z = Z_0 + \rho(\sin\theta\sin Z' + (1-\cos\theta)\cos Z')$$

$$X' = X'_0$$

$$Z' = Z'_0 + \theta$$

Drift Region:

$$X = X_0 + L\sin X'\cos Z'$$

$$Y = Y_0 + L\cos X'\cos Z'$$

$$Z = Z_0 + L\sin Z'$$

$$X' = X'_0$$

$$Z' = Z'_0$$

From the above equations it appears that only five parameters are necessary to specify the trajectory. The sixth parameter is the angle of rotation of the transverse coordinate system about the trajectory. By requiring that the dipole elements bend only in a vertical plane or a horizontal plane the transverse coordinate system will never become rotated along the ideal trajectory. Though this requirement is not absolutely necessary, it does help keep the computation of the beamline geometry simple and easy to understand.

To study the transverse degrees of freedom a right-handed coordinate system (x,y,s) will be adopted. Here, s is the path length along the ideal trajectory, y is the transverse "vertical" displacement from the ideal trajectory, and x is the transverse "horizontal" displacement. The y-s plane is everywhere perpendicular to the X-Y plane from the above discussion. (This is the sixth constraint.) The x-s plane is everywhere perpendicular to the y-s plane. Hill's Equation may now be applied to either transverse plane to determine the motion of a particle in that degree of freedom.

The solution to Hill's Equation may be written in terms of the initial conditions $x_0 \equiv x(0)$, $x'_0 \equiv x'(0)$:

$$x(s) \;\; = a(s)x_0 + b(s)x'_0$$
$$x'(s) = c(s)x_0 + d(s)x'_0 \; ,$$

or in matrix form,

$$\underline{X}(s) \;=\; \begin{bmatrix} x \\ x' \end{bmatrix} \;=\; \begin{bmatrix} a & b \\ c & d \end{bmatrix} \begin{bmatrix} x_0 \\ x'_0 \end{bmatrix} \;=\; M(s/s_0)\underline{X}_0 \; .$$

A piecewise method of solution may be employed to determine the motion of a particle throughout an accelerator or beamline when a set of initial conditions are known. For example, the matrix corresponding to a particle traveling through a region of length L in which K=0 would be

$$M_B = \begin{pmatrix} 1 & L \\ 0 & 1 \end{pmatrix} \quad .$$

For a region in which K>0,

$$M_F = \begin{pmatrix} \cos(K^{1/2}L) & K^{-1/2}\sin(K^{1/2}L) \\ -K^{1/2}\sin(K^{1/2}L) & \cos(K^{1/2}L) \end{pmatrix}$$

and for K<0,

$$M_D = \begin{pmatrix} \cosh(|K|^{1/2}L) & |K|^{-1/2}\sinh(|K|^{1/2}L) \\ |K|^{1/2}\sinh(|K|^{1/2}L) & \cosh(|K|^{1/2}L) \end{pmatrix} \quad .$$

The matrix describing the motion of a particle after traversing a series of magnetic elements is simply the product of the corresponding matrices of the individual elements. Because Hill's Equation contains no first derivatives (i.e., the system is nondissipative) the matrices $M(s/s_0)$ are unimodular.

The matrix corresponding to the motion between points s and s_0 in the beamline or accelerator may be expressed in terms of the amplitude function β (and its slope) evaluated at the two points. If the general solution

$$x = A\beta^{1/2}\sin(\psi(s) + \delta)$$

is rewritten as

$$x = \beta^{1/2}(A\cos\psi + B\sin\psi)$$

then by differentiating and evaluating x and x' at s_0 to find A and B in terms of x_0, x'_0, β_0, and α_0 (and defining $\psi_0 = 0$) the matrix $M(s/s_0)$ is found to be

$$
\begin{bmatrix}
\left[\dfrac{\beta}{\beta_0}\right]^{1/2}(\cos\psi + \alpha\sin\psi) & (\beta\beta_0)^{1/2}\sin\psi \\[3ex]
-\dfrac{1+\alpha\alpha_0}{(\beta\beta_0)^{1/2}}\sin\psi + \dfrac{(\alpha_0-\alpha)}{(\beta\beta_0)^{1/2}}\cos\psi & \left[\dfrac{\beta_0}{\beta}\right]^{1/2}(\cos\psi - \alpha_0\sin\psi)
\end{bmatrix} .
$$

As previously, $\alpha = -(d\beta/ds)/2$ and $\psi = \displaystyle\int_{s_0}^{s}\frac{ds}{\beta(s)}$.

When M corresponds to a complete revolution about a cyclic accelerator, $\beta(s) = \beta(s_0)$, $\alpha(s) = \alpha(s_0)$, and

$$
\psi = \int_{s_0}^{s_0+C}\frac{ds}{\beta(s)} \equiv 2\pi\nu .
$$

Here, C is the circumference of the machine and ν, the number of oscillations undergone during a complete revolution, is referred to as the "betatron frequency" or the "tune." The resulting matrix for a complete revolution is thus

$$
M(s+C/s) = \begin{bmatrix}
\cos 2\pi\nu + \alpha(s)\sin 2\pi\nu & \beta(s)\sin 2\pi\nu \\[2ex]
-\gamma(s)\sin 2\pi\nu & \cos 2\pi\nu - \alpha(s)\sin 2\pi\nu
\end{bmatrix}
$$

where $\gamma(s) \equiv (1 + \alpha^2)/\beta$. In compact form, the matrix for one revolution may be written as

$$
M(s+C/s) = I\cos 2\pi\nu + J\sin 2\pi\nu
$$

where I is the identity matrix and

$$
J \equiv \begin{bmatrix}
\alpha & \beta \\
-\gamma & -\alpha
\end{bmatrix} .
$$

The quantities α, β, and γ are known as the Courant-Snyder parameters.[2] By computing the single-turn matrix for a particular location s using the piecewise method and equating the result with the form of the matrix $M(s+C/s)$ above, values of the Courant-Snyder parameters may be tabulated. The trace of the single-turn matrix, $Tr[M(s+C/s)] = 2\cos 2\pi\nu$ provides a criterion for stable oscillations about the synchrotron:

$$|Tr[M]| \leq 2.$$

Values of the Courant-Snyder parameters at location s may be computed given the values of the parameters at location s_0 and the matrix $M(s/s_0)$. By noting that

$$M(s+C/s) = I\cos 2\pi\nu + J(s)\sin 2\pi\nu,$$

$$M(s_0+C/s_0) = I\cos 2\pi\nu + J(s_0)\sin 2\pi\nu,$$

and

$$M(s_0+C/s_0) = M^{-1}(s/s_0)M(s+C/s)M(s/s_0),$$

then

$$J(s_0) = M^{-1}(s/s_0) J(s) M(s/s_0),$$

or

$$J(s) = M(s/s_0) J(s_0) M^{-1}(s/s_0).$$

The points s_0 and s may correspond to two different points within a particular cyclic accelerator. They may also correspond to the extraction point of an accelerator and a point in the beamline which transports the extracted beam. Since the amplitude functions of the beamline must match those of the injection point of the second accelerator, the matrix M for the entire beamline must satisfy the equation

$$J(\text{inj. pt.}) = M\, J(\text{extr. pt.})M^{-1}.$$

This condition must be met for both transverse degrees of freedom.

As mentioned in Chapter II, particles of momentum $p+\Delta p$, where p is the design momentum, will follow closed trajectories about a synchrotron given by $x(s) = D(s)(\Delta p/p)$. The motion of an off-momentum particle about the design trajectory may be written as

$$x(s) = a(s)x_o + b(s)x'_o + e(s)\Delta p/p ,$$
$$x'(s) = c(s)x_o + d(s)x'_o + f(s)\Delta p/p .$$

The coefficients a, b, c, and d are the same coefficients of the corresponding 2x2 matrices described above. As an example, at the exit point of a rectangular bending magnet of length L and bend angle $\theta = L/\rho$ (ρ = radius of curvature) the trajectory would be

$$x(L) = x_o + Lx'_o + (L\theta)\Delta p/p$$
$$x'(L) = x'_o - \theta \Delta p/p.$$

Each of the quantities a, b, e, c, d, and f may be thought of as a coefficient in a Taylor Series expansion in $\Delta p/p$ about zero. As long as terms of order $(\Delta p/p)^2$ or higher may be neglected, as is certainly the case for the Booster and Main Ring synchrotrons, this representation is quite valid.

The piecewise method may once again be applied by writing

$$\begin{bmatrix} x \\ x' \\ \Delta p/p \end{bmatrix} = \begin{bmatrix} a & b & e \\ c & d & f \\ 0 & 0 & 1 \end{bmatrix} \begin{bmatrix} x_o \\ x'_o \\ \Delta p/p \end{bmatrix} .$$

If $M_{3\times3}$ is the matrix for one complete revolution, then by definition, the closed orbit of an off-momentum particle must satisfy

$$\begin{bmatrix} x_{co} \\ x'_{co} \\ \Delta p/p \end{bmatrix} = \begin{bmatrix} a & b & e \\ c & d & f \\ 0 & 0 & 1 \end{bmatrix} \begin{bmatrix} x_{co} \\ x'_{co} \\ \Delta p/p \end{bmatrix}$$

or, from the definition of the dispersion function, $D \equiv x_{co}/(\Delta p/p)$,

$$\underline{D} = \begin{pmatrix} D(s) \\ D'(s) \\ 1 \end{pmatrix} = \begin{pmatrix} a(s+C/s) & b(s+C/s) & e(s+C/s) \\ c(s+C/s) & d(s+C/s) & f(s+C/s) \\ 0 & 0 & 1 \end{pmatrix} \begin{pmatrix} D(s) \\ D'(s) \\ 1 \end{pmatrix} = M_{3x3}\underline{D} .$$

Solving for D and D',

$$D(s) = \frac{e + (bf-de)}{2 - (a+d)} ,$$

$$D'(s) = \frac{f + (ce-af)}{2 - (a+d)} .$$

Since $\underline{D}$ represents a trajectory, the dispersion function at a point s "downstream" of a point s_0 is found by

$$\underline{D}(s) = M_{3x3}(s/s_0) \ \underline{D}(s_0) .$$

For the beamline joining two synchrotrons, the 3x3 matrix for each transverse degree of freedom must satisfy

$$\underline{D}(inj. \ pt.) = M_{3x3}(beamline) \ \underline{D}(extr. \ pt.)$$

in order to provide a proper match of the off—momentum orbits.

Using the above methods for computing the ideal trajectory, the betatron amplitude functions, and the trajectories of off-momentum particles about the ideal trajectory, a beamline system which transports a particle beam from one synchrotron to another may be designed which adheres to the 20 constraints mentioned earlier in this chapter. As a review, the constraints are

1)-12)   X,Y,Z, and respective slopes must be matched at the extraction and injection points

13)-16)   The horizontal and vertical 2x2 transport matrices must satisfy:

$$J_x(i) = M_x(i/e) J_x(e) M_x^{-1}(i/e)$$

$$J_y(i) = M_y(i/e) J_y(e) M_y^{-1}(i/e)$$

where e = extraction point of first synchrotron

i = injection point of second synchrotron

(J matrices contain β's and α's)

17)-20)   The horizontal and vertical 3x3 transport matrices must satisfy:

$$\underline{D}_x(i) = M_x(i/e)\ \underline{D}_x(e)$$

$$\underline{D}_y(i) = M_y(i/e)\ \underline{D}_y(e)$$

($\underline{D}$ contains D and D')

Several computer codes are available to accelerator designers which perform the calculations mentioned above. Some examples of codes commonly used are TRANSPORT,[3] SYNCH,[4] and MAD.[5] Most of the design codes (including the three mentioned above) provide routines which vary parameters of beamline elements to produce a least squares fit of lattice functions to desired values.

References

1. For a nice discussion on this subject, the reader is referred
    to H. G. Hereward, "How Good is the R.M.S. as a Measure of
    Beam Size?", European Organization For Nuclear Research
    Report CERN/MPS/DC 69-15 (1969).

2. Courant, E. D., and H. S. Snyder. "Theory of the Alternating
    Gradient Synchrotron," Annals of Physics, Vol. 3, No. 1
    (January, 1958), p. 5.

3. K. L. Brown, F. Rothacker, D. C. Carey, F. C. Iselin;
    TRANSPORT -- A Computer Program For Designing Charged
    Particle Beam Transport Systems; May, 1977; Stanford Linear
    Accelerator Report SLAC-91, Rev.2.

4. A. A. Garren, A. S. Kenney, E. D. Courant, M. J. Syphers; A
    User's Guide To SYNCH; June, 1985; Fermi National Accelerator
    Laboratory Report FN-420.

5. F. C. Iselin, E. Keil, E. Nordmark; The MAD Program
    (Methodical Accelerator Design) User's Reference Manual;
    August 15, 1986; Draft for a future European Organization For
    Nuclear Research Report.

IV.   The New 8 GeV Line

General Description

During a nine month period from October, 1985 to July, 1986 the Booster, Main Ring, and Tevatron accelerators were shut down to allow for the construction of the Main Ring overpass at the Collider Detector Facility and the detector building at the D0 straight section. By the end of that period, 12 months after the redesign had been initiated, a new 8 GeV beam transport system between the Booster and Main Ring accelerators had been developed, constructed, installed and was ready for commissioning. The author was in charge of all aspects of the project. A layout of the final design is shown in Figure IV-1. No changes were made to the Booster extraction system, which was described in Chapter II. Rather than having a 1.6 mrad downward slope throughout most of the beamline, the ideal trajectory leaving the second pulsed septum magnet of the Booster extraction system remains parallel to the floor. The first horizontal bend point in the beamline (HB1) remained in its original position. (Beam may be steered toward an already existing beam dump by switching on a set of vertical bending magnets placed immediately upstream of HB1.) Two vertical bending magnets (VB1 and VB2 in Figure IV-1) midway through the beamline direct the trajectory down to roughly the Main Ring level and the beam is then injected horizontally. A 5.5 m thick cement wall was installed in the line to allow access to either the Booster accelerator enclosure or the Main Ring accelerator enclosure during the operation of the other machine.

Figure IV-1

New 8 GeV Beamline Layout
(Horizontal Plane)
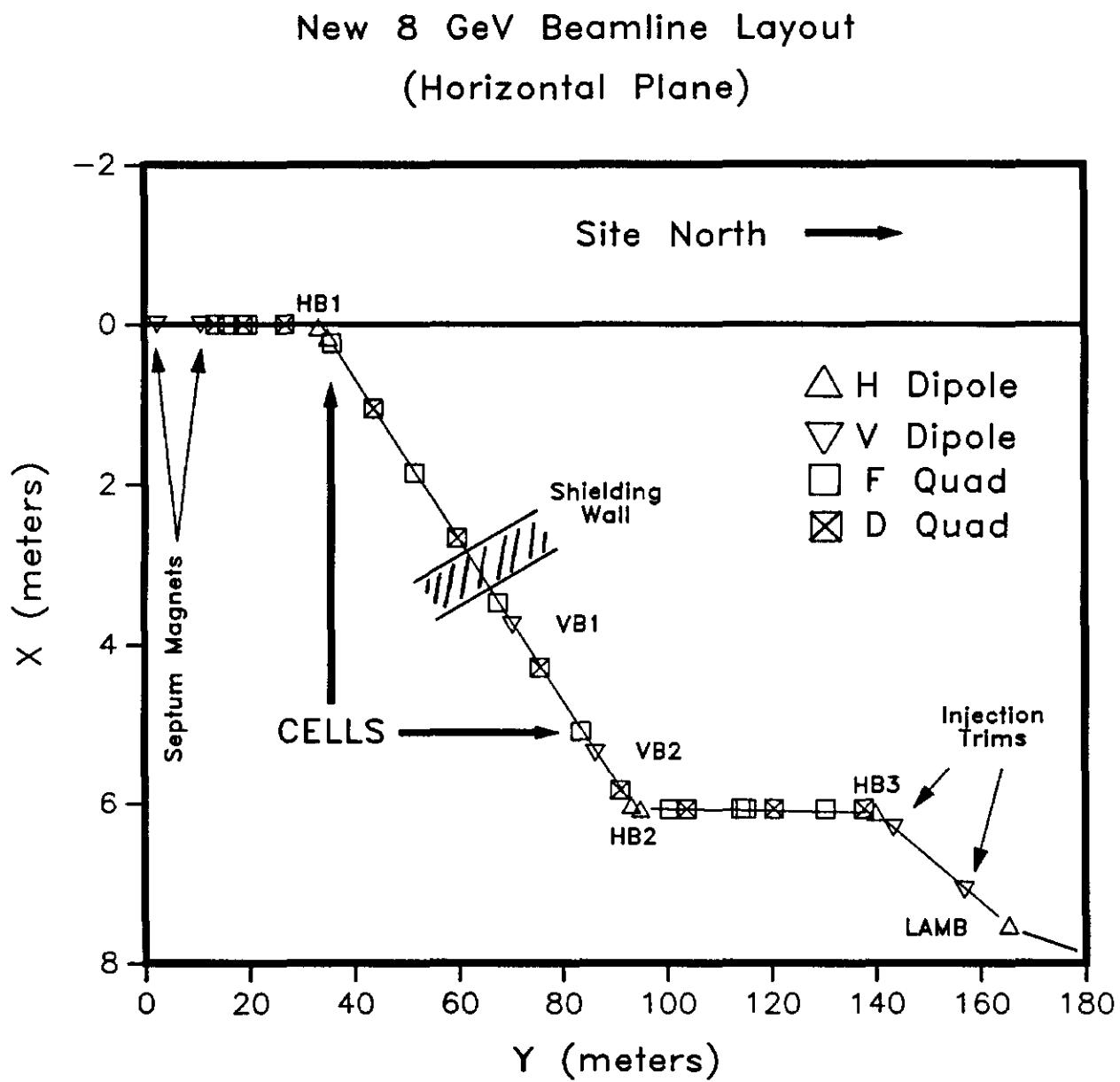
The new focusing system contains 19 quadrupole lenses which alternate in gradient throughout the line. The beamline may be divided into three sections. The middle section, referred to as the "Cells," contains 5 quadrupoles of equal but alternating strengths and spaced equally apart. The betatron phase advance between each of these elements is 45° for both the horizontal and the vertical degrees of freedom. In front of the Cells, the Booster Match section consists of 6 quadrupoles which are used to match the amplitude and dispersion functions of the Booster to those of the Cells. After the Cells, the Main Ring Match section has 8 quadrupoles which match the amplitude and dispersion functions of the Cells to the Main Ring injection point.

Amplitude Functions

Figure IV-2 displays the resulting amplitude functions for both the horizontal and vertical planes. The dramatic reduction in the values of β throughout the line is immediately evident. (c.f. Figure II-6.) Within the Cells, the value of β is the same every other quadrupole. This is typical of the periodic cell structure found in synchrotrons. The value of β_{max} in the cells is roughly 30 meters. The largest value of β in the entire line is 150 m and occurs just prior to the injection point. (The value of β_{max} within the cells of the Main Ring synchrotron is 100 m.) As expected, the sensitivity of the Main Ring match to quadrupole errors is reduced by the smaller values of β. Figure IV-3 shows the dilution of the transverse emittance which would be created by a quadrupole error of the same magnitude used in Figure II-7.

Figure IV-2

Design Amplitude Functions
of New 8 GeV Beamline

Figure IV-3

Transverse Emittance Dilution
Due to Gradient Error of ΔB'/B' = 4%
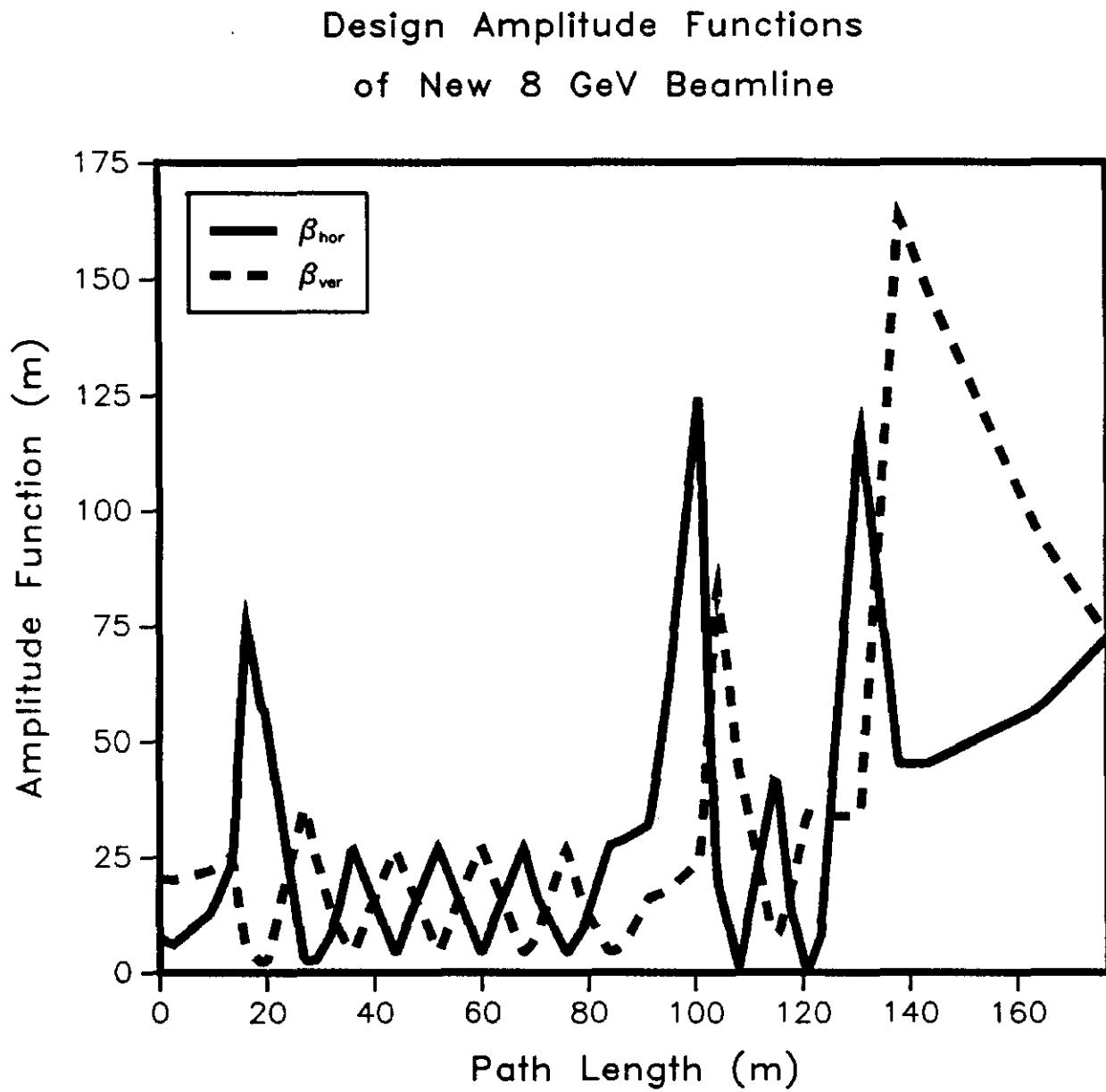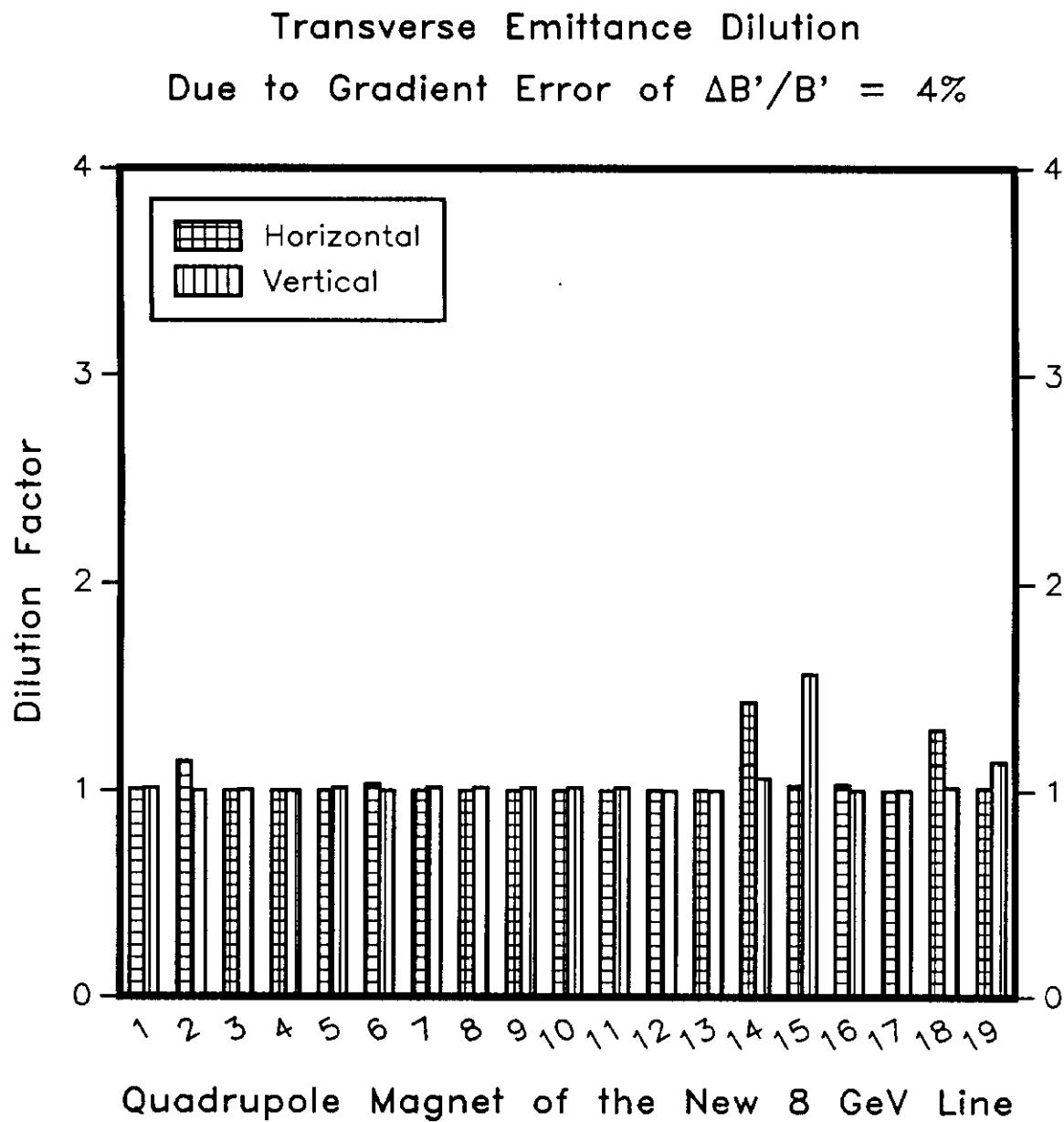
Due to the requirements imposed upon them, the "matching" quadrupoles have a variety of strengths. By having independent control over each of these magnets, the matching of the amplitude functions may be adjusted. Combinations of quadrupole gradients have been developed which permit the adjustment of the values of a particular lattice function (β_y at the injection point, for example) without disturbing the other lattice functions. An example of one such combination is shown in Figure IV-4.

Dispersion Functions

Of the twenty constraints discussed in Chapter II, the matching of the vertical dispersion function at the end of the beamline presented the most problems. Since all the elements of the Booster synchrotron lie in the horizontal plane, the design vertical dispersion function is zero throughout the accelerator. A bending element which steers the trajectory of an ideal particle of momentum p through an angle θ will steer a particle of momentum p+Δp through an angle θ+$\Delta\theta$ where $\Delta\theta = -\theta(\Delta p/p)$. Hence, the slope of the dispersion function will change by an amount $-\theta$ when passing through a bending element. Thus, to create a value of D_y = d meters in a beamline the beam trajectory needs to be displaced by -d meters. A value of D_y = -.4 meters at the beginning of the 8 GeV Line is generated by the vertical extraction process. The value of the vertical dispersion function (caused by the overpasses) of the Main Ring lattice at the injection point is -1.4 meters. Hence, the new beamline needed to produce ΔD_y = -1 m.

Figure IV-4

Amplitude Function vs. Quadrupole Gradients
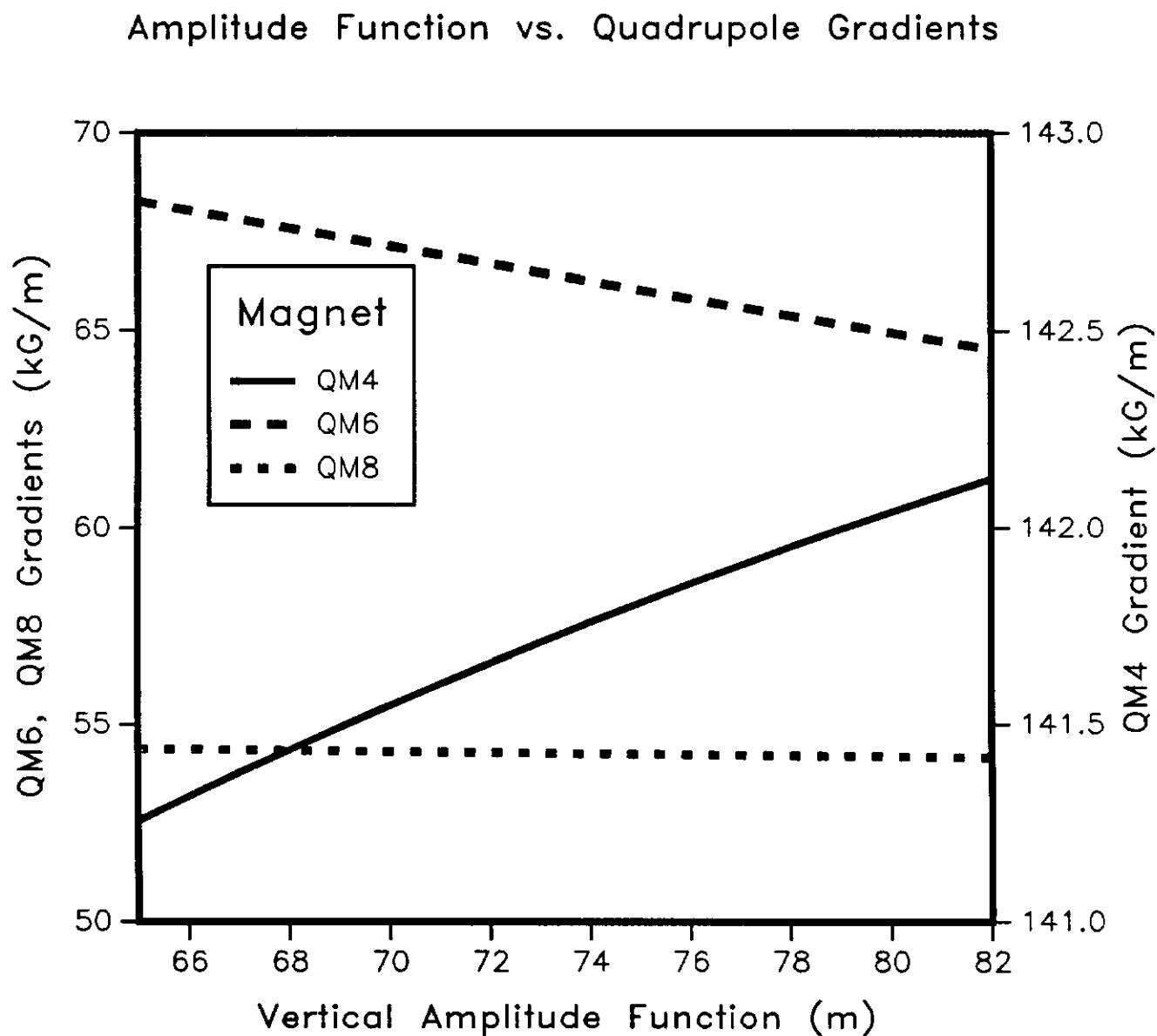
This was achieved by switching the injection process into the Main Ring from the vertical plane to the horizontal plane. If the beam trajectory is not lowered until just before the injection point, then the vertical bending elements would produce $\Delta D \sim +.5$ meter. Thus, the dispersion function just prior to these vertical bends would need to be -2 meters and some type of "dispersion creation" section would need to be added somewhere in the beginning of the line. By switching to horizontal injection, the beam trajectory could be lowered .5 meters to roughly the Main Ring level at any upstream point in the beamline. In particular, if the beam is lowered at a point 180° in betatron phase upstream of the injection point, then the positive dispersion produced by this action will translate to a negative dispersion at the end of the line. Also, since the values of the amplitude functions through the line and at the injection point are roughly 20 meters and 70 meters respectively, then the resulting value of the dispersion function will be amplified by a factor of $(70/20)^{1/2} \sim 2$. With this scenario adopted, the program SYNCH was used to determine the final positions for the vertically bending magnets and the Main Ring Match quadrupole magnets as well as the strengths for the Main Ring Match quadrupoles which would simultaneously fit all the amplitude functions and dispersion functions to their desired values at the injection point. The resulting dispersion functions are shown in Figure IV-5.

The horizontal dispersion function through the Cells was made to alternate from large to small values intentionally to

Figure IV-5

Design Dispersion Functions
of New 8 GeV Beamline
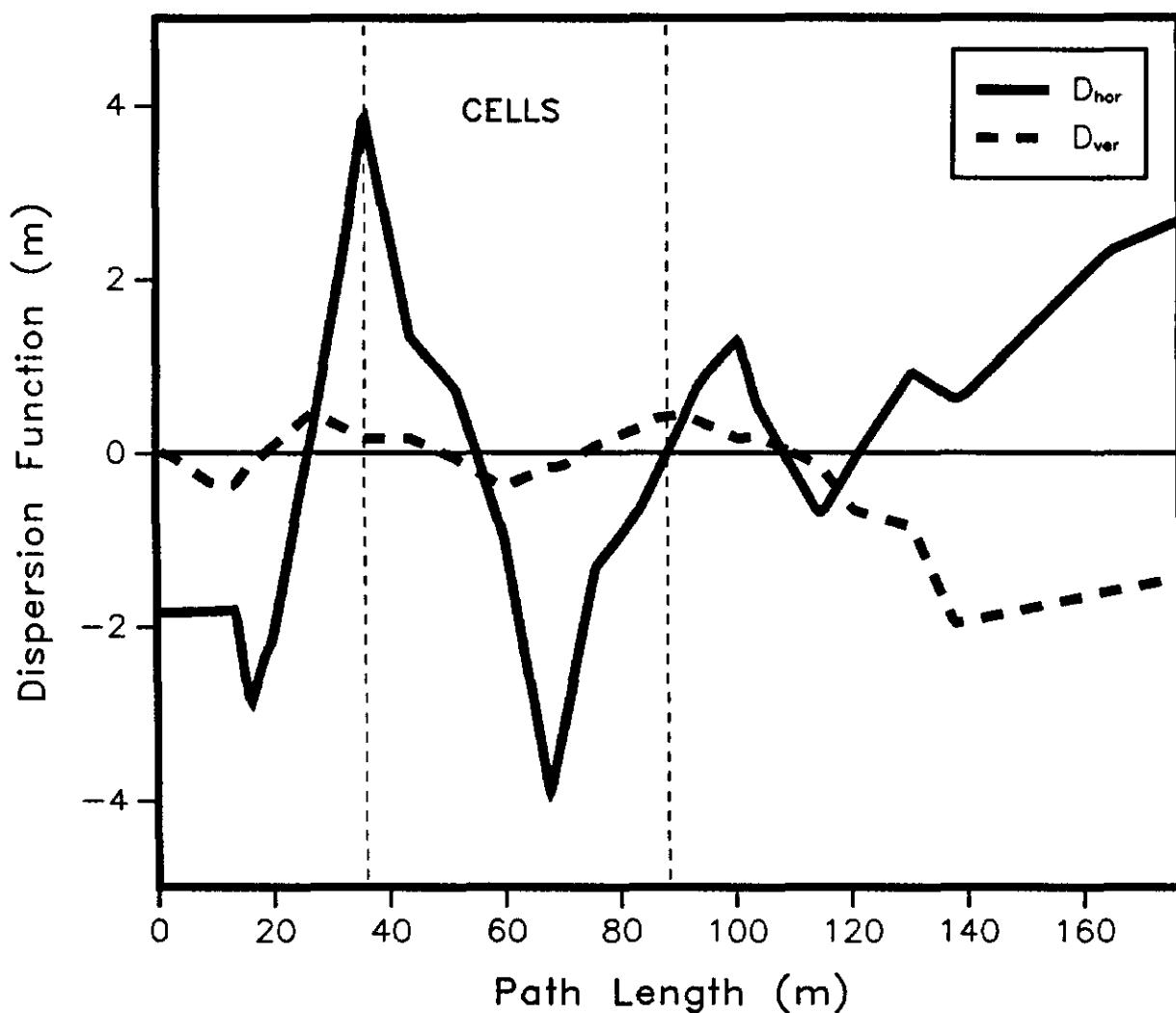
provide a method for performing useful beam measurements. The value of the horizontal dispersion function at the extraction point of the Booster is 1.8 meters. As shown in Figure I-1 the Booster ring is located outside the circumference of the Main Ring. If the x axis for the horizontal degree of freedom of the 8 GeV beamline is defined such that positive x denotes an increased radial position at the Main Ring injection point, then the value used for the horizontal dispersion function at the extraction point of the Booster must be -1.8 meters. The Booster Match quadrupoles plus the first bend center HB1 then modify D_x so that at the entrance to the Cells, D_x = 4 meters and D'_x = 0 in the middle of the sixth quadrupole. Because the phase advance between each quadrupole is 45° throughout the Cells, D_x will oscillate between 4 meters and 0 meters every other magnet while the amplitude function remains at the same value of β_{max} = 27m at every other magnet as seen in Figure IV-2 and Figure IV-5. By obtaining measurements of horizontal beam profiles at alternating β_{max} locations through the Cells, the horizontal transverse emittance may be determined as well as the momentum spread of the extracted Booster beam.

As shown in Chapter III, the variance of a Gaussian shaped beam of particles is related to the transverse emittance by

$$\epsilon = \frac{6\pi\sigma^2}{\beta} .$$

If the distribution of momentum associated with the beam is also assumed to be Gaussian with variance $\langle (\Delta p/p)^2 \rangle \equiv \sigma_p^2$, then the total distribution of particles at location s, assuming no

correlation between the momentum distribution and the beam emittance, is given by

$$\sigma^2(s) = \frac{\epsilon\beta(s)}{6\pi} + D^2(s)\,\sigma_p^2 \ .$$

By measuring σ at two locations where β and D are known, values for ϵ and σ_p may be computed. Figure IV-6 displays curves of constant ϵ and constant σ_p for values of σ measured at the two ideal locations described above. Rather than suppressing D as was done with the old beamline, making D large through the Cells creates an opportunity to perform more precise measurements of σ_p in a very straightforward manner.

Magnets and Power Supply System

As was shown in Figure IV-1, the new 8 GeV Line contains four primary horizontal bend centers and two primary vertical bend centers. A Lambertson-style magnet, which has a strong field region and a "field-free" region separated by a thin septum, is used for the final horizontal bend and is described in more detail later in this chapter. The magnetic elements used for the other five bend centers are ones used in the old beamline. Bend centers HB1 and HB2 contain two magnets each, while bend centers VB1 and VB2 have one magnet each. Each dipole magnet is 60 in. in length, has an aperture of 5 in. x 1.4 in. and has coils consisting of 40 turns of water cooled copper. The bend angle θ produced by a pure dipole field magnet is given by

$$\theta = L/\rho = BL/(B\rho) = \mu_0 NIL/h(B\rho)$$

Figure IV-6

8 GeV Line Emittance Measurements

	β	D
Monitor 1:	24.5 m	3.7 m
Monitor 3:	24.5 m	0.5 m
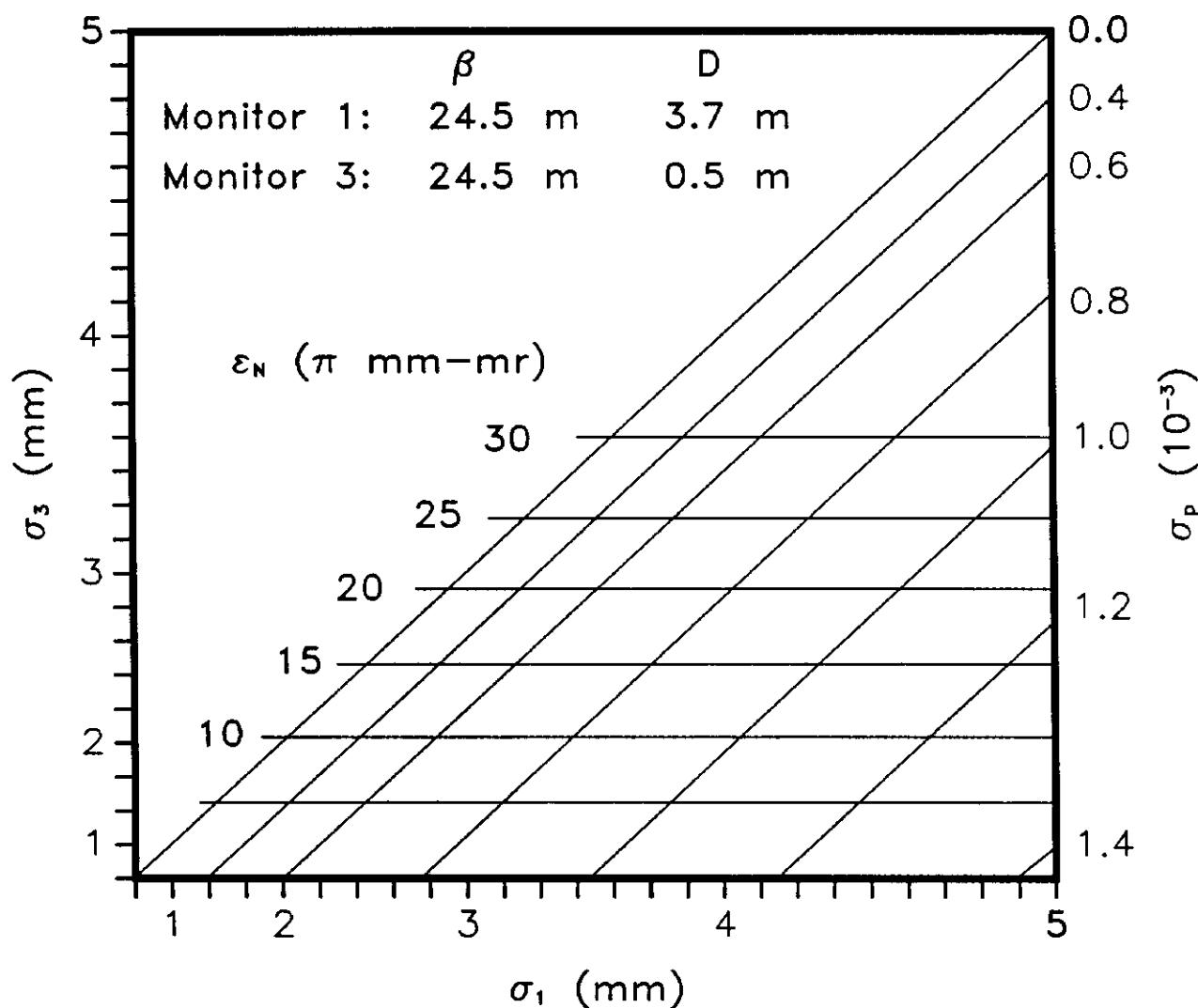
where μ_0 = permittivity of free space, I = current, N = number of turns, L = length of the magnet, h = gap height (1.4 in. for the magnets above), and Bρ = magnetic rigidity = (10/3)P$_{GeV/c}$ Tesla·m = 29.63 Tesla·m for 8 GeV kinetic energy protons.

For the focusing elements of the new line, small aperture quadrupole magnets originally designed for use in the Tevatron I project antiproton storage rings were chosen.[1] These magnets are 18 in. long, have a 3.5 in. pole tip diameter, and have 132 turn coils of water cooled copper. The focal length f of a quadrupole lens is found using

$$q \equiv 1/f = B'L/(B\rho) = 2\mu_0 NIL/D^2(B\rho)$$

where D is the pole tip diameter. The 19 quadrupole lenses required for the beamline vary in strength from q = 0.05/m to a maximum of q = 0.33/m. At about q = 0.25/m (B' = 16 T/m) the small aperture quadrupoles begin to show signs of saturation. Only one element, the fifth Main Ring Match lens, needed a strength q $\gtrsim$ 0.25/m and so two magnets powered in series are used for this lens. Immediately after their construction, each of the new quadrupoles were subjected to detailed magnetic measurements of field vs. current, field harmonics, and hysteresis effects.

In addition to the primary bending and focusing elements, seven position correction bending magnets also are provided. Five of these magnets had been used in the old beamline and have the principal parameters L = 30 in., h = 4 in., and N = 120. The two additional correction dipoles again come from a Tevatron I project design.[2] These magnets, like those used in the antiproton debuncher ring, have L = 25 in., h = 5.6 in., and

N = 400. As correction devices, these magnets are used to counteract undesired steering produced by magnet misalignments and field imperfections as well as to allow fine adjustments to the injection trajectory leading into the Main Ring synchrotron. The maximum deflections expected to be produced by these magnets are less than three percent of those of the major bending elements.

Current for all elements mentioned above is produced via standard commercially available power supplies which are distributed among five already existing power supply galleries. These galleries are located above ground roughly 100 ft from the beamline. All devices are operated DC. The five quadrupole magnets in the Cells are powered by a single supply. Since the bend centers HB1 and HB2 steer the trajectory through equal and opposite angles, the magnets at these bend centers are powered by a single bulk supply as well. The same holds true for bend centers VB1 and VB2. To provide position correction capabilities at each of these bend centers, a trim power supply has been added to each one. The remaining magnetic elements within the beamline are independently powered. Table IV-1 lists each element of the beamline, its strength, and its required current and voltage.

Injection System

The solution to the vertical dispersion function match necessitated lowering the beam trajectory to roughly the Main Ring level 300 ft upstream of the injection point. The beam then had to be steered horizontally onto the the Main Ring horizontal closed orbit. From past experience of using a pulsed septum

Table IV-1

8 GeV LINE MAGNETIC ELEMENTS

Element	B(T)	B'(T/m)	I(Amps)	V(Volts-Supply)
VT1	.151		7.5	10
HT1	.0585		25	10
QB1		-16.0000	408.055	13
QB2		15.0617	378.409	12
QB3		-2.9243	65.222	3
QB4		6.9093	160.213	5
QB5		-13.0297	319.555	10
HB1a	.998		755	145
HB1b	.998		755	145
QB6		13.6697	336.603	11
VT2	.0684		20	15
QD		-11.7091	286.056	45(a)
QF		11.7091	286.056	45(a)
QD		-11.7091	286.056	45(a)
HT2	.0585		25	10
QF		11.7091	286.056	45(a)
VB1	.783		592	72
QD		-11.7091	286.056	45(a)
QM1		5.4217	131.6	4
VB2	.783		592	72(b)
QM2		-5.6899	148.2	4(b)
HB2a	.998		755	145(c)
HB2b	.998		755	145(c)
QM3		15.5471	396.9	12
QM4		-14.1227	348.2	11
VT3	.0684		20	15
QM5a		11.0694	267.3	18(d)
QM5b		11.0694	267.3	18(d)
QM6		-6.8355	175.2	5
QM7		10.1631	248.1	8
QM8		-5.3977	129.3	4
HB3	1.1105		840	40
VT3	.0795		25	15
VT4	.0585		25	10
LAMB	.4545		930	45
In Main Ring :				
VBMP1	.16		260	26(e)
VBMP2	.16		260	26(e)
VBMP3	.16		260	26(e)
VBMP4	.16		260	26(e)

a -- QD's and QF's are powered in series.
b -- VB1 and VB2 are powered in series.
c -- HB1a, HB1b, HB2a, and HB2b are powered in series.
d -- QM5a and QM5b are powered in series.
e -- VBMP1, VBMP2, VBMP3, VBMP4 are powered in series.

magnet to deliver the final major bend angle, as described in Chapter II, a Lambertson-style magnet was chosen which could operate DC. The Lambertson magnet (See Figure IV-7.) provides a field region of .46 Tesla to produce the 35 mrad final horizontal bend. The ideal trajectory leaving the Lambertson then has the proper horizontal position and slope yet is positioned 30 mm above the Main Ring closed orbit (which passes through the "field-free" region of the magnet). Using the last two vertical position correction magnets immediately upstream of the Lambertson, this displacement of 30 mm may be maintained while a downward slope of 0.7 mrad is produced. The beam will then arrive with zero vertical displacement at the same pulsed kicker magnets which were present in the old injection system. These pulsed magnets complete the injection process by cancelling the downward slope, placing the beam onto the proper vertical closed orbit.

Also included in the injection system are four dipole magnets which reside in the Main Ring long straight section, two on either side of the Lambertson magnet. (See Figure IV-7.) These four magnets, powered in series, provide a local vertical displacement of the Main Ring closed orbit of 30 mm. Without the orbit bump the incoming beam would be 60 mm above the Main Ring closed orbit and the kicker magnets would have to deliver twice their present amount of kick, beyond their capabilities. The original magnet choice for the orbit bump created severe problems during the commissioning phase of the project. These difficulties are discussed in Chapter VI. The final magnets

Figure IV-7

New Main Ring Injection Region Layout
(Horizontal Plane)
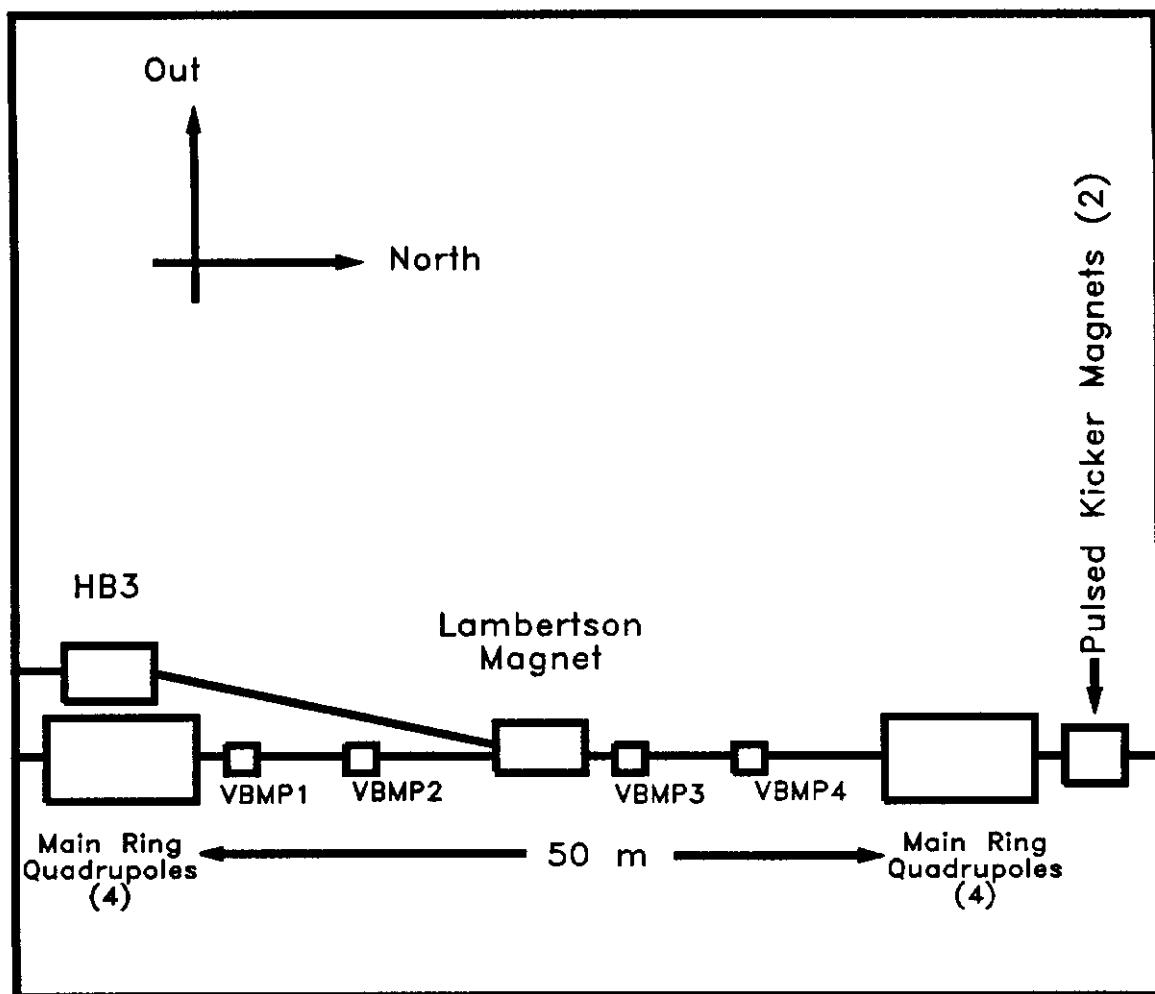
chosen for the orbit bump are those which had been used in the Fermilab Electron Cooling project.[3]   These magnets have 40 turns, apertures of 3 in. x 12 in., and lengths of 48 in.

The four bump magnets also allow for the fine adjustment of the 8 GeV vertical closed orbit through the field-free region of the Lambertson.   The magnets are run DC and as the energy of the beam increases, the effectiveness of the bump magnets decreases. Thus, the beam moves away from the "notch" of the magnet's field-free region (See Figure IV-8.) automatically as the beam is accelerated.

The Lambertson magnet (L = 90 in., h = 1.85 in., N = 18) has a large 4 in. x 4 in. asymmetric field-free region as shown in Figure IV-8.   The Main Ring injection region is located directly above the Tevatron fixed target extraction region.   During colliding beams operation, 150 GeV test beams could conceivably be extracted from the Main Ring and sent to the fixed target experiments.   The asymmetric region allows room for the possible trajectory of Main Ring extracted beam in case this process is called for in the future.   The actual field in the the "field-free" region is on the order of 5 Gauss or less and produces a measurable, but easily correctable, distortion of the Main Ring orbit at 8 GeV.   Detailed magnetic field calculations and magnetic measurements were performed on this magnet, the results of which are presented in the Appendix.

Diagnostics

Several improvements were made to the diagnostics system for the 8 GeV Line.   New electronics were added to the beam profile

Figure IV-8

Injection Lambertson Magnet Cross Section
(Looking "Upstream")
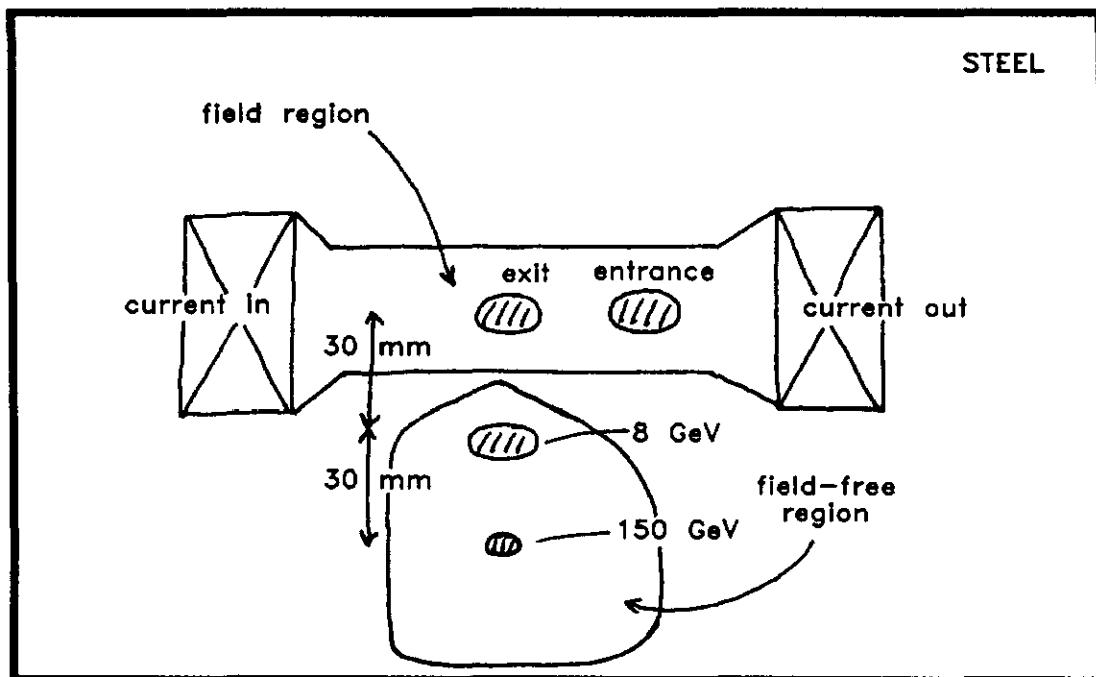
monitoring equipment to allow the data to be quickly processed and easily accessed by the accelerator controls system. New beam position and beam loss monitors were also added to the beamline. The separate systems are described below.

Beam Profile Monitor System

The purpose of the beam profile monitors is to allow for the investigation of problems during the commissioning of the beamline, to provide a method for measuring the transverse emittances and momentum spread of the beam arriving from the Booster synchrotron, and to provide a method for determining the degree of mismatch[*] of the amplitude functions at the injection point of the Main Ring synchrotron. Six profile monitors are located directly in front of each of the quadrupole magnets within the Cells for emittance measurements. Eight monitors are located within the Main Ring lattice to be used for matching measurements. Another five monitors are located in the Booster Match section (3) and the Main Ring Match section (2) for the diagnosis of problems. A last monitor was placed in the beamline leading to the Booster beam dump.

Each of the 20 profile monitors[4] consists of two planes (horizontal and vertical) of 24 wires which may be inserted into the beam path one plane at a time. The wires of the monitors within the beamline are one millimeter apart, the 95% beam width being roughly 10 mm within the Cells. For the monitors located within the Main Ring, where the 95% beam width is 20 mm, the wire spacing is that of the original profile monitor system, 3 mm in the horizontal plane and 1.5 mm in the vertical plane.

All wire planes are made of .05 mm diameter nickel strands which, when spaced 1 mm apart, yield a 5% coverage of the entire wire plane. The rms scattering angle projected to one plane due to multiple coulomb scattering is given by

$$\theta_{rms} = \frac{15 \text{ mrad}}{(p\beta)_{GeV/c}} \sqrt{\frac{\text{thickness}}{\text{radiation length}}}$$

whereas the rms beam angle is

$$\theta_{beam} = \sqrt{\frac{\epsilon}{6\pi\beta}} \quad .$$

For typical 8 GeV Line parameters β = 20 m and ϵ = 1.5 π mm-mrad, and so θ_{beam} = .11 mrad. For nickel wires of thickness .05 mm, θ_{rms} = .07 mrad. Though these numbers are comparable, only a few percent of the beam particles will pass through the wires. In comparison, the nickel foils used in many of the profile monitors of the old beamline were .025 mm thick (yielding θ_{rms} = .03 mrad) and 1.6 mm wide with 3.2 mm spacing. Thus, over 50% of the beam passed through the foils of the monitor.

A new microprocessor based system[5] was developed for gathering and analyzing the profile monitor data. The wire planes may be inserted into the beam path from an applications program on the accelerator controls system and data from all monitors may be processed simultaneously. When in the beam path, the microprocessor automatically computes the mean and variance of the particle distribution as well as a goodness of fit compared to the normal distribution. Figure IV-9 shows a typical display of wire data from one of the wire chambers in the new

Figure IV-9

Typical Beam Profile Monitor Output

Abs-Mean=-1.8 mm   Sigma=2.5 mm   ChiSq=.8

WC3

HORIZONTAL
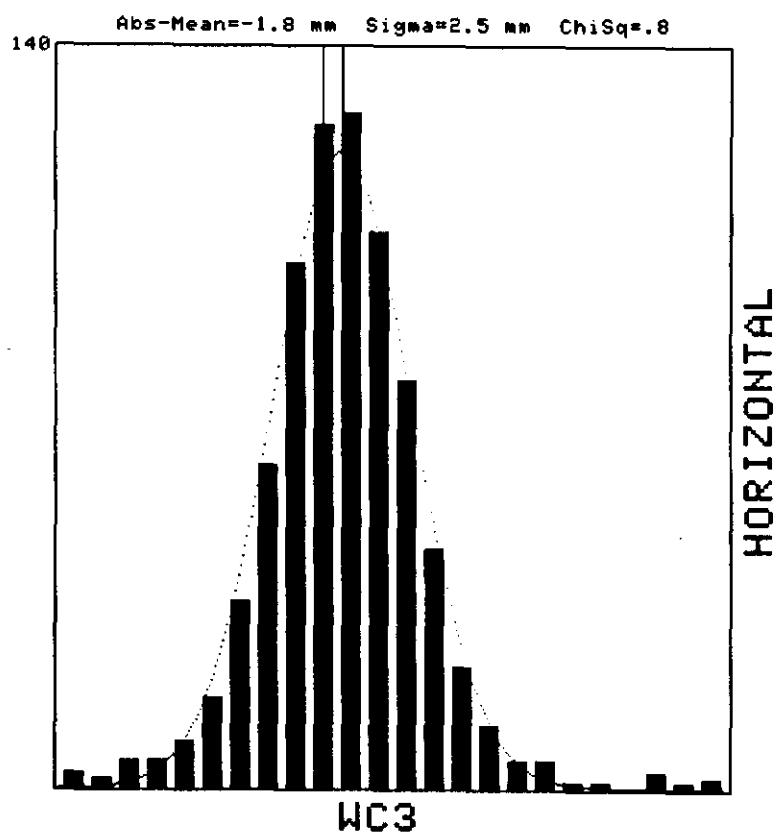
line.   The data may be read and the computations performed at a 15 Hz rate, which permits the analysis of beam from all Booster synchrotron cycles.   The computed values are automatically updated in the accelerator controls system data base and may be plotted in real time from a computer console or stored for future analysis.

Beam Position Monitor System

Noninteracting beam position monitors (BPM's) are also distributed throughout the new 8 GeV Line.   The BPM's are cylindrical stripline detectors similar to those used in the Tevatron accelerator.[6]   For the 8 GeV Line each BPM contains four 50 ohm striplines 6 in. in length spaced 90° apart.   Each of the striplines subtends an arc of 60° and the inside diameter of the detector is 4.5 inches.

If the beam is treated as an infinitely long line charge displaced x mm from the center of the detector, since the potential along the arcs of the striplines is a constant the negative image charge would be located a distance R^2/x mm from the center of the detector, where R is the radius of the detector in mm.   The ratio of the charge density found on one stripline (A) to that found on the other stripline (B) would then be

$$A/B = (R+x)^2/(R-x)^2$$

which yields, to first order in x/R,

$$x \sim (R/4)\ln(A/B) \ .$$

Measurements performed on these instruments show that this is indeed the case and the BPM's have been calibrated to provide position information via the accelerator controls system to within ± 0.2 mm near the center of the detector.

The output of the position detectors is processed through standard Tevatron-style BPM electronics[7] with positions being obtainable from existing accelerator controls system software, as displayed in Figure IV-10. Though each detector has striplines for detecting both horizontal and vertical positions, not all detectors are used for both planes. A total of 12 horizontal and 12 vertical sets of striplines are monitored. Throughout most of the beamline only the striplines in the plane where the beam is large (locations of β_{max} in the Cells, for instance) are used. At the injection and extraction regions, both horizontal and vertical signals from several BPM's allow precise measurements of the beam trajectories at these points.

Beam Loss Monitors

Primarily for use during commissioning and for the diagnosis of problems, 12 beam loss monitors (BLM's) have been mounted on the beampipe throughout the beamline typically near the most narrow aperture restrictions. As with the BPM's, the BLM hardware and electronics has been adopted from the Tevatron project.[8] The loss monitors are cylindrical ion chambers of radius 3 cm containing an effective volume of .11 liter of argon gas at a pressure of about 1 atm. Given $dE/dx = 1.3$ keV/cm for argon gas at 1 atm, a dose of one Rad would correspond to roughly 2×10^9 particles passing through the detector. Operated at 2.5 kV, the detector calibration is roughly 7×10^{-8} Coulombs per Rad and is nearly linear to 100 Rads instantaneous dose.[9] The signal from each BLM is fed into a separate integrating logarithmic amplifier the output of which is fed into an analog

Figure IV-10

Typical Beam Position Monitor Output

(MM)

FLASH FRAME	.5160	

TAKEN 09/30/86 1615:31   2B

UPSTREAM	ML01	-.3
UPSTREAM	QDB3	-.61
UPSTREAM	QDB5	.15
UPSTREAM	QFB6	3.06
UPSTREAM	QFC2	.61
UPSTREAM	QFC4	-3.06
UPSTREAM	QFM1	-2.75
UPSTREAM	QFM3	-2.75
UPSTREAM	QFM5	2.29
DOWNSTREAM	HB83	-9.75
DOWNSTREAM	LAMB	-9.16
END OF STRAIGHT		.7
A 11		4.58
A 13		4.43
A 15		-1.1
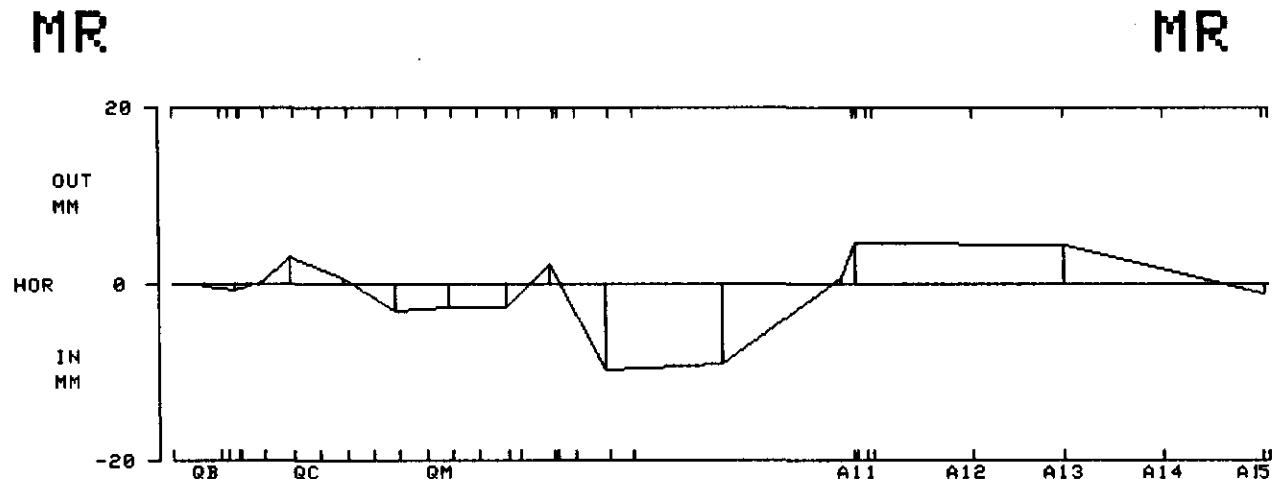
to digital converter. The signals are then read by the accelerator controls system and may be plotted in real time from a console applications program.

Beam Intensity Monitors

To complete the list of diagnostics equipment, one more type of monitor must be mentioned. At the beginning of the beamline just in front of the second pulsed septum magnet and at the end of the line near the entrance of the injection Lambertson, an induction toroid (current transformer) is used to detect the total beam intensity passing through these two regions. The toroids are placed near ceramic gaps in the beamtube which stop the flow of image charges that would otherwise mask the signal generated by the beam. The signals are integrated and sampled by the accelerator controls system. The two beam intensity monitors (BIM's) have been simultaneously cross-calibrated with a single current source. Hence, beam signals may be converted to yield the number of protons entering and leaving the beamline, providing a measure of the overall efficiency of the beam transfer.

Beam Position Correction System

Due to unavoidable magnet field and alignment errors, as well as entry and exit steering errors, a beam position correction system must be included in the design of any beamline. Fine adjustments may be made to the bend strengths of the major bending elements of the beamline, but usually the number of major bends is too few or their locations are inappropriate to provide

proper steering for the correction of the trajectory through all aperture restrictions. In the 8 GeV Line, the beampipe between magnetic elements has an aperture of 4 in. (102 mm). However, the major dipole magnets have gap heights of only 1.4 in. (35 mm). Since the width of the beam may be on the order of 10 mm, distortions of the trajectory of greater than ~10 mm must be avoided in these regions.

As described in Chapter III, a steering error $\Delta\theta = \theta_0 \sin\phi$ can result from a misaligned dipole magnet. More significant are errors produced by the transverse misalignment of a quadrupole magnet. Since the field in a quadrupole magnet along one transverse degree of freedom is given by $B_y = B'x$, then a quadrupole displaced a distance d from the ideal trajectory along the transverse direction will produce a steering error given by

$$\Delta\theta = B_y L/(B\rho) = B'Ld/(B\rho) = (B'L/B\rho)d = d/f$$

where f is the focal length of the quadrupole. In either case, the resulting displacement of a particle downstream of the steering error will be

$$\Delta x(s) = \Delta\theta_0 (\beta(s_0)\beta(s))^{1/2} \sin(\psi(s) - \psi(s_0))$$

as can be seen by letting the general transport matrix $M(s/s_0)$ described in Chapter III operate on the vector $(x, x') = (0, \Delta\theta_0)$. With typical values of $\beta = 20$ m, and a typical quadrupole focal length of 10 m, a single quadrupole magnet displaced by 1 mm would generate a maximum distortion of the trajectory of 2 mm downstream of the error. With 20 quadrupole magnets in the line, the effects of alignment errors can add up quickly.

To determine where to place additional position correction
dipole magnets, a program was written by the author to simulate a
misaligned 8 GeV Line. The program assigns a quadrupole
placement error for each quadrupole in the beamline from a normal
distribution with standard deviation d_{rms}. The equivalent
steering error is then computed for each quadrupole. An initial
trajectory (also obtained from a normal distribution) x_o, x'_o is
then tracked through the elements and the displacement at the end
of each element is found. Steering elements, whose locations are
designated by the user, are then used to minimize the beam
positions through a section of the beamline. The resulting
distribution of beam positions after correction, its rms value
and its maximum value are all stored for future analysis. The
corresponding distribution of corrector strengths is also stored.
The entire process is repeated with a new set of quadrupole
errors as many times as desired by the user.

In the program, the strength of an individual corrector is
obtained using a least squares method to minimize the
displacements downstream of the corrector. The set of N measured
positions is designated by $\{x_i\}$. The corrector is to produce a
set of displacements $\{\Delta x_i\}$, where

$$\Delta x_i = \theta_o (\beta_o \beta_i)^{1/2} \sin\psi_{oi} \; ,$$

such that the quantity $M = \Sigma(x_i + \Delta x_i)^2$ is minimized. The sum is
taken over the N locations. The resulting corrector strength is

$$\theta_o = - \frac{\sum_i x_i \sqrt{\beta_i} \sin\psi_{oi}}{\sqrt{\beta_o} \sum_i \beta_i \sin^2\psi_{oi}}$$

The distribution of maximum beam displacements generated by misaligned quadrupoles (using d_{rms} = 1 mm for each plane) when no correction is performed is shown in Figure IV-11. The seven trim elements are then used in conjunction with the major bending elements to correct the displacements in each of the 2000 trials using the algorithm described above. Each corrector minimized the positions at the ends of the magnetic elements between itself and the next corrector. The resulting distribution of maximum displacements after correction is shown in Figure IV-12.

To improve the positions through the beamline for the 2000 trials, the average correction element strength was 0.1 mrad. The distribution of maximum corrector strengths is shown in Figure IV-13. Less than one percent of the trials had corrector strengths greater than 1.5 mrad. This was the number used for specifying the correction magnets and their power supplies which were described earlier in this chapter. Several variations of corrector placement were studied before the satisfactory results quoted above were produced.

Vacuum and Water Systems

The major vacuum and water systems of the Main Ring and Booster synchrotrons are used to handle the needs of the 8 GeV Line. The "dividing line" between the two synchrotrons is the 18 ft radiation shielding wall midway through the new beamline. On the Booster side of the wall, magnets receive cooling water from the Booster water system. On the Main Ring side, water is delivered from the Main Ring system. No strain is put upon either system from the loads of the 8 GeV Line.

Figure IV-11

Figure IV-12

Distribution of Maximum Displacements
(For 2000 Trials with d_{rms} = 1.0 mm)
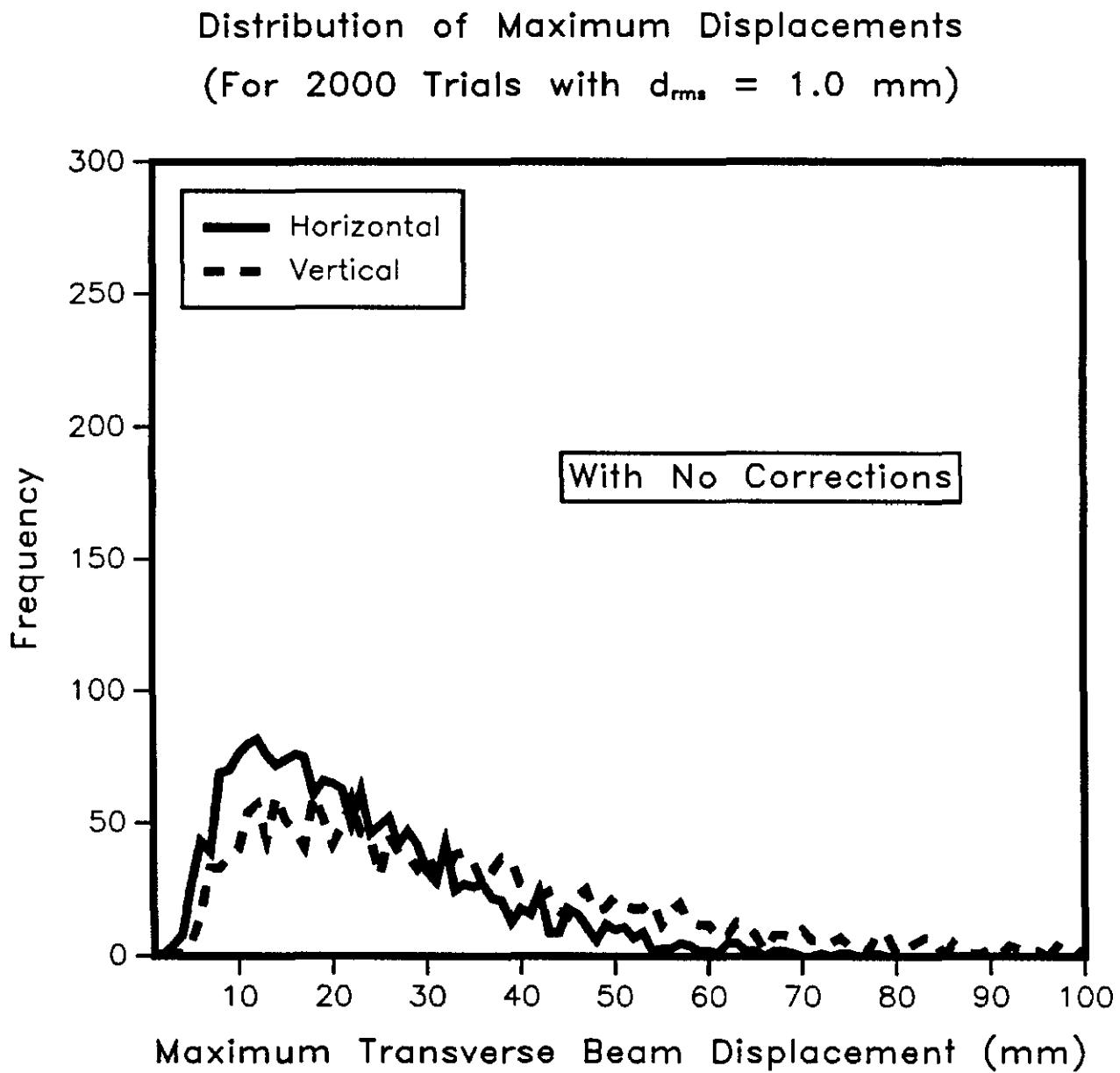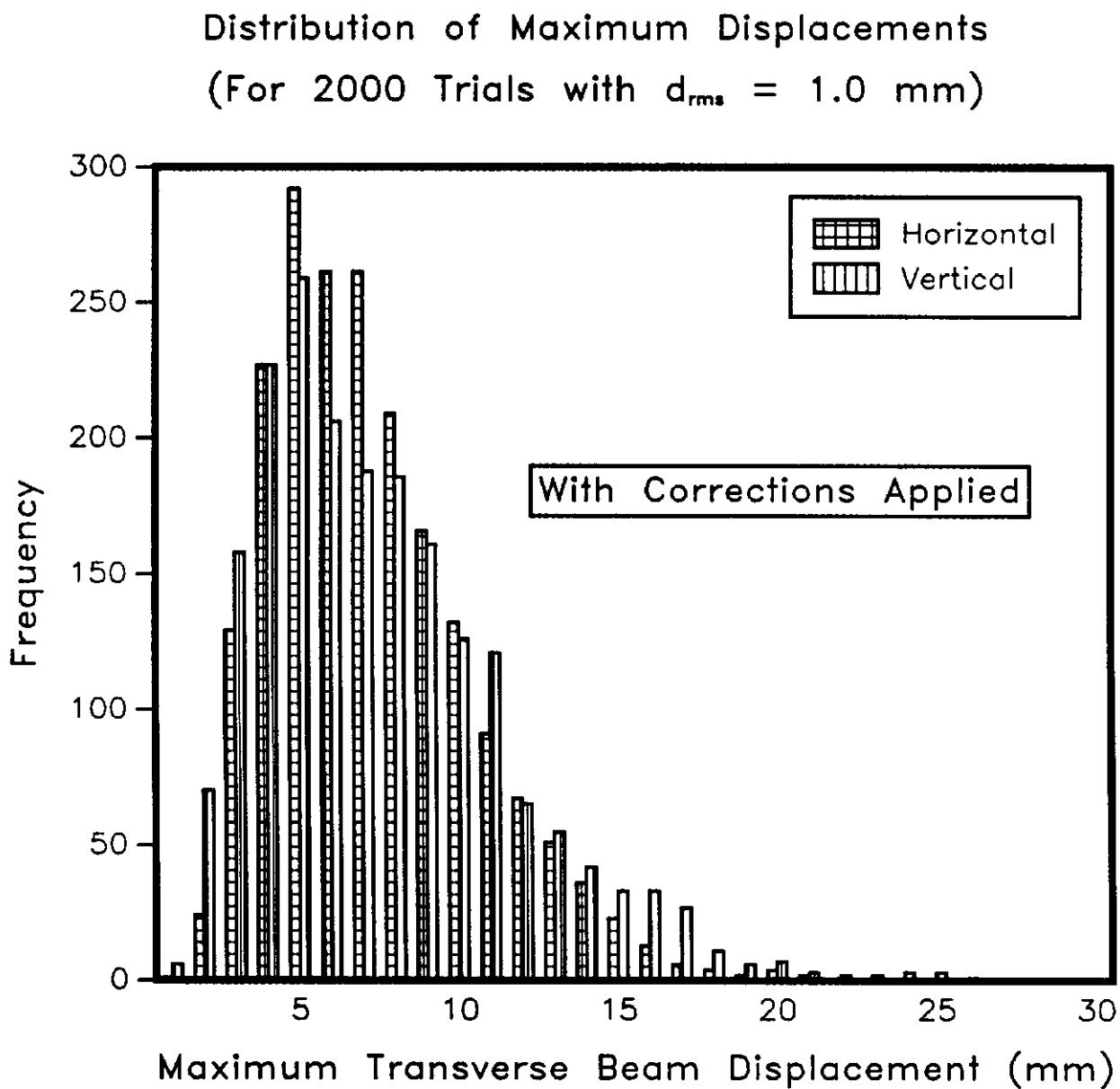
Figure IV-13

Distribution of Correction Element Maxima
(For 2000 Trials with $d_{rms} = 1.0$ mm)
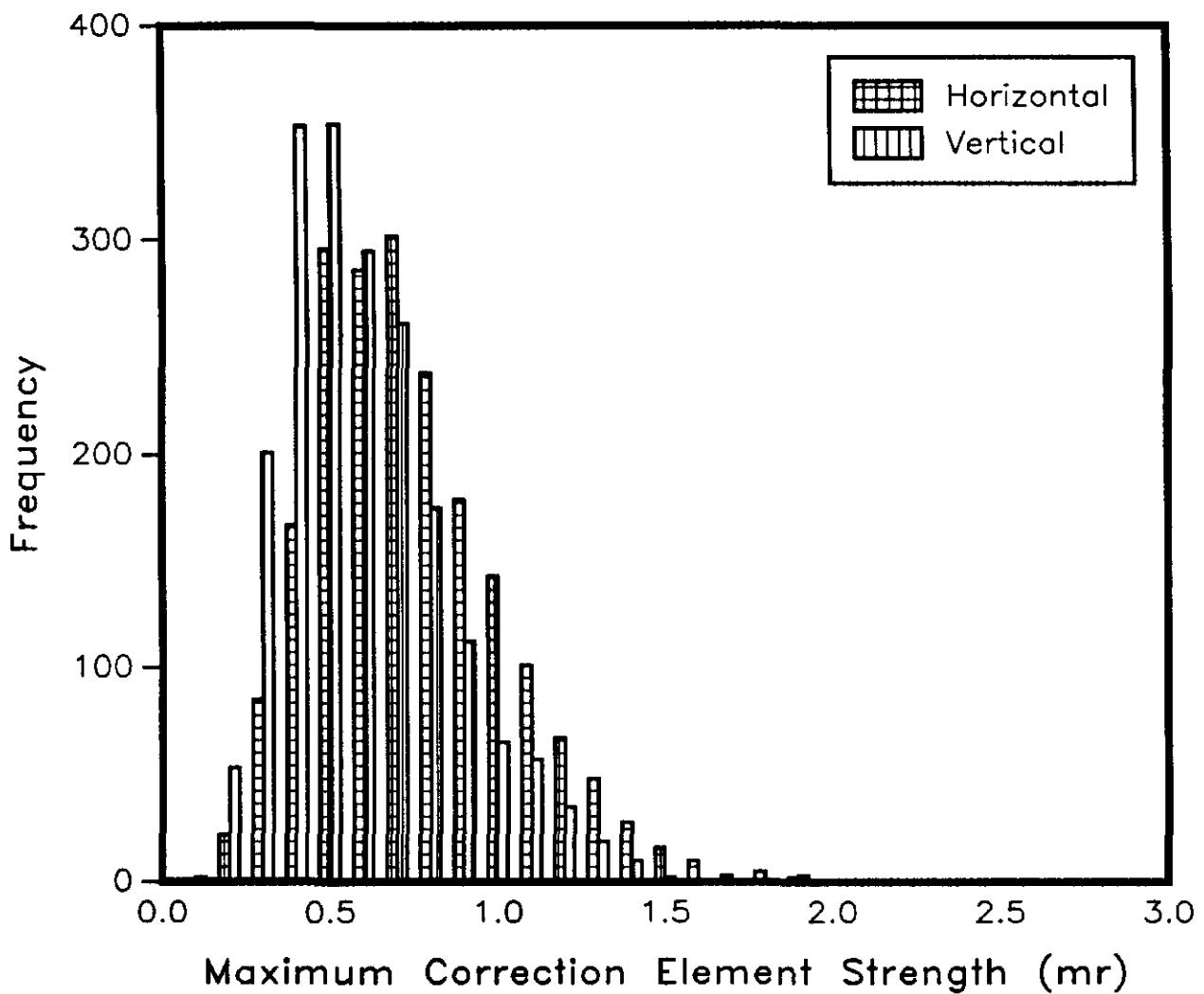
Standard vacuum roughing stations in the two synchrotrons near the Booster extraction and Main Ring injection points pump down the entire line to a pressure of about 10^{-3} torr. Distributed throughout the beamline, 15 ion pumps are used to reduce the pressure to 10^{-6} torr. A vacuum valve is located on the Main Ring side of the shielding wall and can be used to isolate the two vacuum systems. Cold cathode gauges are located periodically through the line to monitor the pressure. All pumps and valves may be controlled remotely.

Budget and Schedule

A final schedule for completion and cost estimate of the entire project are presented in Tables IV-2 and IV-3. Salaries of Fermilab employees who participated in the project are not included. The bulk of the funds for the 8 GeV Line project was provided by the Tevatron I Project.

Table IV-2

8 GeV Line Project Schedule

```
                                        85 | 86
                                    |NOV |DEC |JAN |FEB |MAR |APR |MAY |JUN |JUL |AUG |
MAGNETS
    Quads
            Copper                  |    |    | XXXXXXXX|    |    |    |    |    |    |
            Coils                   |    |    | XXXXXXXXXXXX|    |    |    |    |    |
            Assembly                |    |    |    | XXXXXXXXXXXX|    |    |    |    |
            Measure                 |    |    |    |    | XXXXXXXX    |    |    |    |
            Stands -- Design        |    |    |    | XXXXXXXXXXX|    |    |    |    |
                      Fabricate     |    |    |    |    | XXXXXXXXXX  |    |    |    |
    Lambertson                      --------------------------------------------------
            Measurements of existing Lamb | XXXXXXXXXXXXXX    |    |    |    |    |    |
            Design of Spare         |    | XXXXXXXXXXXX|    |    |    |    |    |    |
            Fabricate & measure Spare |  |    |    |    |    |    |    |    | XXXXX
    Trim Dipoles                    --------------------------------------------------
            Design                  | XXXXXXXXX  |    |    |    |    |    |    |    |
            Fabrication             |    |    | XXXXXXXX    |    |    |    |    |    |
    MR Orbit Bump Dipoles           --------------------------------------------------
            Design                  | XXXXXXXXXXXX    |    |    |    |    |    |    |
            Fabrication             |    |    | XXXXXXXXXXXXXXXXXXXXXXXX|    |    |    |

                                    |NOV |DEC |JAN |FEB |MAR |APR |MAY |JUN |JUL |AUG |
POWER SUPPLIES
    Specifications                  | XXXXX |    |    |    |    |    |    |    |    |
    Design                          |    | XXXXXXXX|    |    |    |    |    |    |    |
    Fabrication                     |    |    |    |    | XXXXXXXXXXXXXX |    |    |
                                    --------------------------------------------------
    Controls
            Design                  |    | XXXXXXXXX|    |    |    |    |    |    |    |
            Fabrication             |    |    |    | XXXXXXXXXXXXXXXXXXXX |    |    |
                                    --------------------------------------------------
    Current Monitoring
            Design                  |    | XXXXXXXXX|    |    |    |    |    |    |    |
            Fabrication             |    |    |    | XXXXXXXXXXXXXXXXXX |    |    |
                                    --------------------------------------------------
    Cabling
            PS Layout               |    |    |    |    | XXXXX |    |    |    |    |
            Cabling Layout          |    |    |    |    |    | XX |    |    |    |    |
            Fabrication             |    |    |    |    |    |    | XXXXXXX|    |    |
                                    |NOV |DEC |JAN |FEB |MAR |APR |MAY |JUN |JUL |AUG |
BEAM DIAGNOSTICS
    Specifications                  | XXXXX|    |    |    |    |    |    |    |    |
    Design                          |    | XXXXXXXXXXX |    |    |    |    |    |    |
    Fabriction                      |    |    |    |    | XXXXXXXXXXXXXXXX|    |    |
```

Table IV-2 (Continued)

```
                                          85 | 86
                                    |NOV |DEC |JAN |FEB |MAR |APR |MAY |JUN |JUL |AUG |
CONTROLS                            |    |    |    |    |    |    |    |    |    |    |
        Design                      |  XXXXXXXXXXXXXXXXXXXXXXX|    |    |    |    |    |
        Hardware Conversion         |    |    |    |    |    |  XXXXXXXXX  |    |    |
        Software                    -----------------------------------------------------
                Front End           |    |    |XXXXXXXXXXXXXXXXXXXXXXXXXXXXX  |    |    |
                Applications        |    |    |XXXXXXXXXXXXXXXXXXXXXXXXXXXXXXX|    |    |

                                    |NOV |DEC |JAN |FEB |MAR |APR |MAY |JUN |JUL |AUG |
VACUUM                              |    |    |    |    |    |    |    |    |    |    |
        Design/Fabrication          |    |    |    |    |    |  XXXXXXXXXX  |    |    |

                                    |NOV |DEC |JAN |FEB |MAR |APR |MAY |JUN |JUL |AUG |
COOLING WATER                       |    |    |    |    |    |    |    |    |    |    |
        Design/Fabrication          |    |    |    |    |  XXXXXXXXXXXXXXX  |    |    |

                                    |NOV |DEC |JAN |FEB |MAR |APR |MAY |JUN |JUL |AUG |
MISCELLANEOUS                       |    |    |    |    |    |    |    |    |    |    |
        Layout/Drawings             |    |    | XXXXXXXXXXXXXX   |    |    |    |    |
        8" Header in Transfer Hall  |    |    |    |  XXXXXX |    |    |    |    |    |
        Tevatron Lambertson bus-work|    |    |    |    |    |    | |XXXXX  |    |    |

                                    |NOV |DEC |JAN |FEB |MAR |APR |MAY |JUN |JUL |AUG |
INSTALLATION                        |    |    |    |    |    |    |    |    |    |    |
        Booster Shutdown            |    |    |    |    |    |    |XXXXXXXXXXXXX  |    |
        Remove Old Line             |    |    |    |    |    |XXXXXXX |    |    |    |
        Remove Labyrinth            |    |    |    |    |    |    XX  |    |    |    |
        Survey                      |    |    |    |XX (rough)    XX  |    |    |    |
                                    -----------------------------------------------------
        Install Water Lines         |    |    |    |    |    |    |XXX |XX  |    |    |
        Install Magnet Stands       |    |    |    |    |    |    |XX  |    |    |    |
        Install Magnets             |    |    |    |    |    |    | XXXXX  |    |    |
        Install Beampipe,Diagnostics,etc.|  |    |    |    |    |    | XXXXX| |    |    |
        Alignment                   |    |    |    |    |    |    |    | XXX   |    |    |
                                    -----------------------------------------------------
        Install Power Supplies      |    |    |    |    |    |    |XXXXXXX |    |    |
        Cable Tray Installation     |    |    |    |    |    |    | XX|    |    |    |
        AC Power Installation       |    |    |    |    |    |    | XXXX   |    |    |
        Cable Installation          |    |    |    |    |    |    | |XXXX| |    |    |
        Cable Termination           |    |    |    |    |    |    | XXXX   |    |    |
        Final Hookup--Power/Water    |    |    |    |    |    |    | XXX  |    |    |
        Install Radiation Shielding Wall|  |    |    |    |    |    | XX|    |    |    |
        Systems Tests               |    |    |    |    |    |    | XXXXXXXXXXX

                                    |NOV |DEC |JAN |FEB |MAR |APR |MAY |JUN |JUL |AUG |
COMMISSIONING                       |    |    |    |    |    |    |    |    |    |    |
        Beam from Booster to 8 GeV Dump|  |    |    |    |    |    |    | XXX   |    |
        Beam to MR C0 Abort         |    |    |    |    |    |    |    | |XXXXX
        MR Circulating Beam         |    |    |    |    |    |    |    | XXX
```

Table IV-3

8 GeV Line Project Budget

Magnets --

Tev I SQA's 20@ $20K =	$398K
Dipoles	~0
Trim Dipoles	$ 33K
Stands/Supports	$ 25K

Sub-Total: $456K

Power Supplies --

Quads	$ 66K
Dipoles	~0
Trim Dipoles	$ 12K
Controls/Monitoring	$ 20K
Cabling, etc.	$ 32K
Elec. Installation	$ 30K

Sub-Total: $160K

Controls/Diagnostics --

BPM's	$ 10K
Multiwires	$ 31K
Loss Monitors	$ 4K
Intensity Monitors	~0
System Conversion	$ 20K

Sub-Total: $ 65K

Misc. Labor --

Install water lines	$ 25K
Install Magnet stands	$ 10K
Install Magnets	$ 15K

Sub-Total: $ 50K

Grand-Total: $731K

References

1. "Design Report--Tevatron I Project," Fermi National Accelerator Laboratory; September, 1983.

2. Ibid.

3. "Fermilab Electron Cooling Experiment--Design Report," Fermi National Accelerator Laboratory; August, 1978.

4. Gerig, R., "8 GeV and Main Ring Multiwire Program," Software Release No. 58, Fermilab Accelerator Division internal report, January 10, 1980.

5. Marsh, W., "Proposal for CAMAC Functions of the CAMAC 192 Module," Fermilab Accelerator Division internal report, June 16, 1986.

6. Shafer, R. E., R. C. Webber, and T. H. Nicol, "Fermilab Energy Doubler Beam Position Detector," IEEE Transactions on Nuclear Science, Vol. NS-28, No. 3, June, 1981.

7. Baumbaugh, A. E., et. al., "Beam Position Monitor System for the Fermilab Tevatron," IEEE Transactions on Nuclear Science, Vol. NS-32, No. 5, October, 1985.

8. Shafer, R. E., R. E. Gerig, A. E. Baumbaugh, and C. R. Wegner, "The Tevatron Beam Position and Beam Loss Monitoring Systems," Proceedings of the 12th International Conference on High Energy Accelerators, Fermilab, 1983.

9. Ibid.

V.   Injection Mismatch and Phase Space Dilution

Introduction to the Problem

In Chapter III, a list of 20 constraints put forth upon a beamline connecting two synchrotrons was presented. These constraints may be grouped into three categories: matching of the ideal beam trajectory, matching of the dispersion functions, and matching of the amplitude functions. The degree to which deviations from an ideal match affect the transverse phase space emittances is the subject of this chapter.

Given a particle with an initial coordinate in phase space, the resulting time average distribution in the transverse coordinate may be obtained for that particle. Using this result an expression for the final distribution of many particles, given their initial distribution, may be found. The area in phase space which will contain 95% of an incoming distribution after dilution may be computed as well. Initial distributions generated by various forms of mismatch may then be inserted into these expressions to yield resulting time average distributions and emittance dilution factors for the particle beam. This process is performed for the three types of mismatch described above and, through a set of simple statistical arguments, general expressions for the variances of these distributions are derived.

Time Average Distribution of a Single Particle

If the transverse motion in one degree of freedom of a single particle is observed at a particular longitudinal location s in a synchrotron, the solution to Hill's Equation yields a trajectory of the particle in transverse phase space given by

$$x^2 + (\beta x' + \alpha x)^2 = \beta A^2$$

where A is a constant determined by the initial conditions x_o and x'_o. The quantities β and $\alpha = -\beta'/2$ are characteristic functions of the ring. If now a new phase space variable $\varsigma \equiv \beta x' + \alpha x$ is defined, then the trajectory may be written as

$$x^2 + \varsigma^2 = a^2$$

which is the equation of a circle in x-ς space with radius $a = (\beta)^{1/2}A$. The quantity a is referred to as the amplitude of the oscillation. Both ς and a have units of length.

A particle enters the accelerator and upon its first passage through point s the particle has phase space coordinates (x_o, ς_o). Upon subsequent revolutions about the machine, the particle will reappear at point s with phase space coordinates (x, ς) which lie on a circle of radius $a = (x_o^2 + \varsigma_o^2)^{1/2}$. The exact location on the circle after each revolution will depend upon the phase advance of the betatron oscillation for one complete revolution. This phase advance may depend upon the amplitude a. (In fact, in a real synchrotron, the phase advance undoubtedly will depend upon amplitude due to nonlinear field imperfections within the machine.) However, over a long period of time, the probability of finding the particle at a specific transverse displacement x may be computed. If the quantities x and ς are parameterized by the relationships

$$x = a \cos\omega t, \qquad \varsigma = a \sin\omega t,$$

then the phase space distribution of the particle will be given by

$$f(x,\varsigma,t) \ dx \ d\varsigma \ = \ \delta(x - a\cos\omega t) \ \delta(\varsigma - a\sin\omega t) \ dx \ d\varsigma$$

where $\delta(u)$ is the Dirac delta function. Integrating over ς yields

$$g(x,t) \, dx \;=\; \delta(x - a\cos\omega t) \, dx \;.$$

To find the time average distribution in x, $g(x,t)$ is integrated over a cycle of period $\tau = 2\pi/\omega$ yielding

$$n_a(x) \, dx \;=\; dx \, \frac{2}{\tau} \int_0^{\tau/2} \delta(x - a\cos\omega t) \, dt \;=\; dx \, \frac{2}{\tau} \int_{-a}^{a} \delta(x-u) \frac{du}{a\omega \left[1-(u/a)^2\right]^{1/2}}$$

or,

$$n_a(x) \, dx \;=\; \frac{1}{\pi a} \, \frac{dx}{\sqrt{1 - (x/a)^2}} \;.$$

So, given the initial condition in transverse phase space (x_0, x'_0), over a long period of time the probability of finding the particle between x and x+dx is $n_a(x) \, dx$.

Time Average Distribution Given an Initial Distribution of Many Particles

Given an initial distribution of particles $n_0(x,\varsigma) \, dx \, d\varsigma$ within the synchrotron at location s, then the resulting time average distribution of the particles may be found. By converting x and ς to polar coordinates, the number of particles which are located within a circle of radius a is given by

$$f(a) \;=\; \int_0^{2\pi} \int_0^{a} n_0(r,\theta) \, r \, dr \, d\theta$$

and the number of particles between two circles of radii a and a+da is

$$\frac{\partial f(a)}{\partial a} \, da \;=\; da \int_0^{2\pi} n_0(a,\theta) \, a \, d\theta \;.$$

Thus, the contribution of a particular ring of radius a and thickness da to the resulting time average distribution in x is

$$n_a(x)\,dx = \frac{1}{\pi}\,\frac{dx\,da}{\sqrt{1-(x/a)^2}}\int_0^{2\pi} n_o(a,\theta)\,d\theta\ .$$

Upon adding up all contributions due to all pertinent rings (i.e., $a \geq |x|$), the resulting time average distribution in x will be

$$n(x)\,dx = \frac{dx}{\pi}\int_{|x|}^{\infty}\int_0^{2\pi}\frac{n_o(a,\theta)}{\sqrt{1-(x/a)^2}}\,d\theta\,da\ .$$

Using the above equation, the resulting time average distribution of particles in one transverse degree of freedom may be computed given the initial distribution of particles delivered by the beamline. A perfect match of the beamline to the synchrotron would produce a resulting time average distribution of $n(x) = \int n_o(x,\varsigma)\,d\varsigma$.

Emittance Dilution

The emittance ϵ has been defined as the area in transverse x-x' phase space which contains 95% of the particles. The differential element of area in x-ς phase space is simply

$$dx\,d\varsigma = \beta\,dx\,dx'\ .$$

Thus, the area in x-ς phase space which contains 95% of the particles is $\beta\epsilon$.

This area may be found by determining the value of a_{95} which satisfies the equation

$$f(a_{95}) = \int_0^{2\pi} \int_0^{a_{95}} n_o(r,\theta) \; r \; dr \; d\theta = 0.95 \; N$$

where N is the number of particles in the beam. If the incoming distribution is Gaussian in x with variance σ_o^2 and is perfectly matched to the synchrotron, the resulting distribution will also be Gaussian with variance σ_o^2. The area in x-ς phase space which contains 95% of the particles will be $\pi a_{95}^2 = \beta\epsilon_o = 6\pi\sigma_o^2$. If the incoming distribution is not perfectly matched to the synchrotron, then the resulting time average distribution in x will be broader than the incoming distribution and the value of a_{95} will be greater than $(6\sigma_o^2)^{1/2}$. Thus, the effective area in phase space which the beam will occupy increases by a factor of

$$F = \frac{\beta\epsilon}{\beta\epsilon_o} = \frac{\pi a_{95}^2}{6\pi\sigma_o^2} = \frac{a_{95}^2}{6\sigma_o^2}$$

due to a mismatch. F is referred to as the dilution factor.

Simplifying Assumptions and Units

Different sources of mismatch will produce different initial distributions n_o and hence will result in different final distributions and dilution factors. Before investigating three of these sources, some simplifying assumptions are made and units are defined which are used throughout the discussions.

All quantities associated with the beamline are denoted by a subscript "1" and those of the synchrotron are denoted by a subscript "2." For example, if s represents the injection point or some other point within the synchrotron "downstream" of the injection point, then $\beta_2(s)$ would be the value of the natural amplitude function of the machine at that point and $\beta_1(s)$ would

be the value of the amplitude function at that point as delivered by the beamline. The distribution of particles at point s is considered to be Gaussian in x_1-ς_1 space and may be written as

$$n(x_1,\varsigma_1) \; dx_1 \; d\varsigma_1 = \frac{N \; e^{-\left[x_1^2 + \varsigma_1^2\right]/2\sigma_1^2}}{2\pi\sigma_1^2} \; dx_1 \; d\varsigma_1 \; .$$

Amplitudes of particle motion in phase space are assumed not to vary with time so that the techniques described in the last two sections may be applied to determine the resulting particle distributions.[1]

Because the resulting trajectory of a particle in x_2-ς_2 phase space is a circle, the resulting time average particle distribution in phase space will always be symmetric about the origin. For the cases of Gaussian beams which are studied, the x_2-ς_2 axes may be rotated through an angle θ to make the original distribution $n_0(x_2,\varsigma_2)$ symmetric about the x_2 axis. For example, if both the position and slope of the incoming trajectory are mismatched by the amounts Δx and $\Delta x'$ respectively, the axes may be rotated and the problem treated as though only the position was mismatched by an amount Δx_{eq}. As shown in Figure V-1, the values of F computed with the axes rotated or not rotated will be the same. This technique reduces the number of types of mismatch to be investigated by a factor of two.

To simplify the problem, all lengths (x, ς, a) are written in units of the standard deviation of the perfectly matched beam. That is, $\sigma_{20} = (\epsilon_0\beta_2/6\pi)^{1/2} \equiv \sigma_0 \equiv 1$. The quantity ϵ_0 is the transverse emittance delivered by the beamline. Similarly, all

Figure V-1

Determination of Equivalent Mismatch
Through Rotation of Phase Space Axes
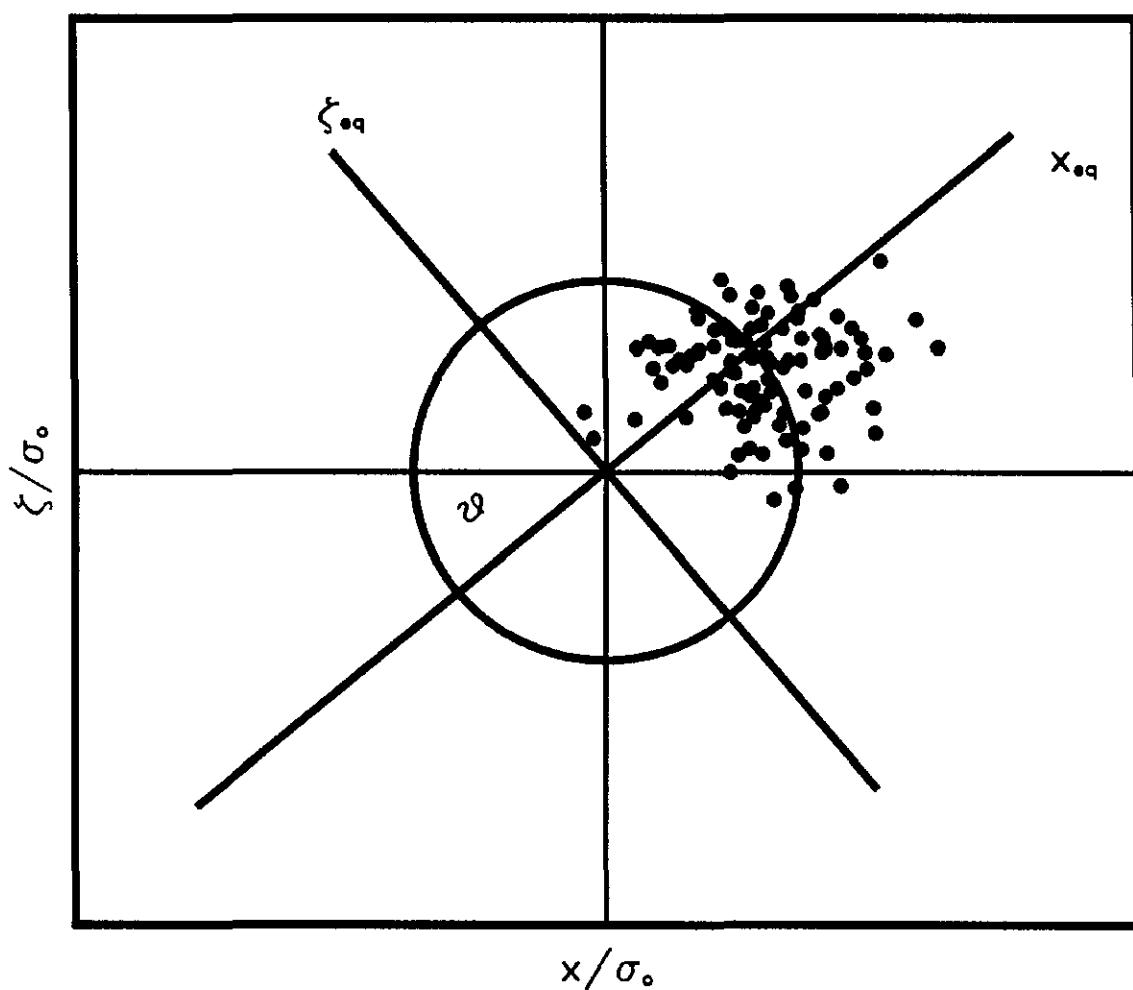
amplitude functions are written in units of the natural amplitude function of the synchrotron $\beta_2 \equiv \beta_o \equiv 1$. In addition, the particle distribution is normalized to one particle, i.e., $N = 1$.

Injection Position Mismatch

For the case of a mismatch of the ideal trajectory, the amplitude functions and dispersion functions delivered by the beamline are assumed to be matched to the synchrotron: $\beta_1 = \beta_2$, $\alpha_1 = \alpha_2$, $D_1 = D_2$, and $D'_1 = D'_2$. If Δx and $\Delta x'$ are the errors in the incoming position and slope for one transverse degree of freedom of the beamline's ideal trajectory, then

$$x_2 = x_1 + \Delta x \qquad \text{and} \qquad x'_2 = x'_1 + \Delta x'$$

which implies

$$\varsigma_2 = \varsigma_1 + \Delta\varsigma \ .$$

The x_2-ς_2 axes may be rotated through an angle θ given by

$$\tan\theta = \Delta\varsigma/\Delta x \ .$$

so that the problem is equivalent to one in which the incoming distribution is displaced only in position by an amount

$$\Delta x_{eq} = (\Delta x^2 + (\beta\Delta x' + \alpha\Delta x)^2)^{1/2} \ .$$

From now on, Δx will be used to represent Δx_{eq}.

Since the amplitude functions are assumed to be matched, $\sigma_1 = \sigma_2 = \sigma_o = 1$ and the incoming distribution may be written as

$$n_o(x_2,\varsigma_2) \ dx_2 \ d\varsigma_2 = \frac{e^{-\left[(x_2-\Delta x)^2 + \varsigma_2^2\right]/2}}{2\pi} \ dx_2 \ d\varsigma_2 \ .$$

Using $n_x(x)dx$ to denote the final time average distribution due to a position mismatch, dropping the subscript "2" for the moment,

$$n_x(x)\ dx\ =\ \frac{dx}{2\pi^2}\int_{|x|}^{+\infty}\int_0^{2\pi}\frac{e^{-\frac{1}{2}\left(a^2+\Delta x^2-2a\Delta x\cos\theta\right)}}{\sqrt{1-(x/a)^2}}\ d\theta\ da$$

or, reducing the expression to a single integral,

$$n_x(x)\ dx\ =\ \frac{dx}{\pi}\int_{|x|}^{+\infty}e^{-(a-|\Delta x|)^2/2}\frac{e^{-|a\Delta x|}\ I_o(a\Delta x)}{\sqrt{1-(x/a)^2}}\ da$$

where $I_o(z)$ is the modified Bessel function of order zero.[2]   The dilution factor F_x for a particular position error Δx is found from

$$F_x\ =\ a_{95}^2/6$$

where a_{95} satisfies

$$f_x(a_{95})\ =\ \int_0^{2\pi}\int_0^{a_{95}}\frac{1}{2\pi}e^{-(r^2+\Delta x^2-2r\Delta x\cos\theta)/2}\ r\ dr\ d\theta$$

$$=\ \int_0^{a_{95}}e^{-(r-|\Delta x|)^2/2}\left[e^{-|r\Delta x|}I_o(r\Delta x)\right]r\ dr\ =\ 0.95\quad.$$

As a check, notice that for $\Delta x = 0$, the expressions for $n_x(x)dx$ and f_x reduce to

$$n_x(x)\ dx\ =\ \frac{1}{\sqrt{2\pi}}e^{-x^2/2}\ dx$$

and,

$$f_x(a_{95})\ =\ 1-e^{-a_{95}^2/2}\ =\ 0.95$$

which implies

$$a_{95}^2\ =\ 6\quad\text{and thus}\quad F_x\ =\ 1\ ,\ \text{as expected.}$$

Numerical integration of the expressions for n_x and f_x
yields the results displayed in Figures V-2 and V-3. If the
injected beam is displaced by more than about twice the standard
deviation of the initial particle distribution, the resulting
time average distribution exhibits a "double hump" appearance.
Up to this point, the variance of the resulting distribution is
equal to the dilution factor, to within a few percent. For Δx
greater than about $2\sigma_0$, the variance is greater than F_x. An
explicit relationship between the variance of the distribution
and the position error Δx is derived later in this chapter.

Dispersion Function Mismatch

For this discussion the ideal trajectory and the amplitude
functions of the beamline are assumed to be matched to those of
the synchrotron: $\beta_1 = \beta_2$, $\alpha_1 = \alpha_2$, $x_2 = x_1 = x$, and $x'_2 = x'_1$.
For a particle of momentum $p+\Delta p$, where p is the ideal momentum,
the equilibrium orbit within the synchrotron is given by (x_2, x'_2)
$= (D\Delta p/p, D'\Delta p/p)$, where D is the dispersion function of the
accelerator. The distribution of momenta $\Delta p/p$ is assumed to be
Gaussian with a mean of zero and a variance σ_p^2. The quantity δ
is defined by

$$\Delta p/p = \sigma_p \delta.$$

Thus, for a particular momentum, the ideal trajectory within the
synchrotron is located at the phase space point

$$(x_2, \varsigma_2) = (D\sigma_p\delta, \Lambda\sigma_p\delta) \quad \text{where } \Lambda \equiv \beta D' + \alpha D .$$

The displacement of the trajectory of a particle of momentum
$p+\sigma_p\delta$ about its respective ideal orbit may be written in terms of

$$\xi = x_2 - D\sigma_p\delta \quad \text{and} \quad \eta = \varsigma - \Lambda\sigma_p\delta.$$

Figure V-2

Particle Distribution Resulting From Position Mismatch
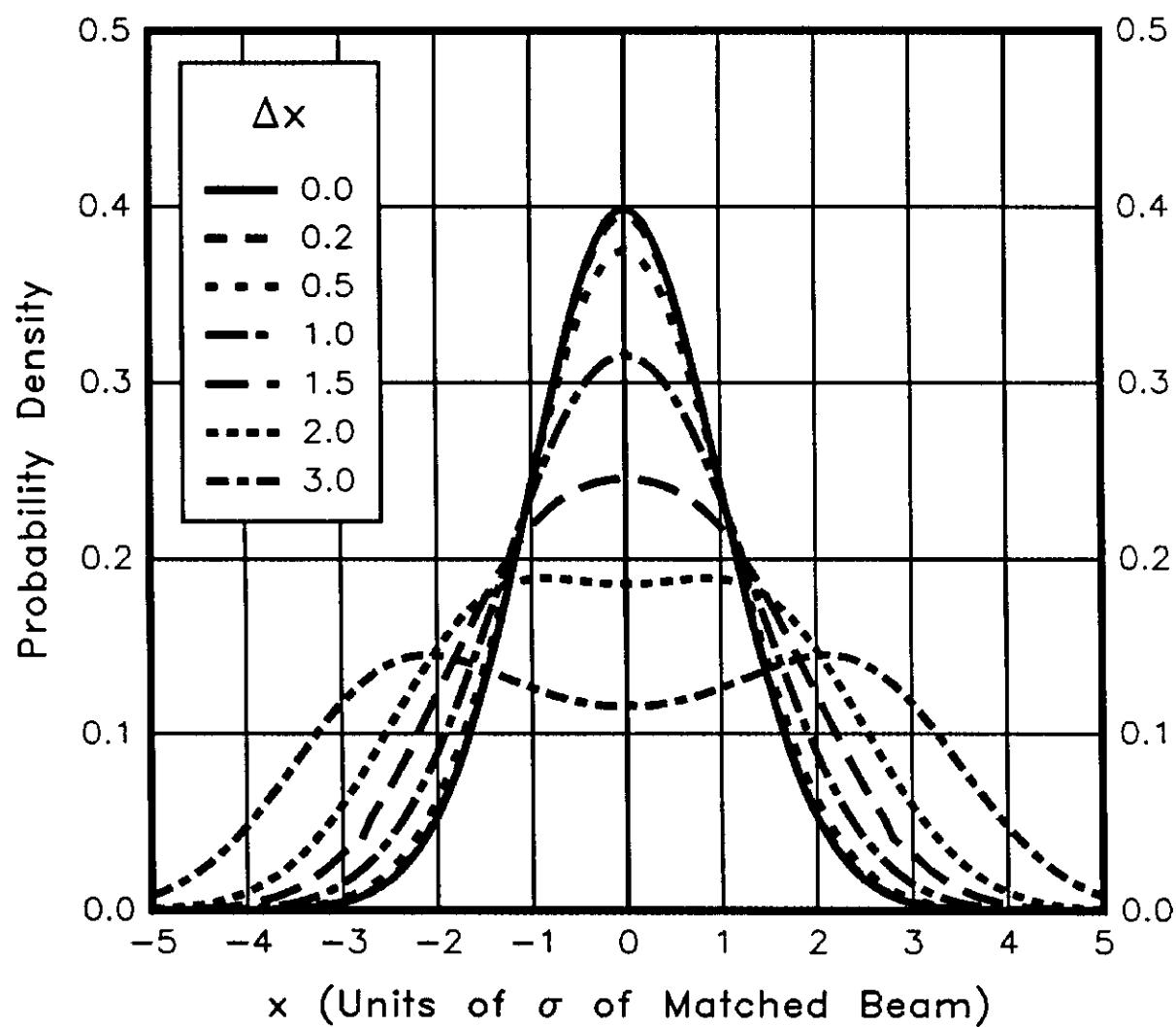
Figure V-3

Dilution of 95% Phase Space Area
Resulting From Position Mismatch
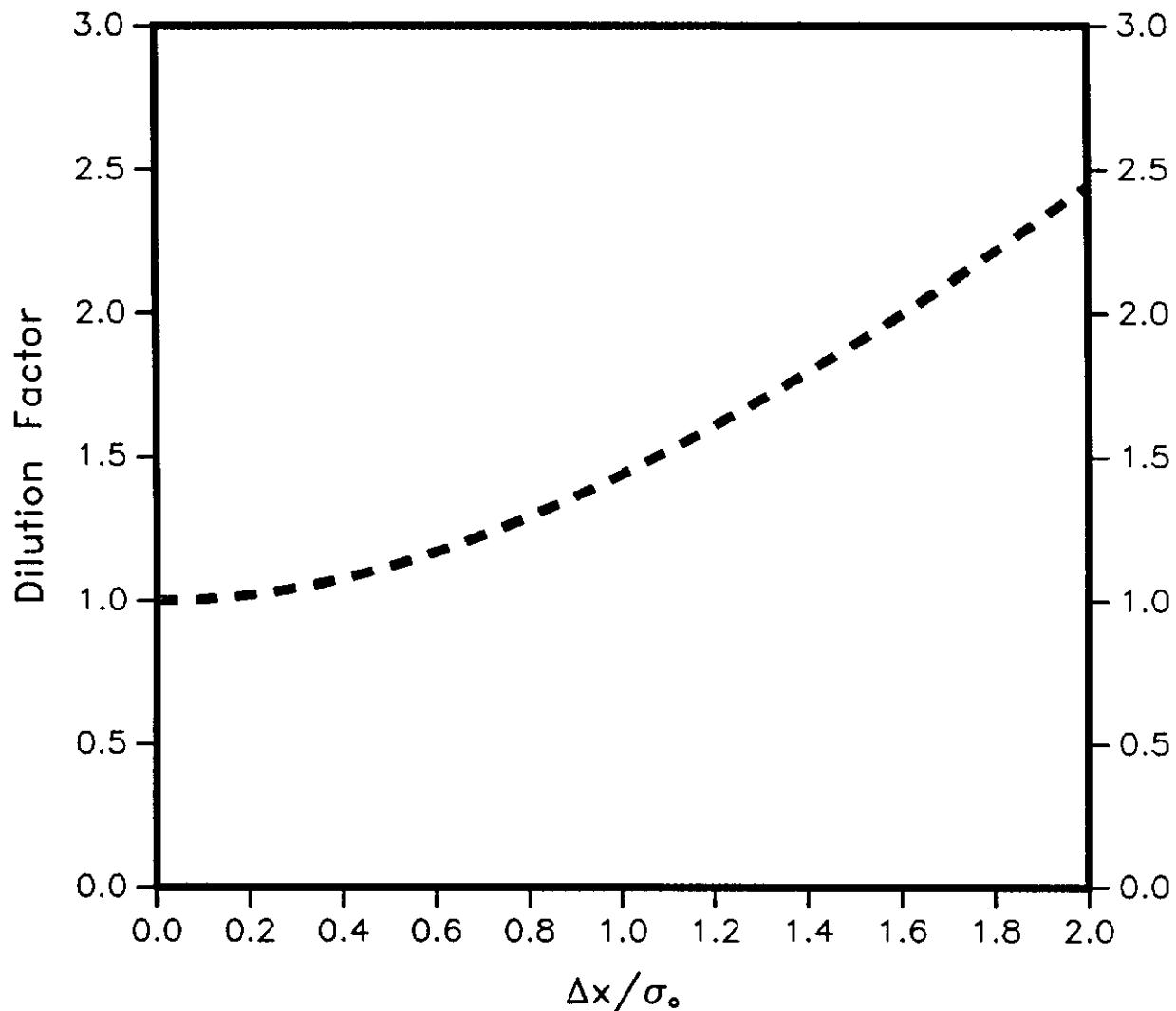
Because a mismatch of the dispersion function may be thought of as a steering error for off-momentum particles, the results of the last section may be used. The dispersion function delivered by the beamline, and its slope, may be written as

$$D_2 = D_1 + \Delta D, \quad \text{and} \quad D'_2 = D'_1 + \Delta D'.$$

As before, an equivalent mismatch of the dispersion function alone may be defined, namely

$$\Delta D_{eq} \equiv (\Delta D^2 + (\beta \Delta D' + \alpha \Delta D)^2)^{1/2}.$$

From now on, ΔD is used to represent ΔD_{eq}. Using these definitions, the resulting time average distribution of particles of momentum $p + \sigma_p \delta$ due to a mismatch of the dispersion function by an amount ΔD is

$$n_\delta(\xi) \, d\xi = \frac{d\xi}{\pi} \int_{|\xi|}^{\infty} e^{-(a-|\Delta \xi|)^2/2} \frac{e^{-|a\Delta\xi|} I_0(a\Delta\xi)}{\sqrt{1 - (\xi/a)^2}} \, da$$

where $\Delta\xi = \Delta D \sigma_p \delta$. In the above equation, the distribution is normalized to the number of particles with momentum $p + \sigma_p \delta$. By integrating over the entire momentum distribution, the resulting time average distribution in x is found to be

$$n_D(x) \, dx = dx \int_{-\infty}^{+\infty} n_\delta(x) \frac{1}{\sqrt{2\pi}} e^{-\delta^2/2} \, d\delta$$

$$= \frac{dx}{\sqrt{2\pi^3}} \int_{-\infty}^{+\infty} \int_{|x-D\sigma_p\delta|}^{+\infty} e^{-\delta^2/2} e^{-(a-|\Delta D\sigma_p\delta|)^2/2} \frac{e^{-|a\Delta D\sigma_p\delta|} I_0(a\Delta D\sigma_p\delta)}{\sqrt{1 - \left(\frac{x-D\sigma_p\delta}{a}\right)^2}} \, da \, d\delta.$$

Here, $D = D_2$ is the dispersion function of the synchrotron.

The phase space dilution factor is given by $F_D = a_{95}^2/6$ where

$$\frac{1}{\sqrt{2\pi}} \int_0^{a_{95}} \int_{-\infty}^{+\infty} e^{-\delta^2/2} \, e^{-(r-|\Delta D\sigma_p\delta)^2/2} \left[e^{-|r\Delta D\sigma_p\delta|} I_o(r\Delta D\sigma_p\delta) \right] r d\delta dr$$

$$= 0.95 \quad .$$

Once again, for $\Delta D = 0$, $a_{95}^2 = 6$ and $F_D = 1$. Also, for $\Delta D = 0$, the distribution n_D becomes

$$n_D(x) \, dx = \frac{1}{\sqrt{2\pi(1+D^2\sigma_p^2)}} \, e^{-x^2/2(1+D^2\sigma_p^2)} \, dx$$

which is a Gaussian distribution with variance $\sigma^2 = 1 + D^2\sigma_p^2$. (Note that $1 = \sigma_o^2 = \epsilon_o\beta_o/6\pi$.) As mentioned in Chapter IV, the variance of the beam distribution at a location in the beamline or synchrotron where the dispersion function is nonzero is given by $\sigma^2 = \sigma_t^2 + D^2\sigma_p^2$ where σ_t is due to the transverse emittance alone. The result of a dispersion function mismatch is to increase the transverse emittance and hence increase σ_t. By studying the resulting time average distribution at a location in the accelerator where $D = 0$, the variance of the distribution at a location where D is nonzero will be given by $D^2\sigma_p^2$ + the variance of $n_D(D=0)$.

Figure V-4 shows the distribution $n_D(D=0)$ for several values of dispersion mismatch. The dilution factor due to a dispersion mismatch is displayed in Figure V-5. The severity of the emittance dilution depends upon both ΔD and σ_p as it must. If all of the particles are of the exact same momentum, the beam

Figure V-4

Particle Distribution Resulting From Dispersion Mismatch

(At Point Where Machine Dispersion = 0.0)

Figure V-5

Dilution of 95% Phase Space Area
Resulting From Dispersion Function Mismatch
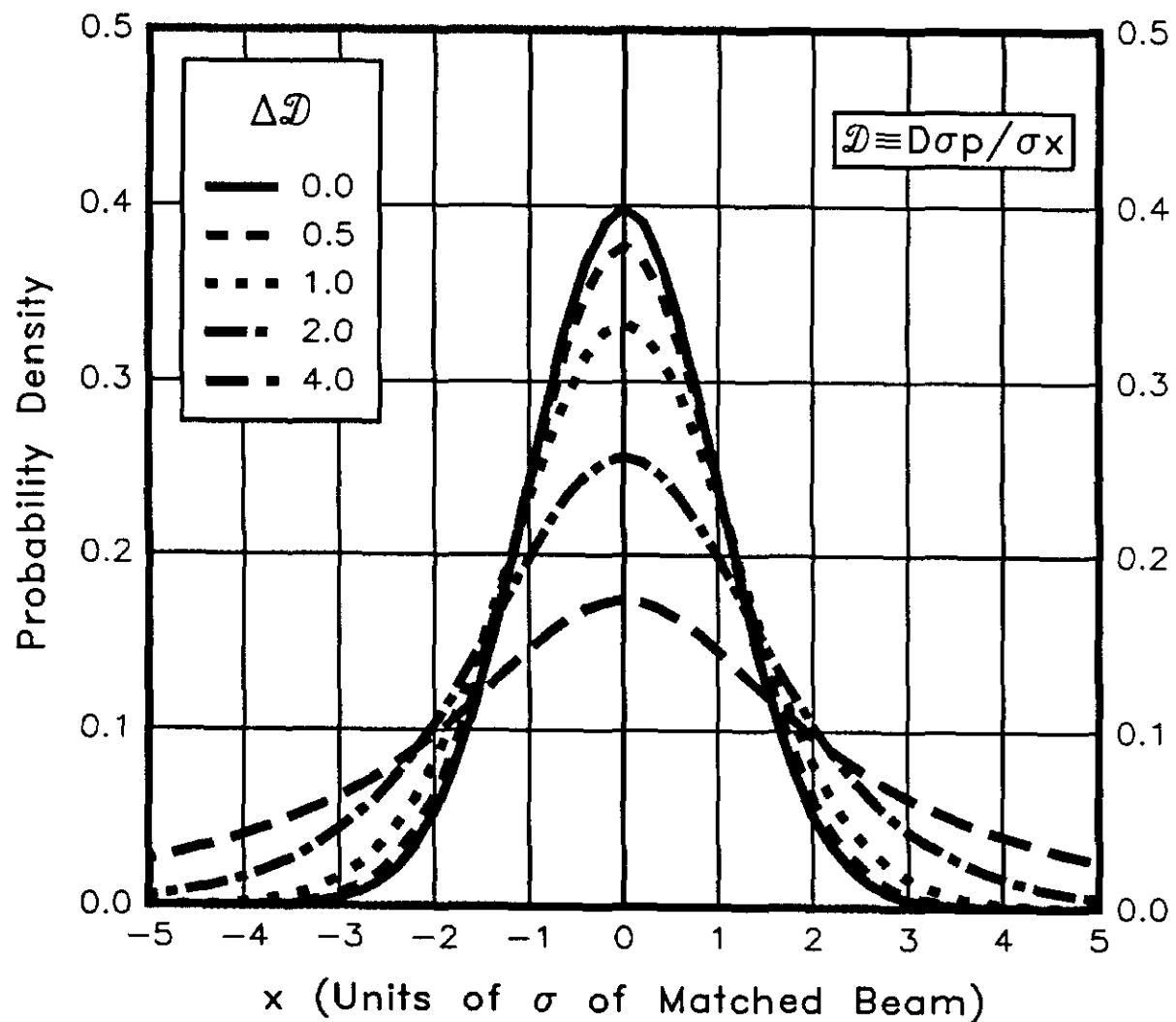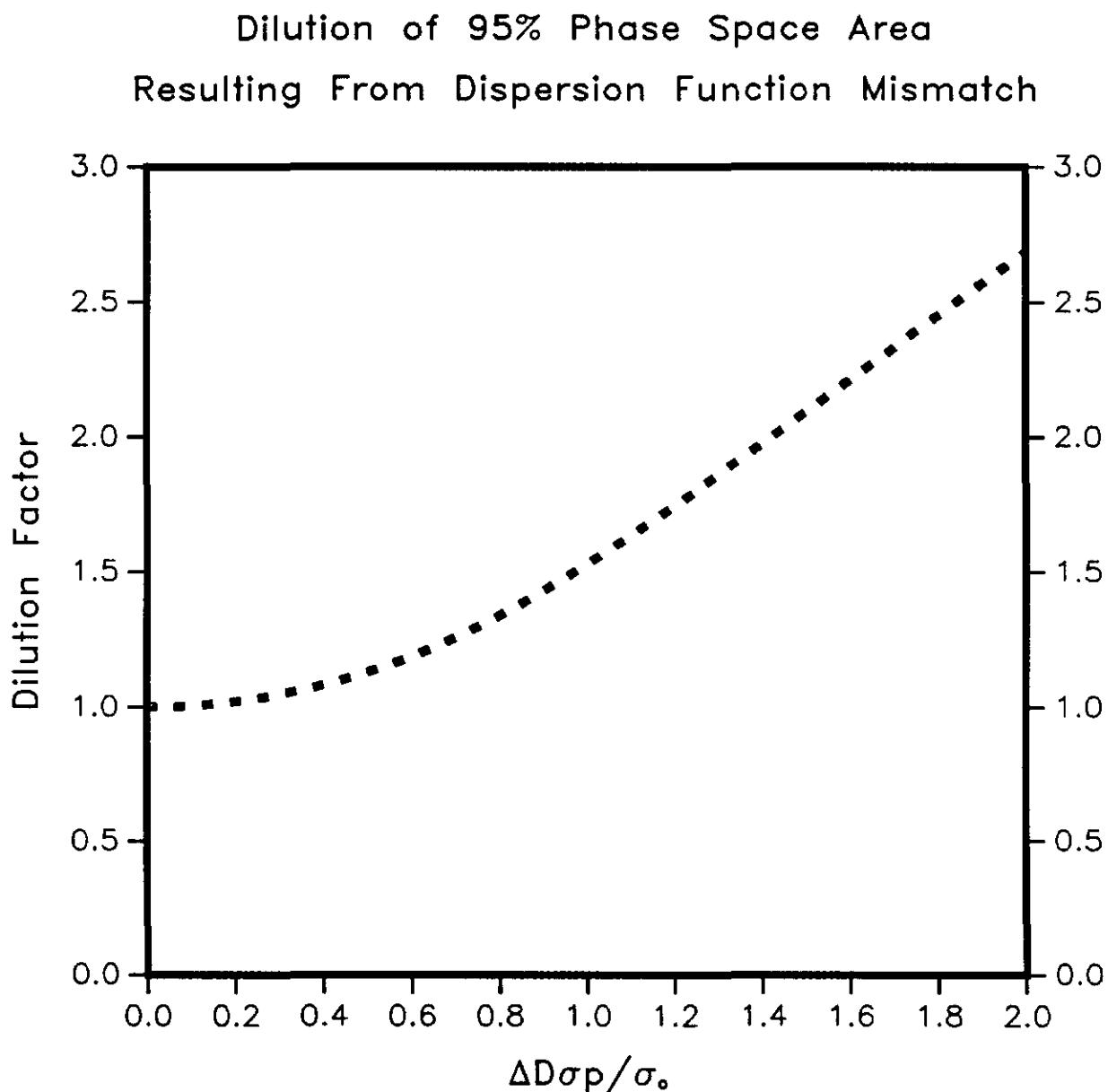
size would not increase no matter how large a value for ΔD is obtained. Likewise, any small deviation from the ideal dispersion function significantly affects the emittance of a beam which has a large enough momentum spread. Even for values of $\Delta D \sigma_p$ as large as 1.5, the variance of the resulting time average distribution provides a good estimate of the dilution factor F_D.

To remind the reader, the quantities Δx and $\Delta D \sigma_p$ used in these discussions are in units of $\sigma_o = (\epsilon_o \beta_o / 6\pi)^{1/2}$ of the ideally matched beam. Thus, for a beam that is inherently large upon entrance to the synchrotron, the effects of mismatches due to steering and dispersion function errors actually may be small.

Amplitude Function Mismatch

For this case, the ideal trajectory as well as the dispersion functions of the beamline are assumed to be matched to the synchrotron: $x_1 = x_2 = x$, $x'_1 = x'_2 = x'$, $D_1 = D_2$, and $D'_1 = D'_2$. Since $\varsigma_1 = \alpha_1 x + \beta x'$ and $\varsigma_2 = \alpha_2 x + x'$ ($\beta \equiv \beta_1$ in units of β_o, and $\beta_2 = \beta_o = 1$), then x_1 and ς_1 may be written in terms of x_2 and ς_2:

$$x_1 = x_2 \quad ,$$
$$\varsigma_1 = (\alpha_1 - \beta\alpha_2)x_2 + \beta\varsigma_2 \; .$$

The equation of a particle trajectory in terms of the beamline phase space coordinates is

$$x_1^2 + \varsigma_1^2 = \beta A^2$$

which, in terms of the synchrotron system, will be

$$x_2^2 + [\; (\alpha_1 - \beta\alpha_2)x_2 + \beta\varsigma_2 \;]^2 = \beta A^2$$

or,

$$[\; 1 + (\alpha_1 - \beta\alpha_2)^2 \;]x_2^2 + 2\beta(\alpha_1 - \beta\alpha_2)x_2\varsigma_2 + \beta^2\varsigma_2^2 = \beta A^2$$

which is the equation of an ellipse. Thus, the incoming particle distribution resulting from a mismatch of the amplitude function and its slope will have the appearance depicted in Figure V-6.

To make the distribution symmetric about the x-axis, the x_2-ς_2 coordinate system may be rotated through an angle θ given by

$$\tan 2\theta = \frac{2\beta(\alpha_1 - \beta\alpha_2)}{1 + (\alpha_1 - \beta\alpha_2)^2 - \beta^2} \quad .$$

Using $\omega \equiv \alpha_1 - \beta\alpha_2$, the axes of the ellipse are of lengths

$$m_1 = \left[\frac{\beta A^2}{\cos^2\theta\left[1 + (\omega+\beta\tan\theta)^2\right]} \right]^{1/2} \quad , \quad m_2 = \left[\frac{\beta A^2}{\sin^2\theta\left[1 + (\omega-\beta\cot\theta)^2\right]} \right]^{1/2} \quad .$$

If the beamline and synchrotron are perfectly matched, then $\beta \to 1$ and $\alpha_1 \to \alpha_2$ which implies $m_1 = m_2 = A$. (θ cannot be determined.) The special case where $\beta \neq 1$ and $\alpha_1 = \alpha_2 = 0$ corresponds to $\theta = 0$ and $m_1 = (\beta A^2)^{1/2}$, $m_2 = (A^2/\beta)^{1/2}$. Therefore the calculation of the dilution factor and time average particle distribution resulting from a mismatch of the amplitude function and its slope can be reduced to the problem of a mismatch of an "equivalent" amplitude function at a point where its slope is zero. The equivalent amplitude function may thus be defined by

$$\beta_{eq} = \frac{\beta}{\cos^2\theta\left[1 + [(\alpha_1-\beta\alpha_2) + \beta\tan\theta]^2\right]} \quad .$$

For the remainder of this discussion, β is used to represent β_{eq}.

The initial distribution of particles delivered by the beamline due to a mismatch of the equivalent amplitude function

Figure V-6

Example of Initial Particle Distribution
Resulting From Amplitude Function Mismatch
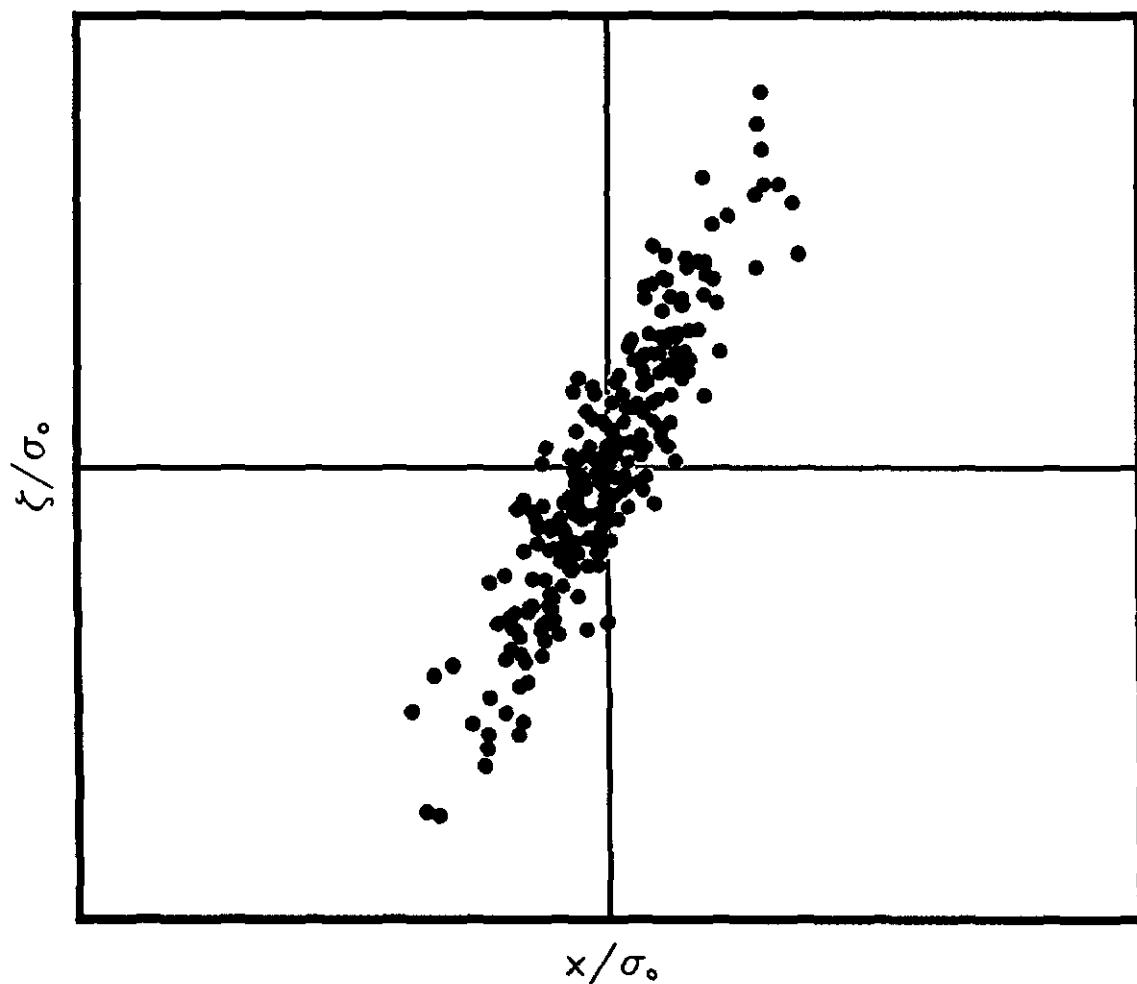
may now be obtained. Since the particle distribution in x_1-ς_1 phase space is

$$n(x_1,\varsigma_1) \; dx_1 \; d\varsigma_1 \; = \; \frac{N \; e^{-\left[x_1^{\,2} + \varsigma_1^{\,2}\right]/2\sigma_1^{\,2}}}{2\pi\sigma_1^{\,2}} \; dx_1 \; d\varsigma_1 \quad ,$$

then using the fact that $dx_1 d\varsigma_1 = \beta dx_2 d\varsigma_2$ along with

$$\epsilon_o = 6\pi\sigma_1^2/\beta = 6\pi\sigma_o^2 \quad ,$$

and $\varsigma_1 = \beta\varsigma_2$ (because $\alpha_1 = \alpha_2 = 0$ in the "equivalent" mismatch case), the particle distribution in x_2-ς_2 phase space is

$$n_o(x_2,\varsigma_2) \; dx_2 \; d\varsigma_2 \; = \; \frac{e^{-\left[x_2^{\,2} + \beta^2\varsigma_2^{\,2}\right]/2\beta}}{2\pi\beta} \; \beta \; dx_2 \; d\varsigma_2$$

or, rewritten with subscripts suppressed,

$$n_o(x,\varsigma) \; dx \; d\varsigma \; = \; \left(\frac{e^{-x^2/2\beta}}{\sqrt{2\pi\beta}} \right) \left(\frac{e^{-\beta\varsigma^2/2}}{\sqrt{2\pi/\beta}} \right) \; dx \; d\varsigma \quad .$$

Upon transforming to polar coordinates, the integral for the resulting time average distribution due to an amplitude function mismatch becomes

$$n_\beta(x) \; dx \quad = \; \frac{dx}{2\pi^2} \int_{|x|}^{\infty} \int_{0}^{2\pi} \frac{e^{-\frac{a^2}{2\beta}\left[\cos^2\theta + \beta^2\sin^2\theta\right]}}{\sqrt{1 - (x/a)^2}} \; d\theta \; da$$

or,

$$n_\beta(x) \, dx \; = \; \frac{dx}{\pi} \int_{|x|}^{+\infty} e^{-a^2/2\beta} \frac{e^{-\left(\frac{a^2}{4} \frac{\beta^2-1}{\beta}\right)}}{\sqrt{1 - (x/a)^2}} I_o\left[\frac{a^2}{4} \frac{\beta^2-1}{\beta}\right] \; da \, .$$

To obtain the dilution factor, $F_\beta = a_{95}^2/6$, a_{95} must satisfy

$$\int_0^{a_{95}} e^{-\frac{r^2}{2\beta}} \, e^{-\left(\frac{r^2}{4} \frac{\beta^2-1}{\beta}\right)} \, I_o\left[\frac{r^2}{4} \frac{\beta^2-1}{\beta}\right] \, r \, dr = 0.95 \; .$$

Figures V-7 and V-8 show the dilution factor F_β and the resulting distribution n_β respectively. To more closely resemble the corresponding figures for position and dispersion mismatches, Figures V-7 and V-8 plot $\Delta\beta/\beta \equiv (\beta_1-\beta_2)/\beta_2 = (\beta-\beta_o)/\beta_o = \beta-1$ along the horizontal axis. As can be seen from the second figure, the amplitude function must be greatly mismatched to produce a significant increase in the variance of the distribution.

The expression for β_{eq} contained the angle of rotation θ which may be found in terms of the values of β and α of the beamline and the synchrotron. By combining these results, a simple expression for β_{eq} in terms of β_1, α_1, β_2, and α_2 may be obtained. Since the value $\tan2\theta$ is given by

$$\tan2\theta = \frac{2\beta(\alpha_1 - \beta\alpha_2)}{1 + (\alpha_1 - \beta\alpha_2)^2 - \beta^2}$$

then $\sin2\theta$ and $\cos2\theta$ may be written as

$$\sin2\theta = Y/R \quad \text{and} \quad \cos2\theta = X/R \; ,$$

where

$$Y = 2\beta(\alpha_1 - \beta\alpha_2)$$
$$X = 1 + (\alpha_1 - \beta\alpha_2)^2 - \beta^2$$

and

$$R^2 = [2\beta(\alpha_1 - \beta\alpha_2)]^2 + [1 + (\alpha_1 - \beta\alpha_2)^2 - \beta^2]^2.$$
$$= [1 + (\alpha_1 - \beta\alpha_2)^2 + \beta^2]^2 - 4\beta^2 \; .$$

Since the equation of the particle trajectory in $x_2-\varsigma_2$ space is

Figure V-7

Dilution of 95% Phase Space Area
Resulting From Amplitude Function Mismatch

Figure V-8

Particle Distribution Resulting From Beta Mismatch
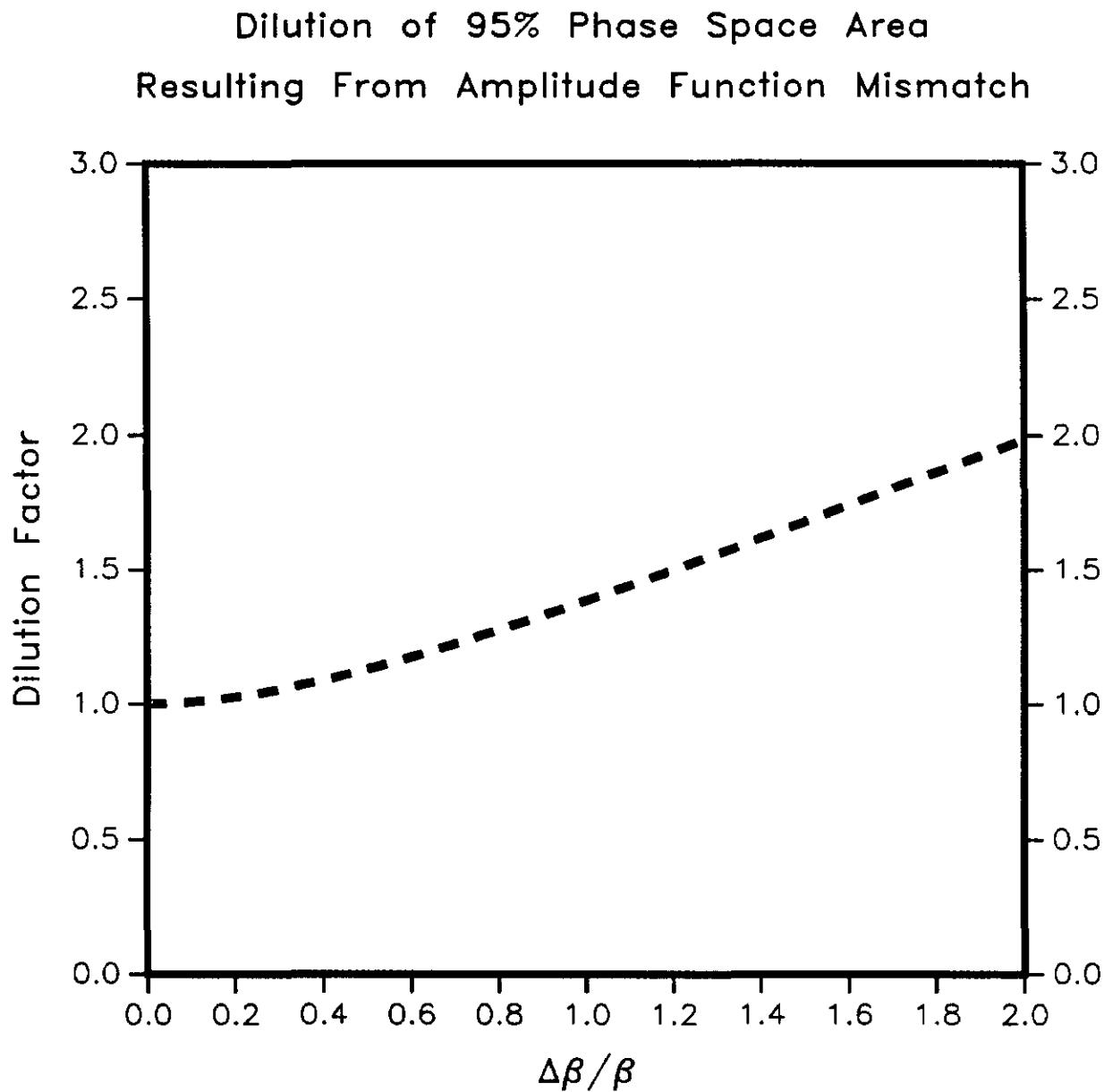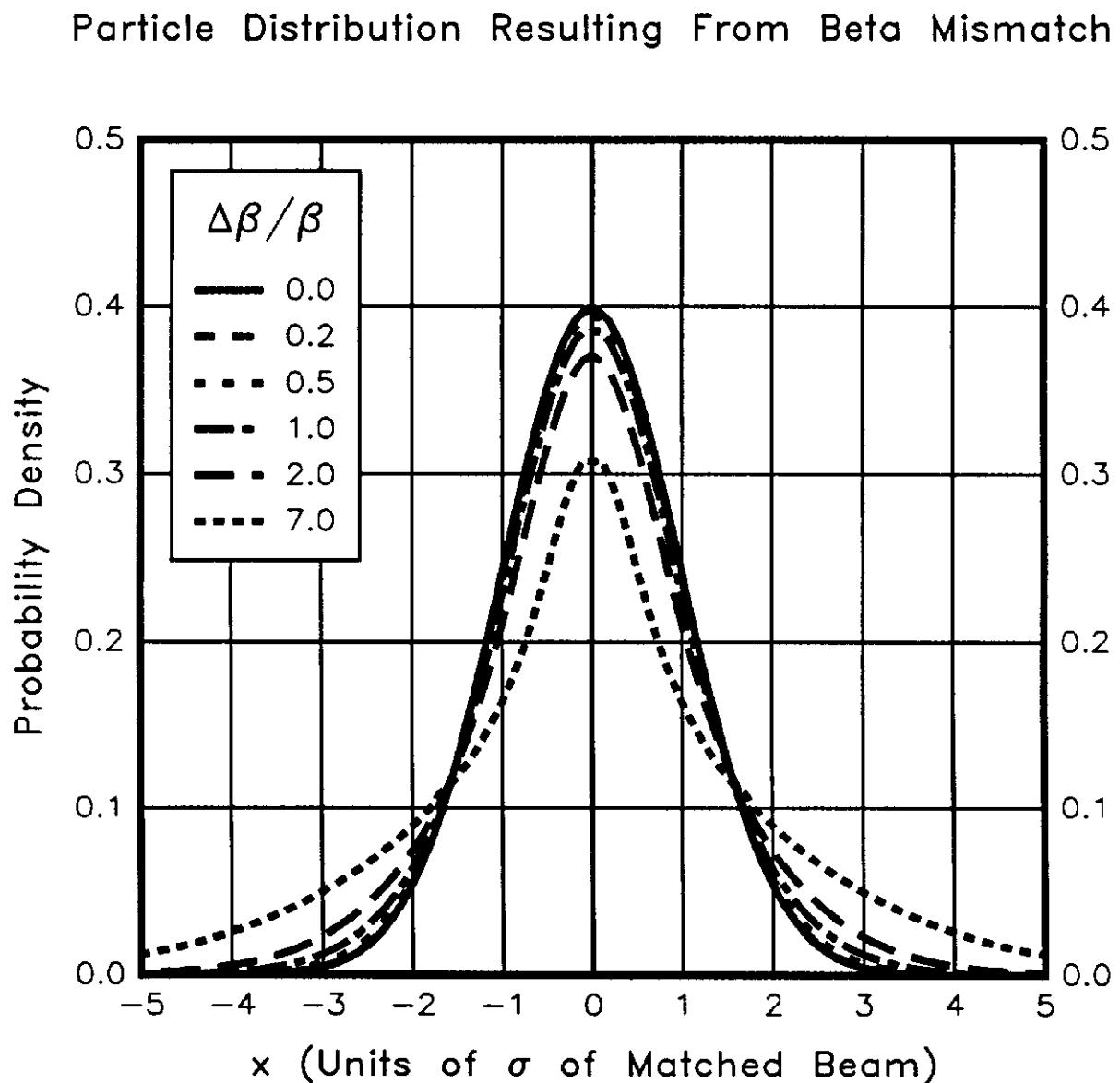
given by

$$[\ 1\ +\ (\alpha_1\ -\ \beta\alpha_2)^2\ ]x_2^2\ +\ 2\beta(\alpha_1\ -\ \beta\alpha_2)x_2\varsigma_2\ +\ \beta^2\varsigma_2^2\ =\ \beta A^2$$

or,

$$a\ x_2^2\ +\ 2b\ x_2\varsigma_2\ +\ c\ \varsigma_2^2\ =\ \beta A^2,$$

then upon rotating through the angle θ, the new coordinates ξ,η will satisfy

$$(a\cos^2\theta\ +\ 2b\cos\theta\sin\theta\ +\ c\sin^2\theta)\xi^2\ +$$

$$(a\sin^2\theta\ -\ 2b\cos\theta\sin\theta\ +\ c\cos^2\theta)\eta^2\ \equiv\ A'\xi^2\ +\ B'\eta^2\ =\ \beta A^2.$$

By inserting the expressions for $\sin 2\theta$ and $\cos 2\theta$ into the above equation along with the expressions for a, b, and c, the quantities A' and B' reduce to

$$A'\ =\ (1\ +\ (\alpha_1\ -\ \beta\alpha_2)^2\ +\ \beta^2\ +\ R)/2\ ,$$

$$B'\ =\ (1\ +\ (\alpha_1\ -\ \beta\alpha_2)^2\ +\ \beta^2\ -\ R)/2\ .$$

By noting that

$$\begin{aligned}
1\ +\ (\alpha_1\ -\ \beta\alpha_2)^2\ +\ \beta^2\ &=\ 1\ +\ \beta^2\ +\ \alpha_1^2\ +\ \beta^2\alpha_2^2\ -\ 2\alpha_1\alpha_2\beta \\
&=\ \beta(\beta\ +\ 1/\beta\ +\ \alpha_1^2/\beta\ +\ \beta\alpha_2^2\ -\ 2\alpha_1\alpha_2) \\
&=\ \beta[\beta(1\ +\ \alpha_2^2)\ +\ (1\ +\ \alpha_1^2)/\beta\ -\ 2\alpha_1\alpha_2] \\
&=\ \beta(\beta_1\gamma_2\ +\ \beta_2\gamma_1\ -\ 2\alpha_1\alpha_2) \\
&\equiv\ \beta(2D)\ ,
\end{aligned}$$

and hence

$$R^2\ =\ 4\beta^2 D^2\ -\ 4\beta^2\ =\ 4\beta^2(D^2\ -\ 1)\ ,$$

the expression for A' reduces to

$$A'\ =\ \beta[D\ +\ (D^2\ -\ 1)^{1/2}]\ .$$

(D is not to be confused with the dispersion function.)

Because A' is of the form $u + v$ and B' is of the form $u - v$, then

$$A'B'\ =\ u^2\ -\ v^2\ =\ \beta^2 D^2\ -\ \beta^2(D^2\ -1)\ =\ \beta^2$$

which implies $(A'/\beta)\ =\ (\beta/B')$.

So, finally, the equation of the particle trajectory in the rotated coordinate system becomes

$$A'\xi^2 + B'\eta^2 = A'\xi^2 + (\beta^2/A')\eta^2 = \beta A^2$$

or,

$$(A'/\beta)\xi^2 + (\beta/A')\eta^2 = A^2$$

which is an ellipse with axes of lengths

$$m_1 = (A^2\beta/A')^{1/2} \equiv (A^2/\beta_{eq})^{1/2}$$

$$\text{and } m_2 = (A^2A'/\beta)^{1/2} \equiv (\beta_{eq}A^2)^{1/2} .$$

This suggests a new definition of β_{eq} in terms of the values of α and β delivered by the beamline and the natural values of α and β of the synchrotron, namely,

$$\beta_{eq} = D + (D^2 - 1)^{1/2}$$

where

$$D = (\beta_2\gamma_1 + \beta_1\gamma_2 - 2\alpha_1\alpha_2)/2.$$

The significance of the quantity D may be seen by computing the determinant of the matrix ΔJ where J contains the Courant-Snyder parameters as defined in Chapter III:

$$\det(\Delta J) = -(\alpha_2 - \alpha_1)^2 + (\gamma_2 - \gamma_1)(\beta_2 - \beta_1)$$

$$= -[\alpha_2^2 - 2\alpha_1\alpha_2 + \alpha_1^2 - \gamma_2\beta_2 + \gamma_1\beta_2 + \gamma_2\beta_1 - \gamma_1\beta_1]$$

$$= -[-1 - 2\alpha_1\alpha_2 - 1 + \gamma_1\beta_2 + \gamma_2\beta_1]$$

$$= -2D + 2 ,$$

or,

$$D = 1 - \det(\Delta J)/2 .$$

The quantity $-\det(\Delta J)$ is positive definite and may be reduced to the form

$$-\det(\Delta J) = \frac{\left(\frac{\Delta\beta}{\beta}\right)^2 + \left(\Delta\alpha - \alpha\frac{\Delta\beta}{\beta}\right)^2}{1 + \frac{\Delta\beta}{\beta}} \geq 0 .$$

This quantity is also an invariant. Suppose M is the 2 x 2 transport matrix from point s_a to point s_b. Then, as shown in Chapter III, $J_b = MJ_aM^{-1}$. If now J_a is altered by an amount ΔJ_a, then

$$J'_b = M(J_a + \Delta J_a)M^{-1} = MJ_aM^{-1} + M\Delta J_aM^{-1}$$

which implies

$$\Delta J_b = J'_b - J_b = M\Delta J_aM^{-1}$$

and so $\det(\Delta J_b) = \det(M) \ \det(\Delta J_a) \ \det(M^{-1})$

$$= \det(\Delta J_a).$$

Thus $\det(\Delta J)$ is invariant with s. This implies that the degree of mismatch due to amplitude functions may be measured at any point within the synchrotron, not just at the "injection point."

General Expressions for the Variances of Particle Distributions After Dilution

Using a simple statistical argument the resulting variance after dilution of an initially mismatched particle beam may be derived. The variances obtained with this method agree with the variances of the distributions arrived at by the straightforward method of the previous sections and allows one to write down simple formulas for the variances of the resulting time average distributions.

Given a particle with phase space amplitude a determined by the initial phase space coordinates x_0, ς_0, the subsequent motion in phase space is defined by the circle $x^2 + \varsigma^2 = a^2$. A distribution of particles of the form $g(x,\varsigma) = f(x)f(\varsigma)$ will have $\langle x^2 \rangle = \langle \varsigma^2 \rangle$. Since $\langle x^2 \rangle + \langle \varsigma^2 \rangle = a^2$, then $\langle x^2 \rangle = \langle \varsigma^2 \rangle = a^2/2$.

Therefore, a single particle with initial coordinates corresponding to amplitude a will provide a contribution of $a^2/2$ to the variance of the resulting time average distribution in x.

An initial distribution having a variance of σ_o^2 and which has rotational symmetry about the point $(\Delta x, 0)$ is of the form

$$n_o(\rho, \phi) = f(\rho)/2\pi$$

where the distance from the point $(\Delta x, 0)$ is denoted by ρ and the angle ϕ is the angle between the x axis and the line segment of length ρ, as shown in Figure V-9. The distance a from the origin of a particle with coordinates ρ and ϕ is thus given by

$$a^2 = \rho^2 + \Delta x^2 - 2\rho\Delta x \cos\phi \ .$$

The final variance of the distribution in x averaged over a long period of time will then be

$$\sigma^2 \equiv \langle x^2 \rangle = \int (a^2/2) n_o d\Sigma = \int (\rho^2/2) n_o d\Sigma + \int (\Delta x^2/2) n_o d\Sigma - \int \rho\Delta x \cos\phi d\Sigma$$

where $d\Sigma$ is the differential element of area in x-ς phase space. Therefore,

$$\sigma^2 = (2\sigma_o^2)/2 + \Delta x^2/2 - (\Delta x/2\pi) \int \rho^2 f(\rho) d\rho \int \cos\phi d\phi$$

$$= \sigma_o^2 + \Delta x^2/2$$

or,

$$\sigma^2 = 1 + \Delta x^2/2 \ ,$$

where σ and Δx are in units of σ_o. This is the expression for the variance of the distribution resulting from a position mismatch of the ideal trajectory and is in agreement with the distributions displayed in Figure V-2.

In exact analogy the resulting variance due to a mismatch of the dispersion function may be obtained. Since ΔD corresponds to an initial position error of $\Delta D \sigma_p \delta$ for a particle of momentum

Figure V-9

Definition of ρ, φ
For Position Mismatch
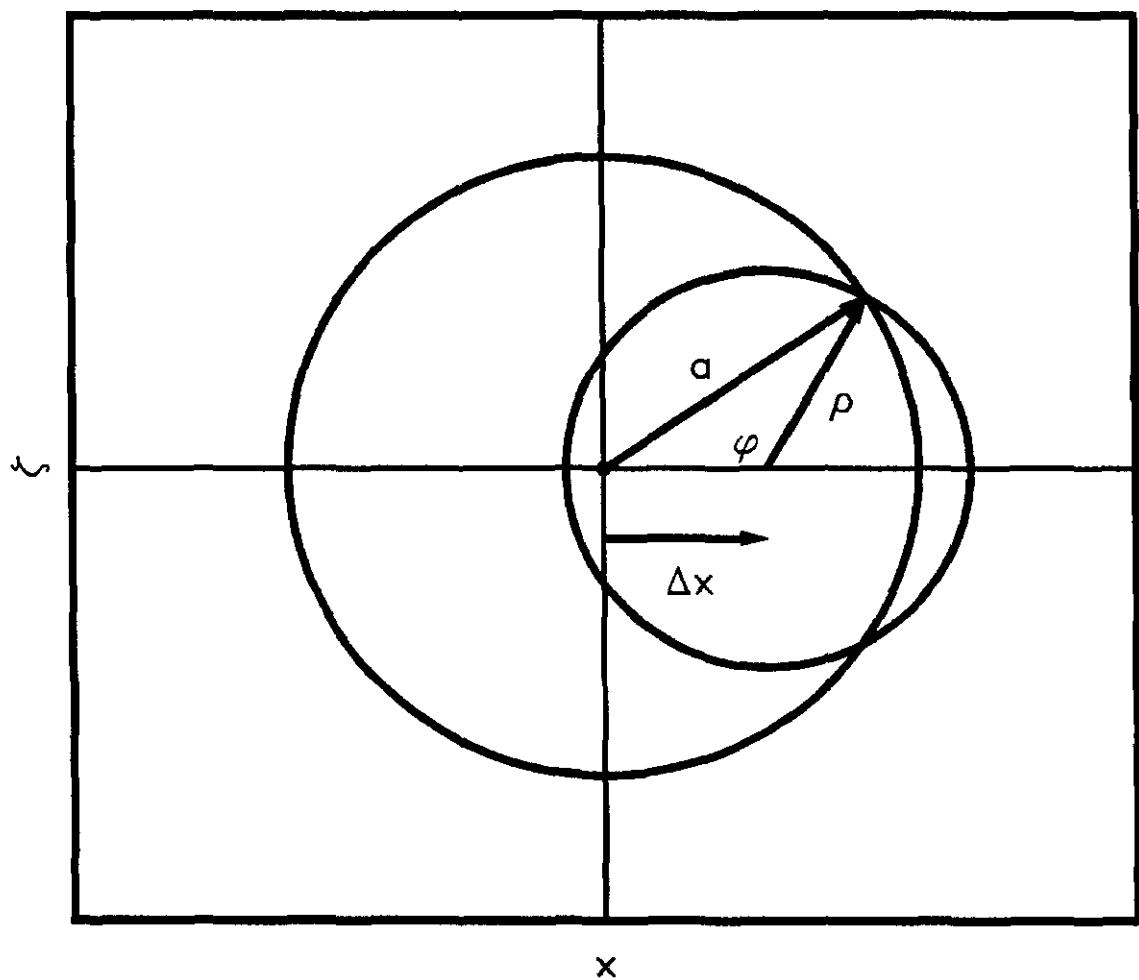
$p+\sigma_p\delta$, $\langle\xi^2\rangle = 1 + (\Delta D\sigma_p\delta)^2/2$, using the expression from the preceding paragraph. The position relative to the origin for a particle of momentum $p+\sigma_p\delta$ is given by $x_\delta = \xi + D\sigma_p\delta$ and thus

$$x_\delta^2 = \xi^2 + 2D\sigma_p\delta\xi + D^2\sigma_p^2\delta^2,$$

which yields

$$\langle x_\delta^2\rangle = \langle\xi^2\rangle + D^2\sigma_p^2\delta^2 = 1 + (\Delta D\sigma_p)^2\delta^2/2 + D^2\sigma_p^2\delta^2$$

since $\langle\xi\rangle = 0$. Therefore, upon averaging over momentum,

$$\langle x^2\rangle \equiv \sigma^2 = 1 + (\Delta D\sigma_p)^2/2 + D^2\sigma_p^2 .$$

Again, σ and $D\sigma_p$ are in units of σ_o. This expression again agrees with the distributions obtained earlier and shown in Figure V-4.

For an amplitude function mismatch the initial distribution was written as

$$n_o(x,\varsigma)\ dx\ d\varsigma = \left[\frac{e^{-x^2/2\beta}}{\sqrt{2\pi\beta}}\right]\left[\frac{e^{-\beta\varsigma^2/2}}{\sqrt{2\pi/\beta}}\right] dx\ d\varsigma .$$

from which the variances $\langle x^2\rangle = \beta$ and $\langle\varsigma^2\rangle = 1/\beta$ are immediately evident. Given this initial distribution, the variance of the resulting time average distribution in x will be

$$\sigma^2 = \int (a^2/2)n_o d\Sigma = \int (x^2/2)n_o d\Sigma + \int (\varsigma^2/2)n_o d\Sigma$$

$$= \langle x^2\rangle/2 + \langle\varsigma^2\rangle/2 = \beta/2 + 1/2\beta = (\beta^2+1)/2\beta$$

$$= ([D+(D^2-1)^{1/2}]^2 + 1)/2[D+(D^2-1)^{1/2}] = D$$

where here, $D = (\beta_2\gamma_1 + \beta_1\gamma_2 - 2\alpha_1\alpha_2)/2$. Written in terms of $\Delta\beta/\beta = \beta-1$, the form of this final variance more closely resembles the form of the two variances found for position and dispersion mismatches, namely

$$\sigma^2 = 1 + \frac{1}{2}\left[\frac{\Delta\beta/\beta}{\sqrt{1 + \Delta\beta/\beta}}\right]^2 .$$

The variance σ^2 is in units of the variance of the matched beam, σ_0^2. Once again, this formula for the resulting variance agrees with the results of the earlier distribution calculations.

As the original definition of the phase space emittance was $\epsilon = 6\pi\sigma^2/\beta$ for a Gaussian distribution, a dilution factor could naively be defined as

$$\epsilon/\epsilon_0 = \sigma^2/\sigma_0^2$$

so long as the resulting distribution after dilution resembles a Gaussian. Therefore, the expressions for the variances presented above are compared with the functions F_x, F_D, and F_β derived earlier for small degrees of mismatch, as shown in Figure V-10. As can be seen, σ^2/σ_0^2 agrees with F reasonably well for the values of Δx, ΔD, and $\Delta\beta/\beta$ (all typically less than 1) which would normally be encountered in the 8 GeV beam transfer process examined in this thesis. Thus, the results of this section may be used to describe the emittance dilution generated by mismatches on the order of those generated by the 8 GeV Line.

Normalized Emittance and Adiabatic Shrinking

As two of the dilution factors derived in this chapter depend upon the original beam size, the variation in beam size with energy should be mentioned. According to classical mechanics, the action variable $J = \int pdq$ of periodic motion, where the integral is carried out over a complete period of libration, is an adiabatic invariant under slow changes to the system.[3] Because the energy of the particle beam is varied slowly, the action variable for the motion in one transverse degree of freedom may be written as

$$\int p_x dx = mc \int \gamma\beta_x \, dx = mc\gamma\beta \int x'dx = mc\gamma\beta\epsilon = \text{constant}.$$

Figure V-10

Comparison of Variances with Dilution Factors
(a) Positon Mismatch
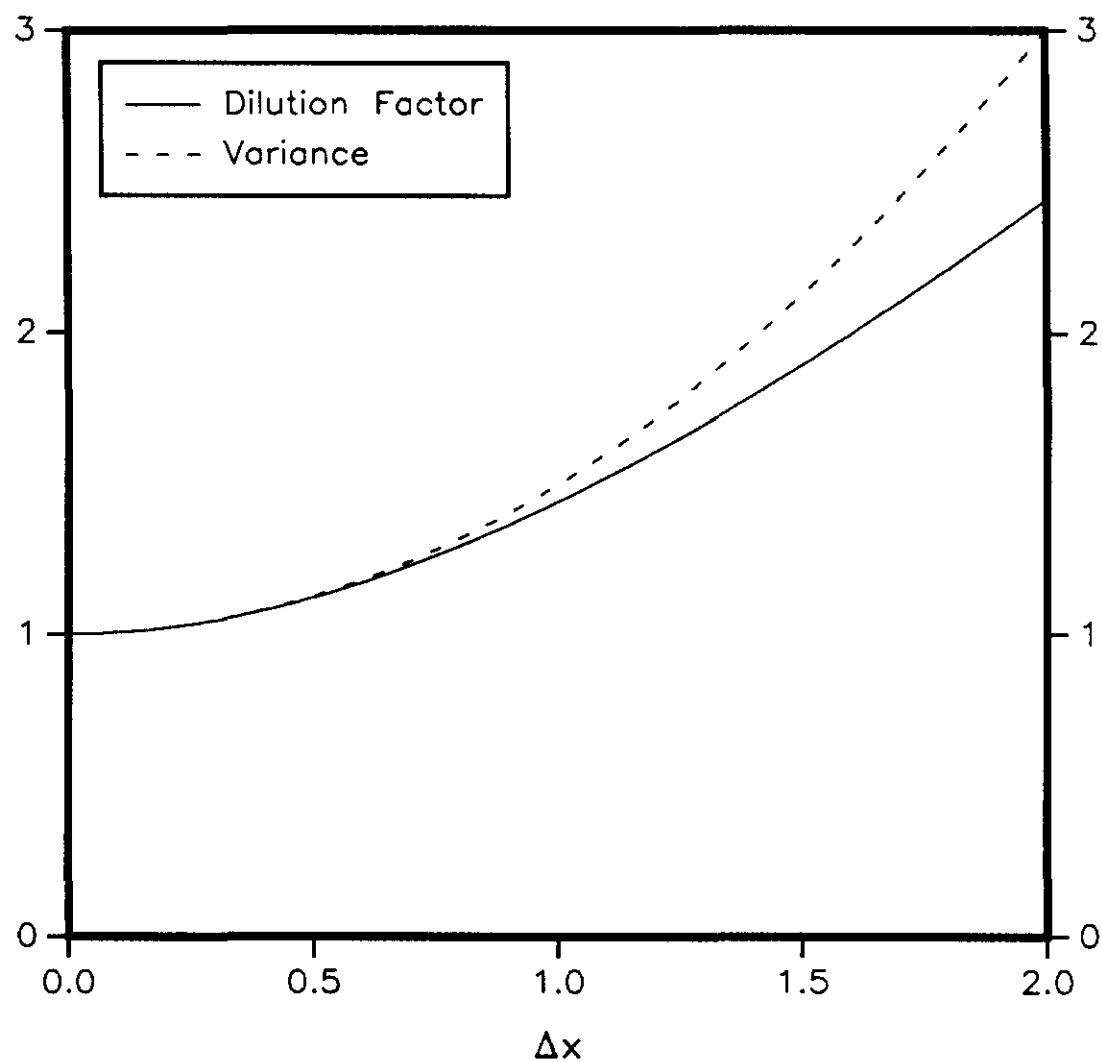
Figure V-10 (Continued)

(b) Dispersion Function Mismatch
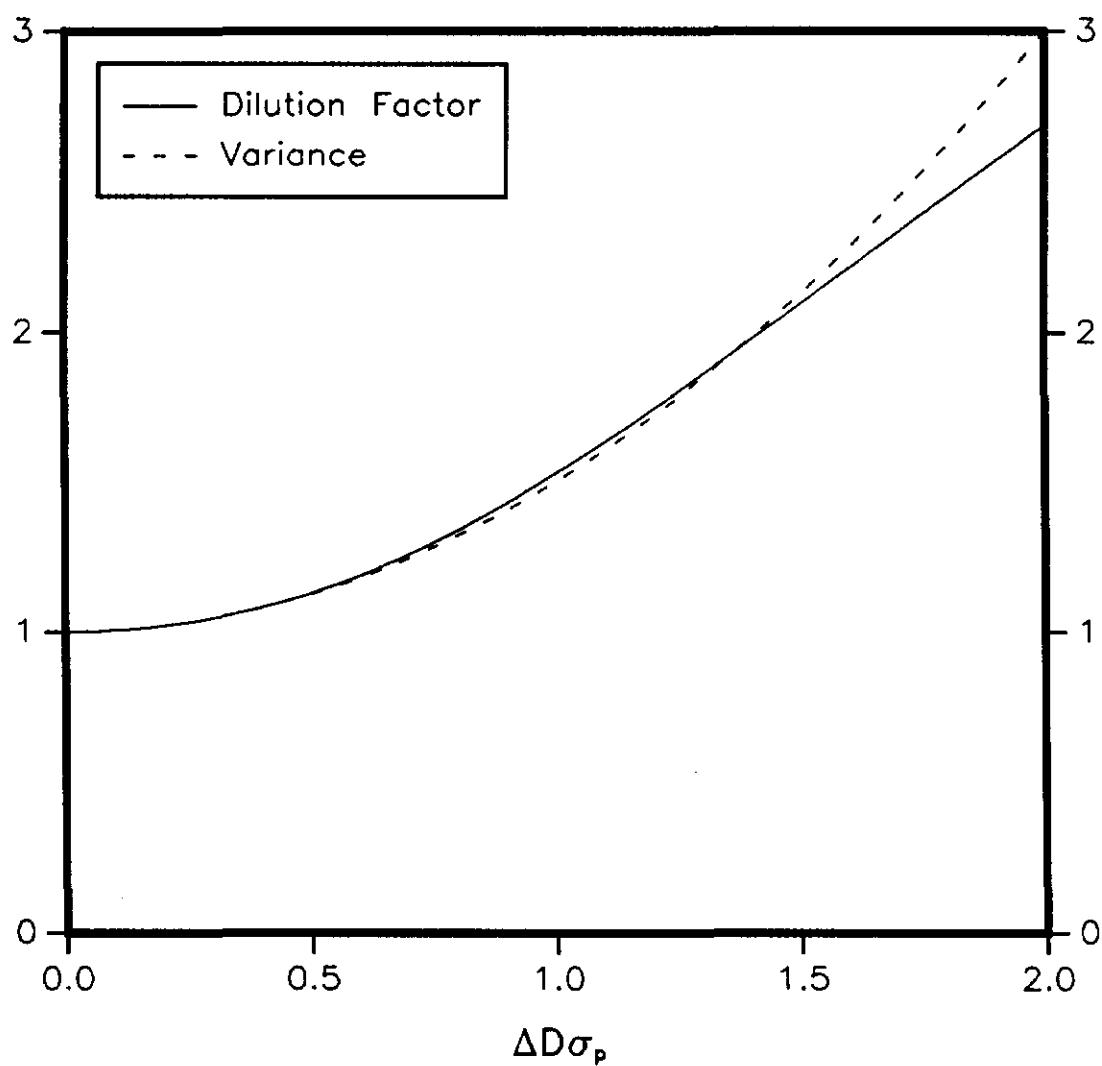
Figure V-10 (Continued)

(c) Amplitude Function Mismatch
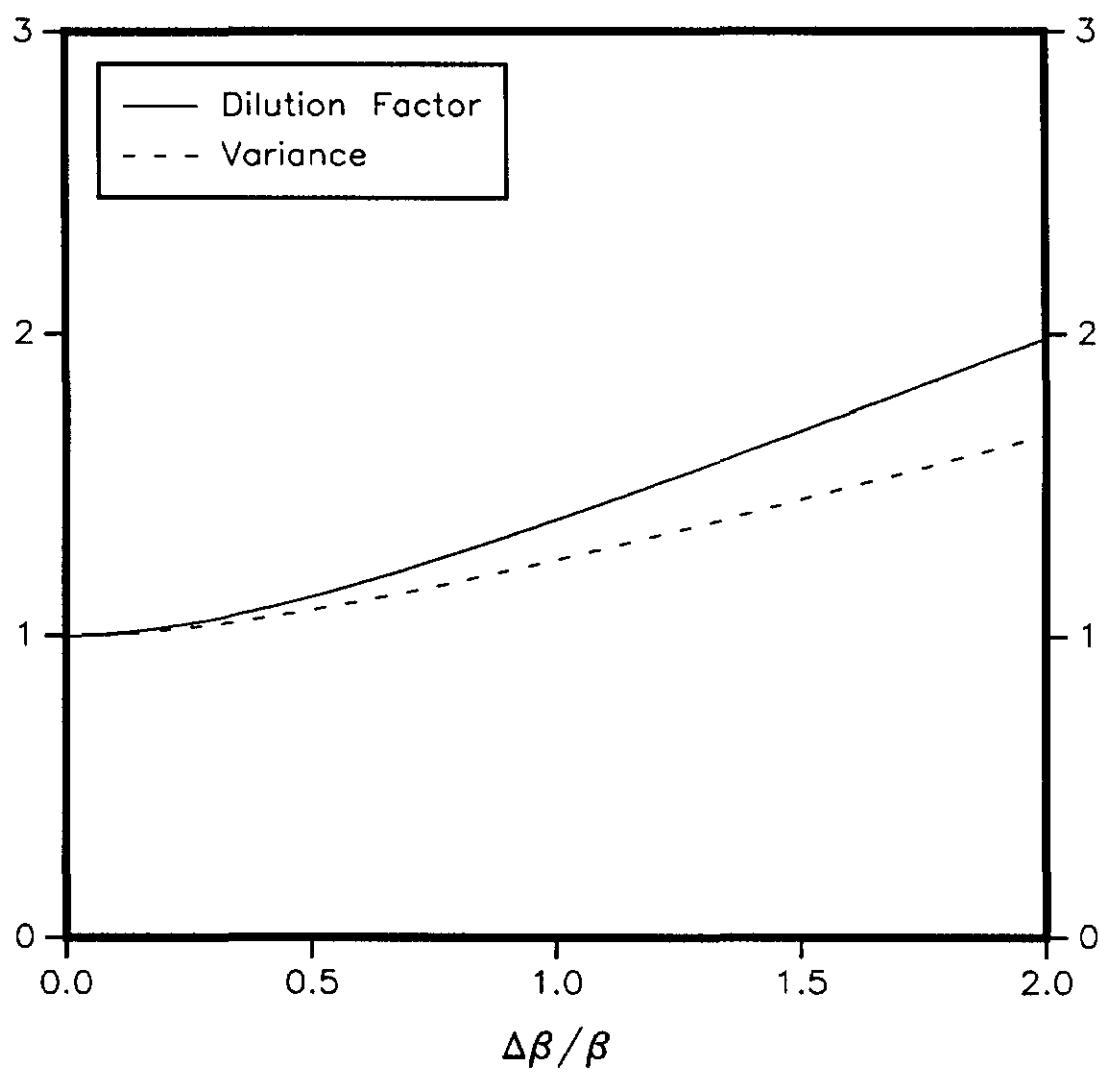
For the ideal accelerator, the quantity $\epsilon_n = (\gamma\beta)\epsilon$ would be constant throughout the entire acceleration process. ϵ_n is referred to as the normalized emittance.

The beam size is related to the emittance by

$$\sigma_o = \sqrt{\frac{\epsilon\beta_o}{6\pi}} = \sqrt{\frac{\epsilon_n\beta_o}{6\pi(\gamma\beta)}}$$

where β_o is the amplitude function and the quantity $(\gamma\beta)$ is the kinematic factor. Therefore the beam size varies inversely with the square root of the momentum. This process is sometimes referred to as adiabatic shrinking. Because the variances of the distributions resulting from position and dispersion mismatches depend upon the size of the incoming beam σ_o, the effects of these mismatches become much more important for higher beam energies.

Summary

The important results of this chapter are gathered on the following page for quick reference.

The transverse phase space dilution factors due to injection amplitude function, position, and dispersion function errors are given by

$$F_\beta \sim \frac{\sigma^2}{\sigma_o^2} = 1 + \frac{1}{2}\left[\frac{(\Delta\beta/\beta)_{eq}}{\sqrt{1 + (\Delta\beta/\beta)_{eq}}}\right]^2 = D$$

$$\text{where} \quad \left(\frac{\Delta\beta}{\beta}\right)_{eq} \equiv D + \sqrt{D^2 - 1} - 1$$

$$\text{and} \quad D = \frac{1}{2}\left[\beta_1\gamma_2 + \beta_2\gamma_1 - 2\alpha_1\alpha_2\right] \quad ;$$

$$F_x \sim \frac{\sigma^2}{\sigma_o^2} = 1 + \frac{1}{2}\left[\frac{\Delta x_{eq}}{\sigma_o}\right]^2$$

$$\text{where} \quad \Delta x_{eq} \equiv \sqrt{\Delta x^2 + \left[\beta\Delta x' + \alpha\Delta x\right]^2}$$

$$F_D \sim \frac{\sigma^2}{\sigma_o^2} = 1 + \frac{1}{2}\left[\frac{\Delta D_{eq}\sigma_p}{\sigma_o}\right]^2$$

$$\text{where} \quad \Delta D_{eq} \equiv \sqrt{\Delta D^2 + \left[\beta\Delta D' + \alpha\Delta D\right]^2} \quad .$$

$$\sigma_o \equiv \sqrt{\frac{\epsilon_n\beta_o}{6\pi(\gamma\beta)}}$$

References

1. Some accelerators are equipped with beam damping systems used to damp out betatron oscillations of the beam centroid caused by a position mismatch. These systems do not completely compensate the position mismatch, however, and dilution will still occur. These systems would have no effect on amplitude function or dispersion function mismatches.

2. Abramowitz, M., and I. A. Stegun, Handbook of Mathematical Functions, New York: Dover Publications, Inc., 1970, p. 374.

3. Goldstein, Herbert, Classical Mechanics, 2nd ed. Addison-Wesley Publishing Co., 1981, p. 531.

VI. Operational Experience with the New 8 GeV Line

Problems Encountered During Commissioning

By the end of July, 1986 beam was being extracted from the
Booster accelerator and being transported to the 8 GeV beam dump
using the upstream elements of the new beamline. On August 2,
1986 beam was first transported through the entire beamline to
the Main Ring synchrotron. To study the new 8 GeV Line and the
injection process, the Main Ring beam abort system was set up to
dispose of the beam on its first passage through the synchrotron.
The abort is situated one third of the ring circumference away
from the injection point. A Main Ring dipole magnet which had
been electrically connected with the wrong polarity prevented
beam from reaching the abort. Once this problem was fixed, beam
was successfully transported to the abort on August 4, 1986 and
detailed studies of the new transport system could begin.

Several minor problems were encountered which are typical of
many accelerator start-up periods. A number of controls problems
(database entries, remote control and proper readback of power
supplies, proper readback of profile monitor data) took time to
track down and correct due to the new instrumentation. In
addition to the new 8 GeV Line requirements imposed upon it, the
entire Booster accelerator controls system had been modified over
the nine month shutdown, sometimes adding to the confusion.
Also, a few power supply problems needed to be resolved. The
Lambertson magnet power supply had a large amount of ripple,
causing the horizontal trajectory of the injected beam to wander.

A persistent problem with the AC power being delivered to the fourth Main Ring Match quadrupole required some extra attention. The third and fourth vertical orbit bump magnets needed to be realigned to provide more aperture for the injected beam. At one time, the beam profiles through the downstream end of the line did not have the appearance expected. The vacuum valve midway between the Booster and Main Ring synchrotrons was later discovered to be partially closed, but not closed enough to trigger the remote status microswitch.

Three problems with the new system did require hardware modifications. The first two have to do with beam losses which were occurring on the third horizontal bend magnet and on the Lambertson magnet. The value of the vertical amplitude function at the location of the third horizontal bend magnet is roughly 150 m. The normalized vertical beam emittance coming from the Booster was expected to be roughly 10 π - 15 π mm-mrad. This would indicate the beam size at this bending magnet should be roughly σ = 5-6 mm. For a total beam width of about 6σ, the minimum aperture required at this location would be about 35 mm. The 1.4 in. gap of the magnet just barely meets this requirement. According to the beam intensity monitors (BIMs) about four percent of the particles were being lost during the transfer through the beamline. The highest beam loss was occurring at the third horizontal bend, even after the beam was centered through this aperture to minimize the loss there. This magnet was replaced by a magnet of similar size but which has a 2.3 in. gap. The new magnet is discussed in Chapter IV. Since this

replacement, the BIMs indicate 100 percent efficiency for the beam transport through the beamline up to the Lambertson magnet.

The beam loss monitors on the Lambertson magnet also showed appreciable signals as the beam passed through the field region. The original magnet used for the injection Lambertson is one which had been built for a previous project that was never completed. Because the field-free region of this magnet was centered below the field region (See Figure IV-8) the beam upon entrance to the field region was at a horizontal displacement of $\Delta x = \rho(1 - \cos\theta) = (2.286m/35mrad)(1 - \cos(.035)) = 40$ mm with respect to the center of the aperture. The beam loss is due to the edge of the beam scraping the beam tube at the upstream end of the magnet. The position of the beam through the field region was varied until the beam loss was minimized (though it could not be completely eliminated) and the Main Ring closed orbit was altered through the field-free region accordingly.

As a new Lambertson magnet of similar design was being built as a spare, some changes were made to the design of the new magnet in an attempt to correct the beam loss problem. The field-free region of the new magnet is displaced horizontally by roughly 20 mm with respect to its position in the older magnet to provide more room for the incoming beam in the field region. In addition, the field-free region laminations were extended in the longitudinal direction at both ends of the new magnet to reduce the values of the end fields seen by the circulating beam. These design changes are discussed in more detail in the Appendix. The new magnet fabrication was completed in February, 1987 and the

device is scheduled to be installed in May, 1987 during a two week shutdown. The original Lambertson magnet will be kept as a spare.

The third and most serious problem requiring a hardware change was caused by the magnets used for the vertical orbit bump in the Main Ring. The original magnets chosen for the orbit bump were small trim magnets previously used for the Main Ring extraction system when the Main Ring synchrotron was used as a 400 GeV fixed target accelerator. These particular magnets have 4 in. x 5 in. apertures. The bend field vs. vertical position through the magnets was later calculated using a relaxation code, the results of which are shown in Figure VI-1.[1] For the extraction of 400 GeV beam where the beam size is on the order of .02 in., the field nonuniformity is tolerable. However, at 8 GeV where the beam size is on the order of 1 in., the sextupole component of these bending magnets generated significant beam distortions. The distribution of the incoming beam essentially saw a large quadrupole error, the strength of which varied with position through the dipoles. This error affected the matching of the amplitude functions to those of the Main Ring. Also, since these magnets reside within the Main Ring synchrotron, the distortions altered the betatron oscillation frequencies as well as the sextupole components of the ring. Both of these problems could be corrected by standard Main Ring correction element quadrupoles and sextupoles. However, as the acceleration process began, the effects of the orbit bump magnets would decrease and hence the tunes and sextupole components would change. Once the

Figure VI-1

Original Vertical Orbit Bump Magnet
Horizontal Field Component vs. Vertical Position

Figure VI-2

New Vertical Orbit Bump Magnet
Horizontal Field Component vs. Vertical Position
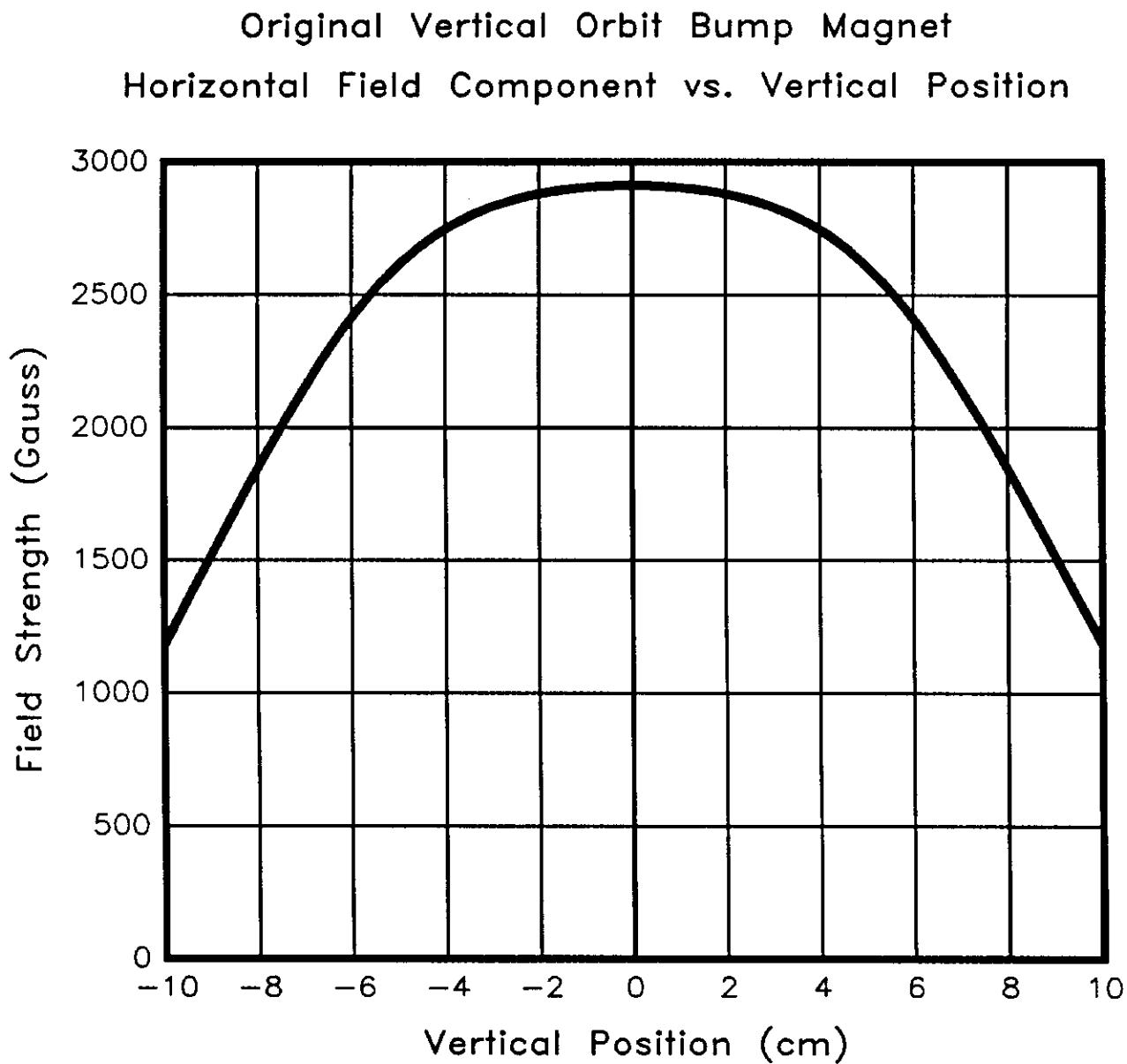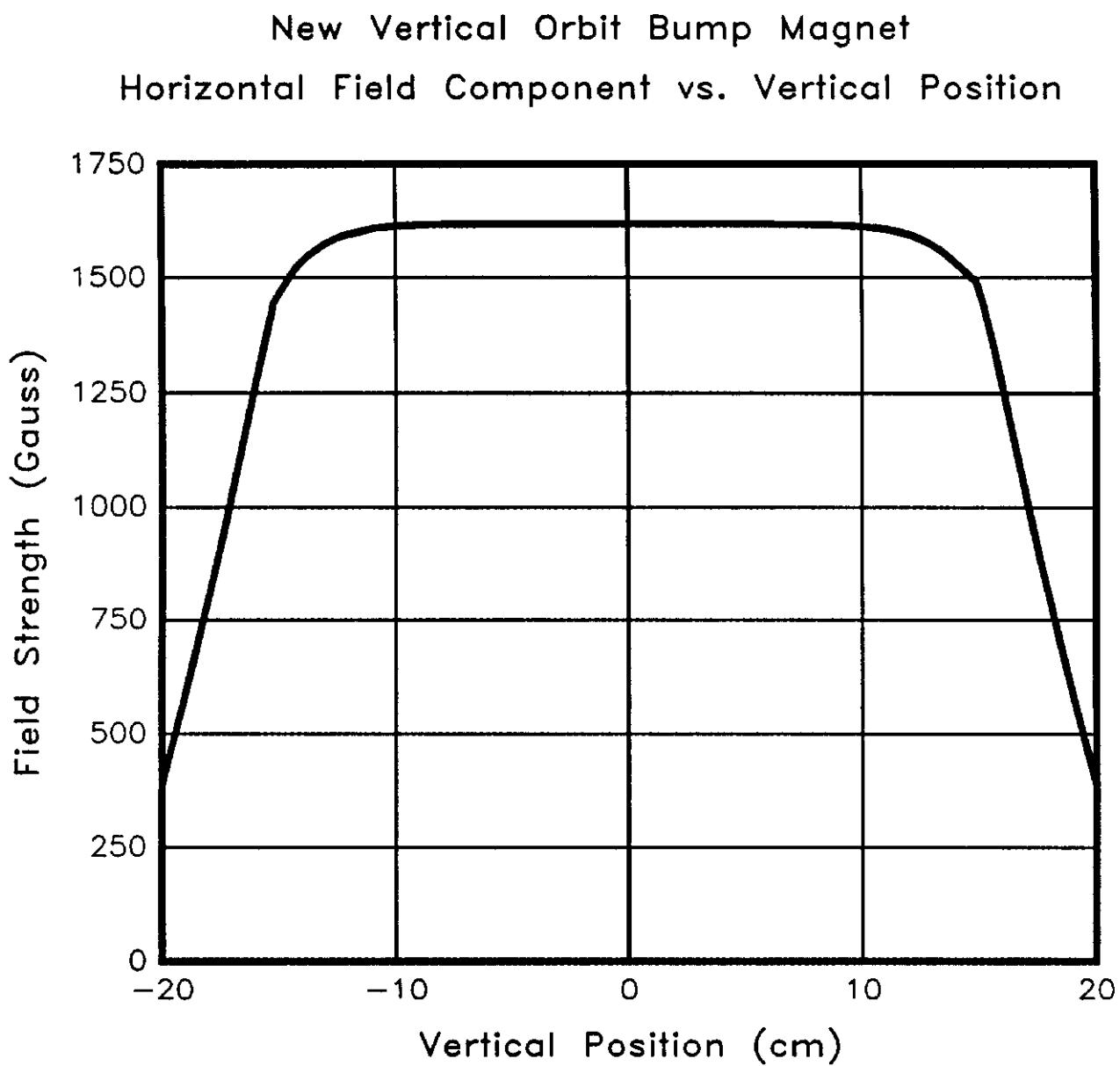
problem with the orbit bump magnets was identified and understood, they were replaced with dipoles of much higher quality. These new magnets were described in Chapter IV and their calculated bend field is shown in Figure VI-2. A more detailed account of the effects which the original magnets had on the circulating Main Ring beam is provided in the Appendix.

Correction of Beam Trajectory

Originally, the position of the beam as seen on the beam position monitors (BPMs) was tuned manually using the correction elements discussed in Chapter IV. Although the BPMs were carefully aligned during the installation of the beamline, small offsets in the readbacks from these devices were expected. By adjusting the beam position through the quadrupole magnets until a large change in a quadrupole magnet current brought about little or no change in the downstream positions, the ideal trajectory was sought. Since that experiment, an automatic beamline position correction program has been developed which runs on the accelerator controls system from the Main Control Room.[2] The program utilizes the algorithm presented in Chapter IV to calculate corrector strengths necessary to minimize beam displacements from desired positions. The program may then send these changes to the appropriate devices automatically and iterate through this procedure until the positions are within a designated tolerance.

As a result of the beam trajectory correction, the maximum position errors throughout the line are less than 3 mm for each plane. The average corrector strength is approximately 0.2 mrad

and the maximum corrector strength is 0.6 mrad, far below the design maximum correction of 1.5 mrad.

The injection positions have been adjusted to within $\Delta x_{eq} =$ 1.0 mm of the Main Ring closed orbit for both the horizontal and vertical planes. To check this condition, the BPM system is used to obtain 8 GeV closed orbit positions as well as the first-turn positions around the ring. (To determine the closed orbit at a particular location, the average position as seen by the BPM over several turns is computed.) Because the amplitude function has roughly the same value at each detector (~100 m), the difference between the two sets of data will have a maximum value roughly equal to Δx_{eq}. Figure VI-3 shows BPM difference data of this sort obtained during Main Ring operation. For $\Delta x_{eq} = 1$ mm and a typical beam size of $\sigma_0 = 5$ mm, the dilution factor due to position mismatch would be 1.02.

Emittance Measurements

Since the beginning of the new 8 GeV Line operation, emittance measurements have become rather routine. With the new microprocessor-based system and associated applications programs, profile data may be obtained and analyzed with ease. Figure VI-4 shows typical profile data from three of the horizontal monitors in the Cells region of the beamline. All three monitors are at locations of $\beta_x = 24.5$ m. However, the monitors labeled WC1 and WC5 are at locations where $|D_x| = 3.7$ m while the monitor labeled WC3 is at a location where $|D_x| = 0.5$ m. Using the variances computed by the microprocessors, the beam sizes may be plotted in real time on a color graphics display in the Main Control room.

Figure VI-3

Determination of Δx_eq from BPM Data

FLASH FRAME   .5184
  FILE 77 01/30/87 0541:52 29
OWL SHIFT DAILY SAVE; INJECTIO

              MINUS

DISPLAY FRAME   .546
  FILE 76 01/30/87 0541:24 29
OWL SHIFT DAILY SAVE; LOW FLD

(MM)   03/05/87 0731

	E	F	A	B	C	D
VX11	-.15	-.91	3.52	-1.41	.31	1.22
VX12	-1.08	-1.08	-1.39	-1.22	.76	.92
VX14	-1.69	.15	-.93	.46	1.07	-.31
VX16	-.31	1.53	.62	1.38	-.31	-1.38
VX18	1.38	.93	1.37	.3	-1.37	-.92
VX21	1.22	-.93	.15	-.92	-.61	.76
VX23	-.62	-1.38	-1.08	-1.07	.61	1.36
VX25	-1.85	-.46	-1.21	0	1.06	.15
VX27	-.93	.91	0	1.07	.3	-1.22
VX29	.93	1.23	1.08	.76	-1.06	-1.08
VX33	1.69	-.31	.77	-.45	-1.22	.46
VX35	.31	-1.56	-.63	-1.22	.15	1.37
VX37	-1.7	-.77	-1.24	-.46	1.06	.46
VX39	-1.38	.77	-.46	.91	.6	-.92
VX43	.15	1.55	1.08	.77	-.61	-1.37
VX45	1.82	0	1.08	-.46	-1.38	-.31
VX47	.77	-.92	-.31	-1.23	-.15	1.07
VX49	-.92	-.93	-1.41	-.31	1.26	.48

MR   **MR**

RMS (MM) = 1.043   DP/P (%) = .0052   MOM CORR RMS = 1.041
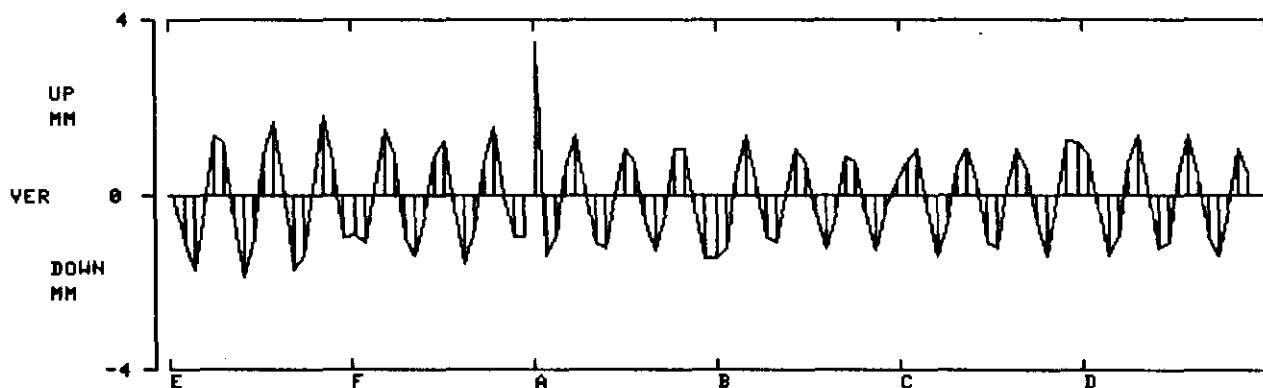
Figure VI-4

Typical Data from Cells Profile Monitors

Abs-Mean=-.3 mm   Sigma=3.6 mm   ChiSq=0
66
WC1
HORIZONTAL
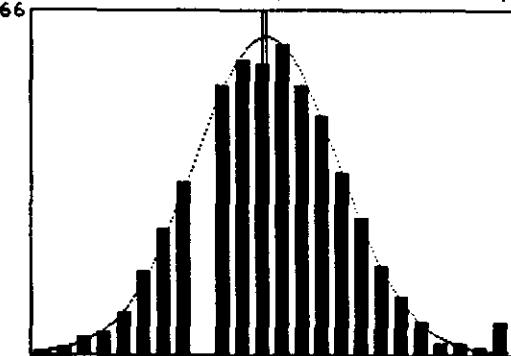
Abs-Mean=-3.3 mm   Sigma=3.6 mm   ChiSq=.1
111
WC5
HORIZONTAL
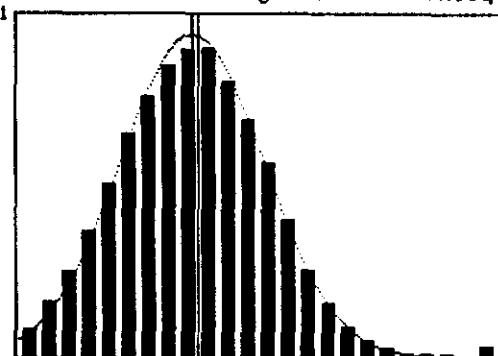
Abs-Mean=-1.5 mm   Sigma=2.4 mm   ChiSq=.3
121
WC3
HORIZONTAL
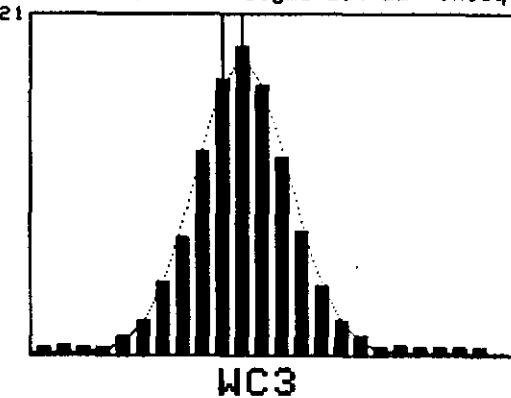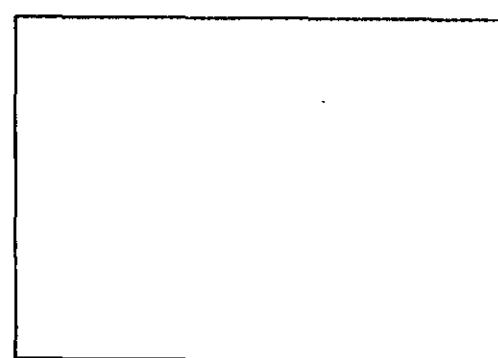
Figure VI-5

8 GeV Emittance Measurements
of April 15, 1987

Figure VI-6

Dependence of Main Ring Injection Efficiency on Booster Momentum Spread
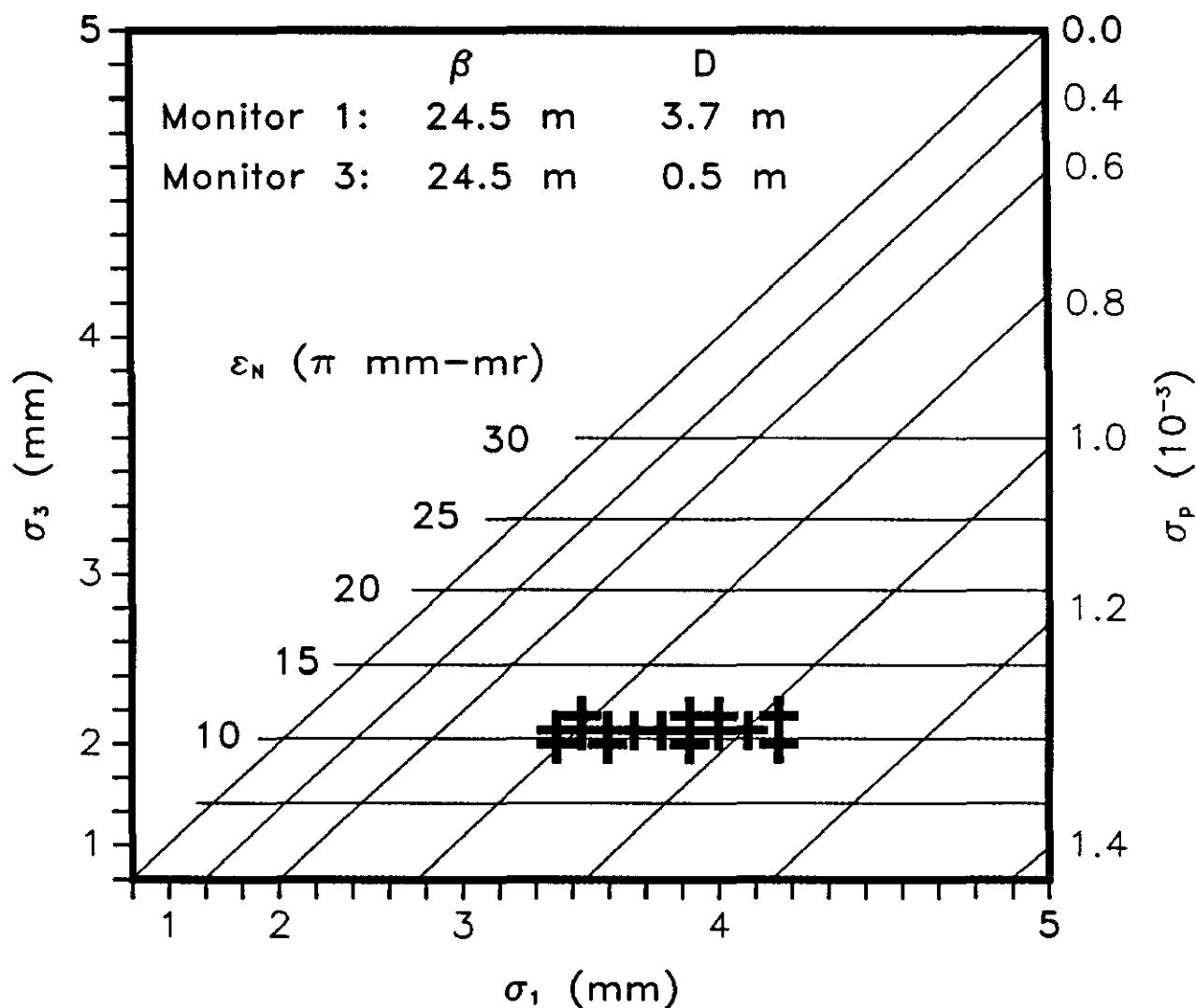
(Data of November 4, 1986)
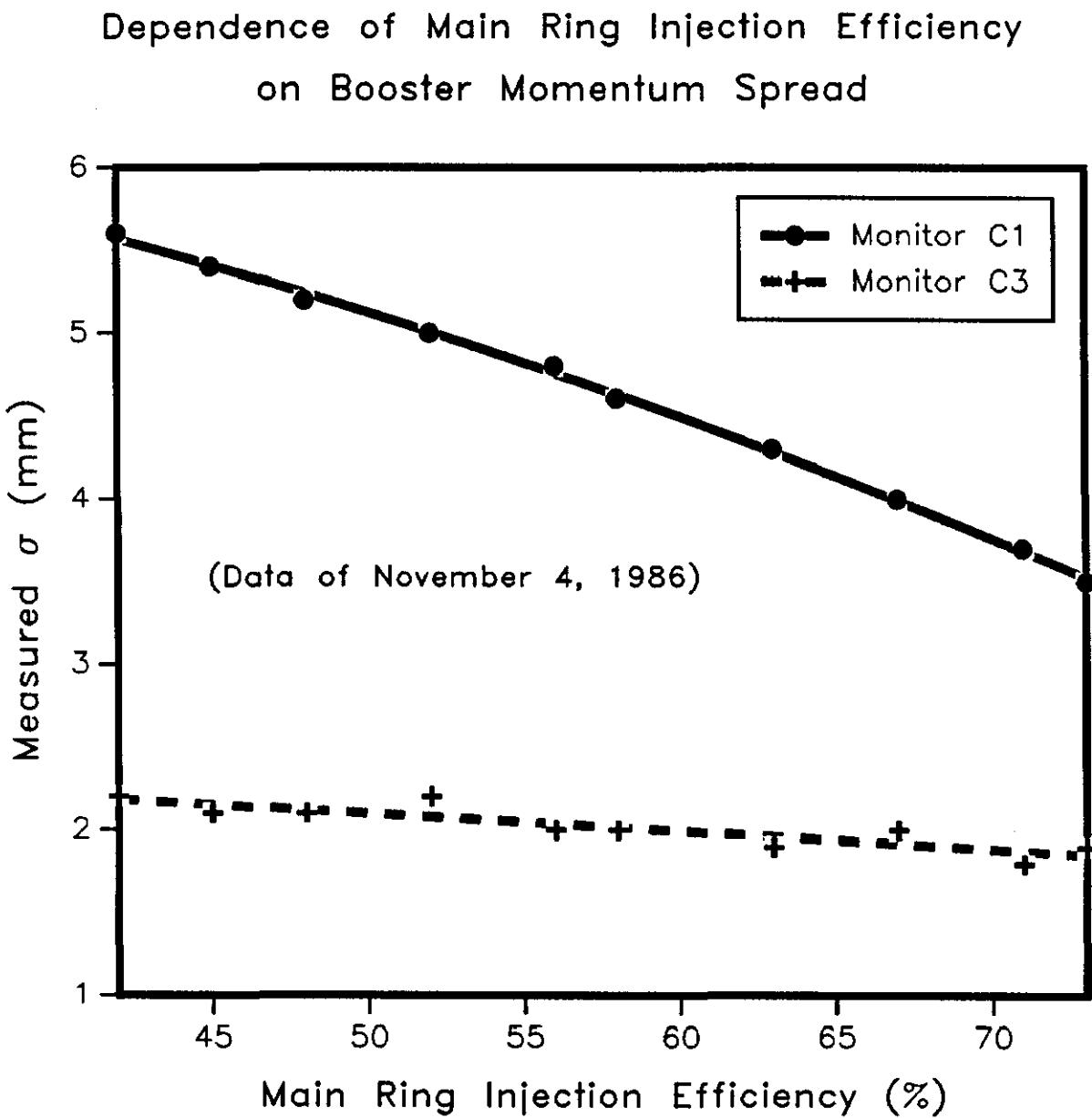
One such plot is shown in Figure VI-5. From this particular graph, the horizontal normalized emittance and the variance of the momentum distribution may be read. By allowing the plot to update over an extended period of time, the uncertainties in these two quantities may be obtained easily. (For Figure VI-5, roughly 200 points were obtained.)

Since all of the profile data may be stored in the controls system database, other types of analyses may be performed. For instance, Figure VI-6 shows the beam sizes as seen on wires WC1 and WC3 correlated with the efficiency of the Main Ring injection process. The variation of WC1 wire size indicates that the Booster efficiency was intimately tied to the momentum distribution on this particular date. This type of plot has been used to diagnose problems with the Booster RF system.

Dispersion Measurements

On December 9, 1986 an attempt was made to measure the dispersion functions through the 8 GeV Line and determine the amount of mismatch of these functions to those of the Main Ring. To perform the measurements, BPM signals were recorded as the Booster RF frequency at extraction was varied. An automatic radial position feedback signal of the Booster RF system had to be disconnected to ensure that the Booster position at extraction would change as the frequency was varied. To obtain the values of the dispersion functions at the locations of the BPMs, the value of $\Delta p/p$ was found from the relationship

$$\Delta f/f = (1/\gamma^2 - \alpha_p)(\Delta p/p)$$

where f is the revolution frequency or the RF frequency, γ is the Lorentz factor, and α_p is the so-called momentum compaction factor,

$$\alpha_p \equiv (\Delta C/C)/(\Delta p/p)$$

with C = machine circumference. The value of α_p is roughly equal to $\langle D_x \rangle/R$, where the average is carried out over the bending magnets of the accelerator which have radius of curvature R. A more precise value may be computed by most accelerator design codes, like those described in Chapter III. For the Booster accelerator, $\alpha_p = .0337$ and $\gamma = 9.526$ at extraction so that

$$1/\gamma^2 - \alpha_p = -0.0227 \ .$$

Therefore, a value for $\Delta p/p$ may be obtained for each increment of the RF frequency $\Delta f/f$. The dispersion function is then given by $D = \Delta x/(\Delta p/p)$ where Δx is the change in position created by Δf.

The 8 GeV Line horizontal and vertical dispersion functions obtained from the measurements described above are displayed in Figure VI-7 and Figure VI-8 along with their design values. Within the accuracy of the measurement the values are in good agreement. The real test is the degree to which these functions conform to the Main Ring dispersion functions past the injection point. Figure VI-9 and Figure VI-10 show the measured dispersion functions delivered by the beamline along with the corresponding Main Ring design dispersion functions. The region of large vertical dispersion is caused by the overpass at the Collider Detector Facility. The beam was being aborted on the first turn and hence beam was not observed past the position labeled "CO" where the abort system is located.

Figure VI-7
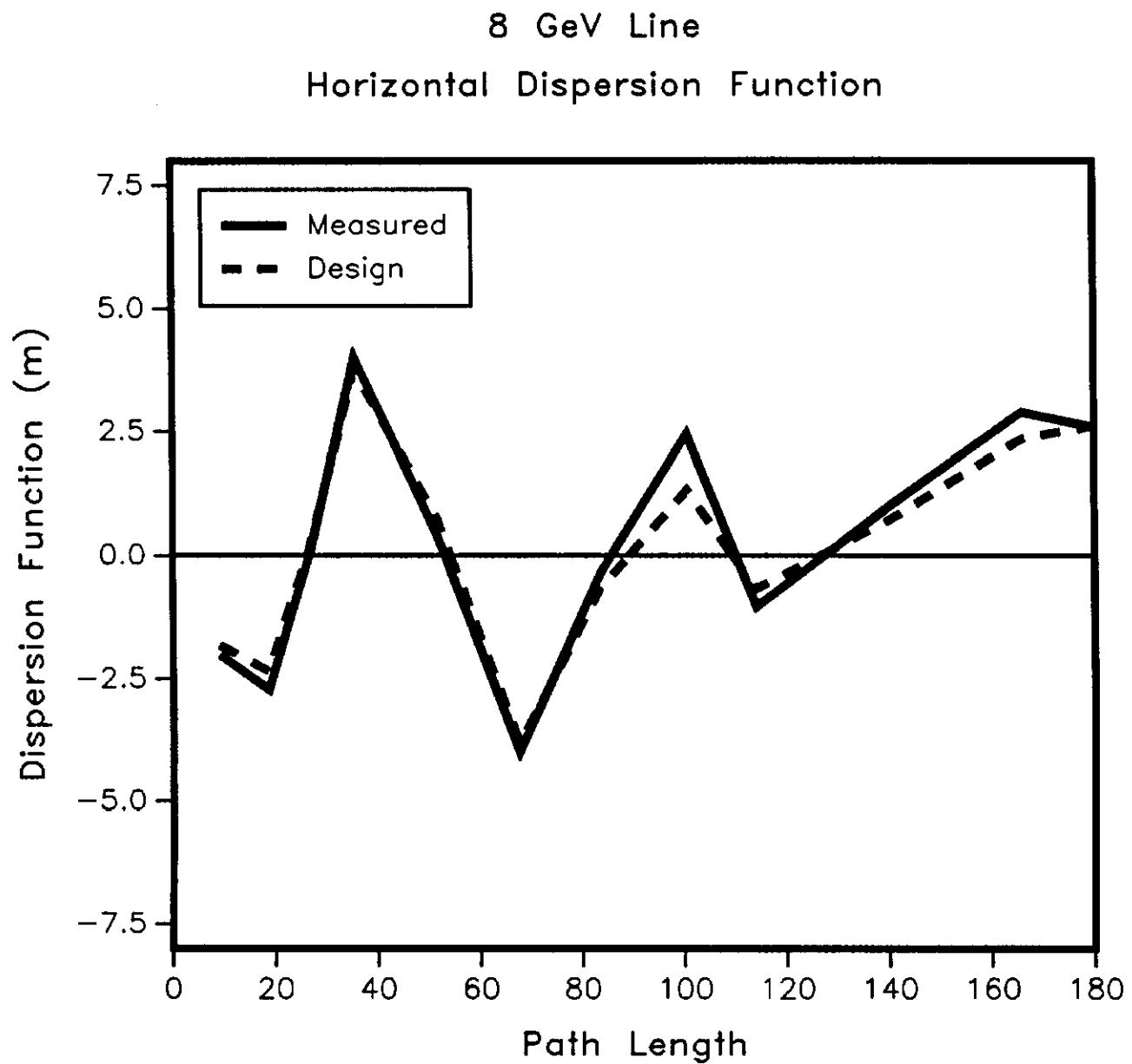
8 GeV Line

Horizontal Dispersion Function

Figure VI-8

8 GeV Line

Vertical Dispersion Function

Figure VI-9

Main Ring
Horizontal Dispersion Function

Figure VI-10

Main Ring
Vertical Dispersion Function
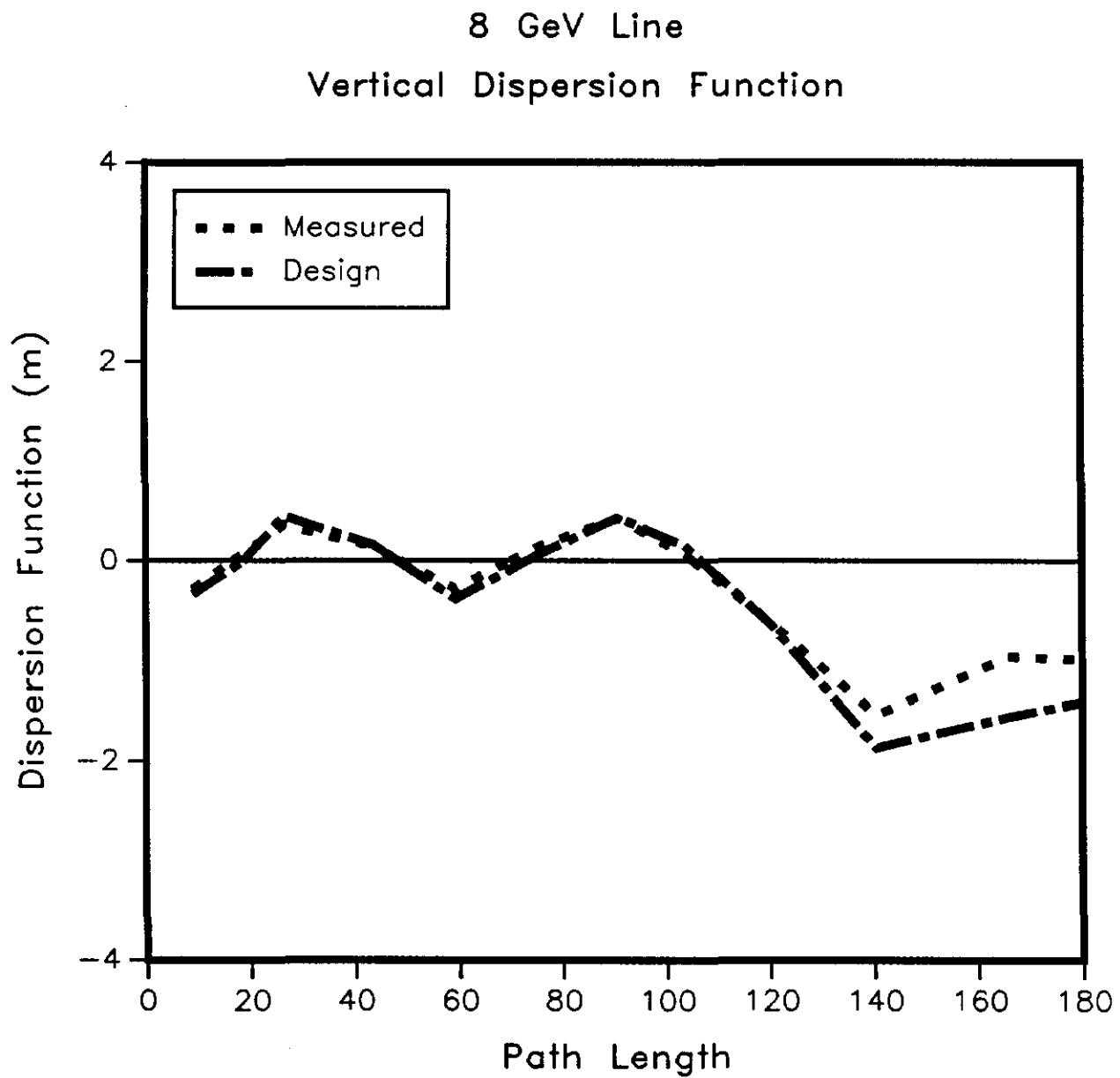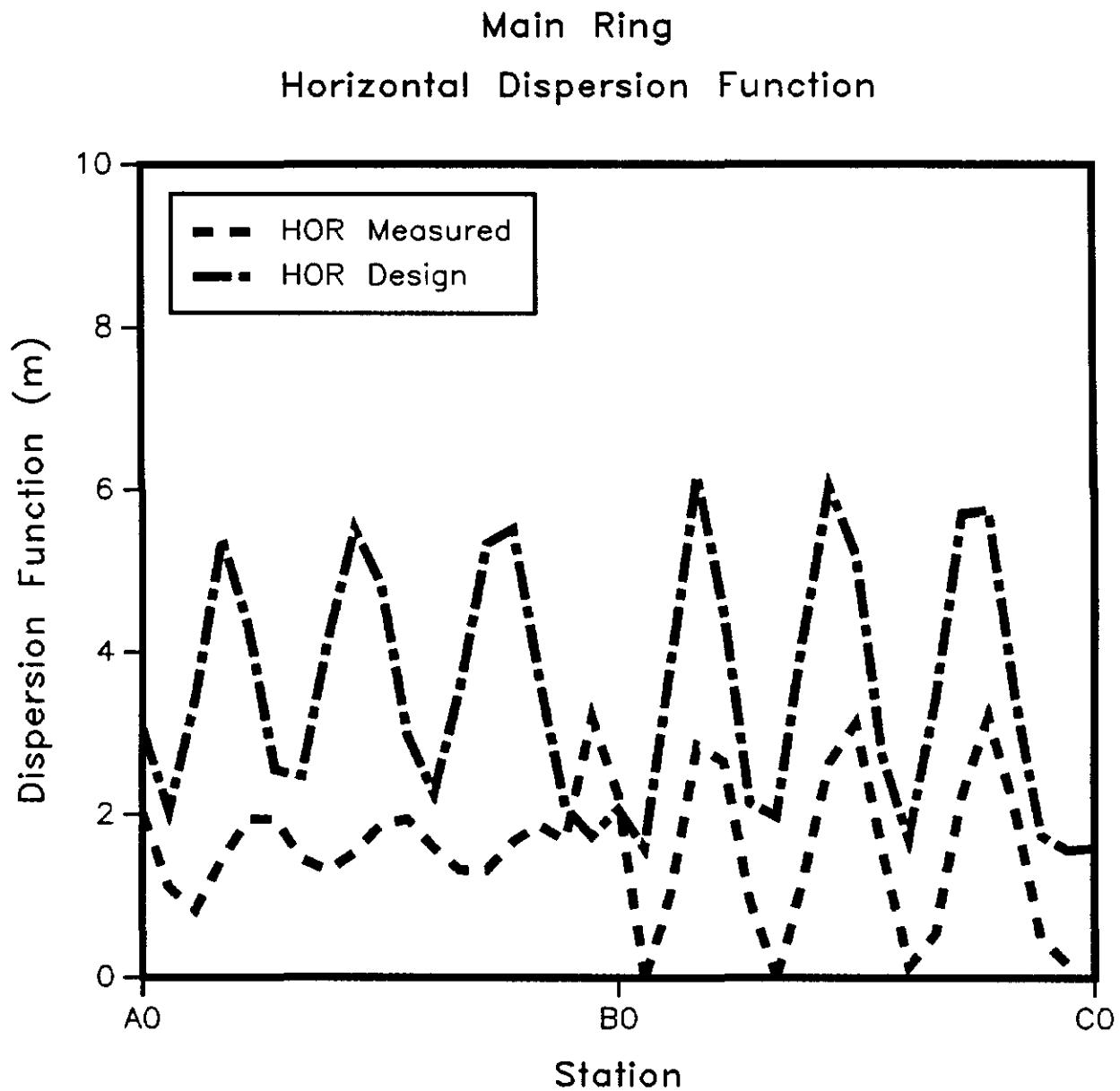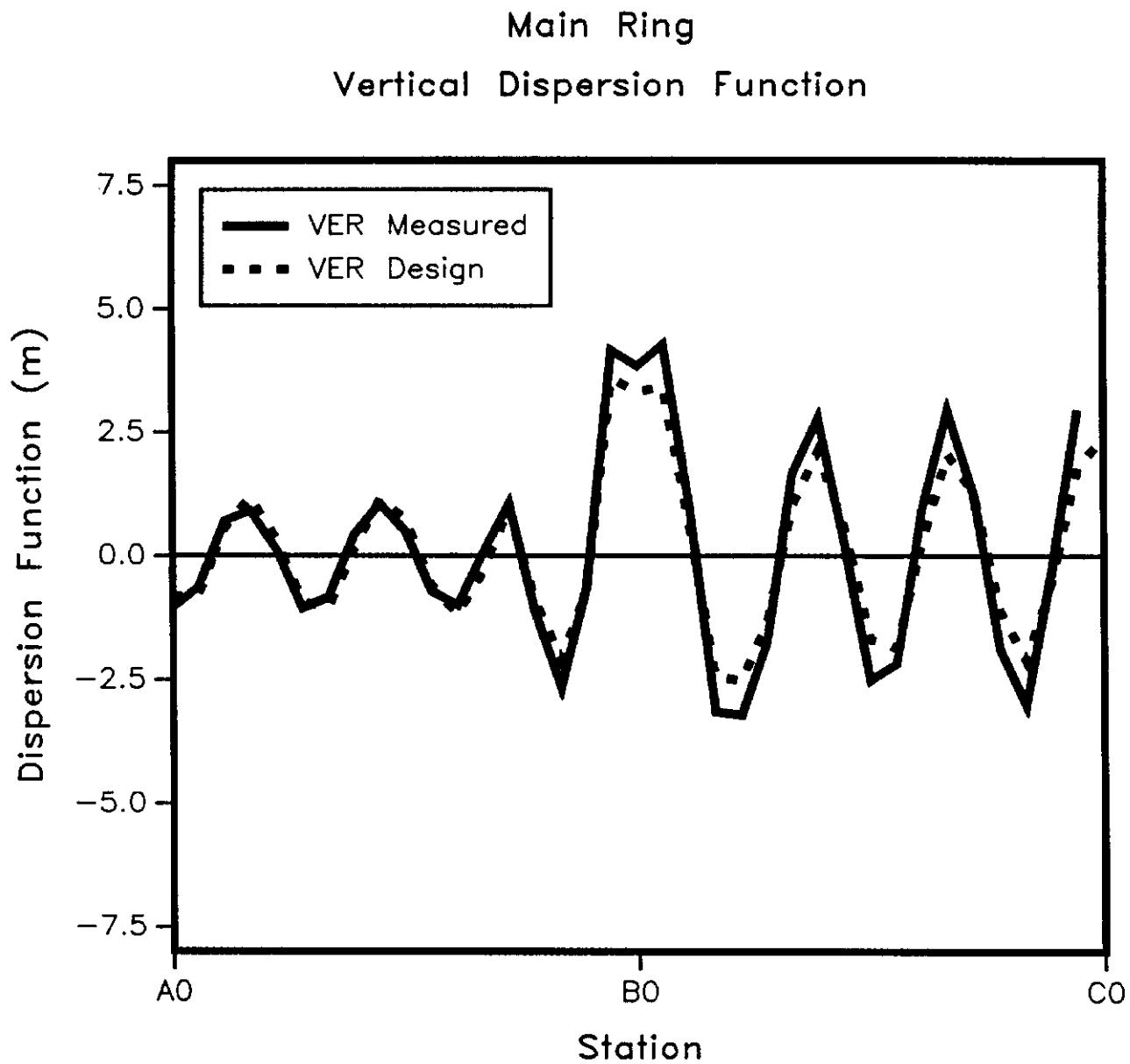
The vertical dispersion function delivered by the beamline appears to be well matched to the synchrotron. The horizontal function appears to be grossly mismatched. However, the pattern observed in the horizontal data is not what would be expected of a pure dispersion function mismatch. One would expect the difference between the delivered function and the design function to oscillate about zero. Clearly this is not the case with the data shown in Figure VI-9. After the study session was over, the horizontal position through the Lambertson magnet was noticed to be several millimeters to the radial outside from the nominal position. As discussed earlier, this can result in significant beam loss at the upstream end of this magnet. The changes in the RF frequency were also forcing the beam further to the radial outside, compounding the problem. A significant portion of the beam is thought to have been scraped off during the measurements, affecting the detected centroid of the beam in an unpredictable manner. Horizontal profile monitor data which were taken during this study period appear to support the hypothesis. Further study time has been requested to repeat the measurement.

To obtain a value for ΔD_{eq} for each plane, the method employed for position mismatch may be used again. Subtracting the two curves in each of Figures VI-9 and VI-10 and finding the maximum values of these differences yields the desired values. For the vertical plane, $\Delta D_{eq} = .5$ m whereas for the horizontal data, if it is taken at face value, $\Delta D_{eq} = 1.5$ m (one half of the peak-to-peak variation). Taking $\sigma_o = 5$ mm and $\sigma_p = 0.8 \times 10^{-3}$ in agreement with profile monitor data taken during the same study

period, the dilution factors due to dispersion function mismatch are 1.003 in the vertical plane and 1.03 in the horizontal plane.

Amplitude Function Measurements

By aborting the beam during its first revolution, the signals obtained from the profile monitors located within the Main Ring accelerator reflect the initial distribution of particles being delivered by the 8 GeV beamline. The emittance of this beam may be obtained by profile measurements using the monitors within the Cells region of the beamline as described earlier. Hence, the amplitude functions at the locations of the Main Ring profile monitors being delivered by the beamline may be obtained and compared with design.

Eight profile monitors reside within the Main Ring at the locations of the first eight quadrupole lenses past the injection straight section. If the matrix $M(s_i/s_o)$ which transports the transverse beam trajectory (x, x') from location s_o to location s_i is known, then using the methods of Chapter III the value of the amplitude function at s_i will be

$$\beta_i = a_i^2 \beta_o - 2a_i b_i \alpha_o + b_i^2 \gamma_o$$

where a_i and b_i are the 1-1 and 1-2 elements of the matrix $M(s_i/s_o)$ and $\gamma_o = (1 + \alpha_o^2)/\beta_o$. By obtaining measurements of β_i at various profile monitor locations, an estimate of β_o and α_o at a particular reference point may be determined.

A program has been written which runs on the accelerator controls system that analyzes profile monitor data to obtain estimates for β_o and α_o.[3] The effects of momentum dispersion on the beam size are subtracted and a grid search is performed which

varies the values of β_o and α_o in an attempt to find the minimum of $\Sigma(\beta_i - a_i{}^2\beta_o - 2a_ib_i\alpha_o + b_i{}^2\gamma_o)^2$, where here, β_i is the measured value of β at the ith monitor. The point s_o typically used in the calculation corresponds to the middle of the injection long straight section. The design values of the parameters β and α at this point are β_x = 72.6 m, β_y = 73.3 m, α_x = -0.723, and α_y = 0.729 . Results of vertical profile measurements taken December 9, 1986 are shown in Table VI-1. The estimated values α_y = 0.763 and β_y = 63.3 m in conjunction with the design values yield the number β_{eq} = 1.23. Thus, the vertical dilution factor is 1.02. From horizontal profile data taken the same evening, β_{eq} = 1.90 and the horizontal dilution factor due to amplitude function mismatch is thus 1.21. It is believed that most of this horizontal emittance blow-up is caused by the problem of beam loss on the Lambertson magnet.

The resulting variance due to all three sources of mismatch working simultaneously may be estimated for each plane using the same statistical arguments developed in Chapter V. The variance of the distribution resulting from a combination of amplitude function errors, dispersion function errors, and position errors is given simply by

$$\sigma^2 = (\beta_{eq}{}^2+1)/2\beta_{eq} + (\Delta x_{eq})^2/2 + (\Delta D_{eq}\sigma_p)^2/2 \ .$$

Hence, the total dilution factors would become

$$F_x = 1.26 \quad \text{and} \quad F_y = 1.04 \ .$$

<u>Table VI-1</u>

Results of Profile Measurements of December 9, 1987

Normalized Emittance: $\epsilon_y = 15\ \pi$ mm-mr

$\sigma_p = .82 \times 10^{-3}$

<u>Monitor</u>	$\underline{\alpha}$	$\underline{\beta}$	$\underline{\beta(\text{fit})}$	$\underline{\alpha(\text{fit})}$
WA11	3.75 mm	50.78 m	39.36 m	3.33 mm
WA12	4.65 mm	79.47 m	84.13 m	4.68 mm
WA13	3.15 mm	37.83 m	29.70 m	2.79 mm
WA14	5.25 mm	104.1 m	104.7 m	5.23 mm
WA15	3.00 mm	32.89 m	28.22 m	2.79 mm
WA16	4.65 mm	76.05 m	81.35 m	4.78 mm
WA17	3.00 mm	33.14 m	24.40 m	2.59 mm
WA18	4.95 mm	92.79 m	94.36 m	4.99 mm

β_o, α_o minimize $\Sigma[\beta - \beta(\text{fit})]^2$:

$$\beta_o = 63.3\ m \qquad \beta(\text{design}) = 73.3\ m$$

$$\alpha_o = 0.763 \qquad \alpha(\text{design}) = 0.729$$

$$\therefore \beta_{eq} = 1.229$$

$$F_\beta = 1.02$$

References

1. Holsinger, R. F. POISSON Group User's Guide; February, 1981; Field Effects, Inc., Carlisle, Massachusetts.

2. Development of this program courtesy R. Joshel, FNAL

3. Development of this program courtesy D. E. Johnson, FNAL.

CONCLUDING REMARKS

Several improvements were made to the 8 GeV beam transport system. The sensitivity of the transverse emittance growth due to errors in the gradients of the quadrupole magnets was significantly reduced. The mismatch of the vertical dispersion function was resolved. A new injection scheme aided in the vertical dispersion matching process. In addition, upgrades to the profile monitor system as well as an optical design more congenial to beam measurements have improved the diagnostic capabilities of the line. The quality of the magnetic elements in the line was also improved through the use of Tevatron I project quadrupole magnets and the new injection Lambertson magnet. Detailed magnetic measurements have been performed on all of these devices. There is no evidence of significant emittance dilution or hindrance of Main Ring performance due to the injection process.

From the results of Chapter V, the consequences of the three forms of mismatch, position errors, amplitude function errors, and dispersion function errors, have been put into proper perspective. For the errors produced by the new FNAL 8 GeV Line all three sources of mismatch are of roughly the same degree, each contributing a few percent to the total dilution factor.

The results of Chapter V are completely general and may be applied to other accelerator injection systems. For example, the transport line between the Main Ring and Tevatron accelerators may be considered. Since the amplitude functions of these two

machines are essentially identical, the effects of beta mismatch are negligible. The design vertical dispersion function in the Tevatron is zero everywhere. The value delivered by the short beamline connecting the Main Ring to the Tevatron injection point is roughly 1.5 m, generated by both the Main Ring D0 overpass and the fact that the beam is displaced vertically when delivered from one machine to the other. The beam size at 150 GeV is reduced from $\sigma = 5$ mm to $\sigma = 1$ mm due to adiabatic shrinking. With a momentum spread of $\sigma_p \sim 1 \times 10^{-3}$, typical of coalesced bunches used for colliding beams operation, the dilution of the vertical phase space emittance would be approximately 2.1. Coupled with the effect of a 1 mm position error upon entrance to the Tevatron the total dilution factor would be roughly 2.5. The results of the 8 GeV Line study have helped to emphasize the importance of these sources of emittance dilution within the FNAL accelerator system and other accelerator systems as well.

BIBLIOGRAPHY

Blewett, M. H., editor, "Theoretical Aspects of the Behaviour of Beams in Accelerators and Storage Rings," CERN Report No. 77-13.   Geneva: CERN.   1977.

Bryant, P., S. Turner, editors, "CERN Accelerator School -- General Accelerator Physics, Volumes I, II," CERN Report No. 85-19.   Geneva: CERN.   1985.

Cole, F. T., editor, "National Accelerator Laboratory -- Design Report."   Batavia: Universities Research Association. 1968.

Cole, F. T., M. R. Donaldson, D. A. Edwards, H. T. Edwards, P. F. M. Koehler, editors, "A Report on the Design of the Fermi National Accelerator Laboratory Superconducting Accelerator." Batavia: Fermi National Accelerator Laboratory.   1979.

Courant, E. D., H. S. Snyder, "Theory of the Alternating Gradient Synchrotron," Annals of Physics, Vol. 3.   New York: Academic Press.   1958.

Jowett, J. M., M. Month, S. Turner, editors, "Nonlinear Dynamics Aspects of Particle Accelerators," Lecture Notes in Physics No. 247.   New York: Springer-Verlag.   1985.

Month, M., editor, "Physics of High Energy Particle Accelerators," AIP Conference Proceedings No. 105.   New York: AIP.   1983.

Month, M., P. F. Dahl, M. Dienes, editors, "Physics of High Energy Particle Accelerators," AIP Conference Proceedings No. 127.   New York: AIP.   1985.

Month, M., M. Dienes, editors, "Physics of Particle Accelerators," AIP Conference Proceedings No. 153.   New York: AIP.   1987.

APPENDIX

AI.   Lambertson Magnet Measurements

Several calculations and measurements were performed on the Lambertson-style magnet used in the injection region of the new 8 GeV beamline.   The results presented in this section are those associated with the new magnet which was discussed in Chapter VI. The same measurements were performed on the old magnet but only the most significant result, the end field measurement, is presented at the end of this section.   An end view and a side view of the magnet are shown in Figure AI-1 and Figure AI-2 respectively.   The coordinate system used throughout the following discussions is indicated in the figures.   The field region of the magnet $(y > 0)$ is 90 in. long, whereas the field-free region $(y < 0)$ is extended an additional 8 in. on each end of the magnet.   The calculations and measurements were performed with the magnet operating at a nominal current of 920 Amp.   As stated in Chapter IV, the gap height of the field region is 1.85 in., and the number of turns in the magnet is 18.

A commercially available software program, POISSON,[1] was used to model the fields expected to be observed within the magnet.   The results of the calculations are displayed in Figures AI-3 through AI-6.   The point $x = 0$, $y = -1.5$ cm corresponds to the position of the circulating beam with the vertical orbit bump magnets operating at their nominal current.   At high energy, the beam will pass through the point $x = 0$, $y = -4.4$ cm. By fitting the central regions of the curves to polynomial functions,

estimates of the quadrupole and sextupole components of the
magnetic field may be obtained as well as the resulting effects
of these fields on the behavior of the circulating Main Ring
beam.

The more important results at y = -1.5 cm yield $B_y \simeq 3.4$ G
and $B_x \simeq 1.5$ G. Hence, the steering errors introduced by the
"field-free" region in the two transverse planes would be

$$\Delta\theta_x = B_y L/(B\rho) = (.0034)(2.286)/(296.5) = .026 \text{ mr},$$

$$\Delta\theta_y = B_x L/(B\rho) = (.0015)(2.286)/(296.5) = .012 \text{ mr}.$$

These errors would introduce a maximum distortion of the Main
Ring closed orbit on the order of 1 mm. The quadrupole component
is determined to be B' $\equiv \partial B_y/\partial x = .095$ G/cm from Figure AI-4.
This would alter the frequencies of betatron oscillations (the
tunes) by the amounts

$$\Delta\nu_x = \beta(s)B'L/(4\pi B\rho) = (60)(.0095)(2.286)/(4\pi)(296.5) = .0003,$$

$$\Delta\nu_y = \beta(s)B'L/(4\pi B\rho) = (90)(.0095)(2.286)/(4\pi)(296.5) = .0005.$$

The sextupole component B'' $\equiv \partial^2 B_y/\partial x^2 = 1.06$ kg/m^2 obtained from
the calculations alters the chromaticity of the machine by the
amount

$$\Delta\xi = \beta(s)D(s)B''L/(4\pi B\rho) = (60)(1.06)(2.286)/(4\pi)(296.5) = .04,$$

that is, the change in the horizontal tune for a particle of
momentum p+Δp would be $\Delta\nu = \Delta\xi(\Delta p/p)$.

The measurements of the fields within the actual magnet were
performed on a test stand at the Fermilab Magnet Test Facility.
A Hall probe was placed within the magnet body supported by a G10
rod which could be moved in any of three directions (x, y, and z)
independently. The vertical field component B_y in the field

region was measured as a function of current. Both transverse field components were then measured as a function of transverse position in the field-free region in the vicinity of the two circulating beam positions $x = 0$, $y = -1.5$ cm (injection) and $x = 0$, $y = -4.4$ cm (extraction). The results of these measurements are displayed in Figures AI-7 through AI-13. As can be seen, the measurements are in good agreement, at least qualitatively, with the POISSON calculations.

The last set of measurements performed were those of the vertical field component in the field-free region as a function of longitudinal position z. The point $z = 0$ is defined as the end of the laminations of the field region ($y > 0$) as seen in Figure AI-2. The field-free region of the original Lambertson-style magnet used in the 8 GeV Line was extended out to $z = 3.5$ in. Measurements of B_y as a function of z indicated that the end fields were enormous in this magnet. The results of the measurement are shown in Figure AI-14. As can be seen, the peak field strength is roughly 150 G. By integrating the field strength over z, the total amount of bend provided by the end region is found to be

$$\Delta\theta_x = (\int B_y dz)/(B\rho) \sim (.0058 \text{ kG m})/(296.5 \text{ kG m}) = .020 \text{ mrad}.$$

For the two ends, the total bending would be roughly .040 mrad, to be compared to the bending brought about by the body of the magnet of $\Delta\theta = .026$ mrad. Thus, the orbit displacement due to the entire magnet is likely to be more on the order of 2.5 mm. (This orbit displacement was actually measured while the original magnet resided in the Main Ring and was indeed 2-3 mm in amplitude.)

Before the original magnet was installed in the Main Ring tunnel, a simple test was performed whereby a thin (.25 in.) piece of steel 4.75 in. wide and 6 in. long was placed at the end of the magnet in the septum plane and a rough measurement of B_y versus z was obtained. The maximum field strength observed was roughly 30 G. When the new magnet was being designed, the decision was made to lengthen the bottom ($y < 0$) half of the magnet so that the laminations of the field-free region extended a full 8 in. past the field region laminations.

Once the new magnet was built, the end field measurements were performed and the peak field was dramatically smaller than in the original magnet, the peak field observed being 17 G. Figure AI-15 shows the results from both the old and the new magnet measurements together. The integrated field strength for the ends of the new magnet is down by a factor of about 16 from that of the original magnet. This new magnet is scheduled to be installed in early May, 1987.

Figure AI-1

Injection Lambertson Magnet
End View
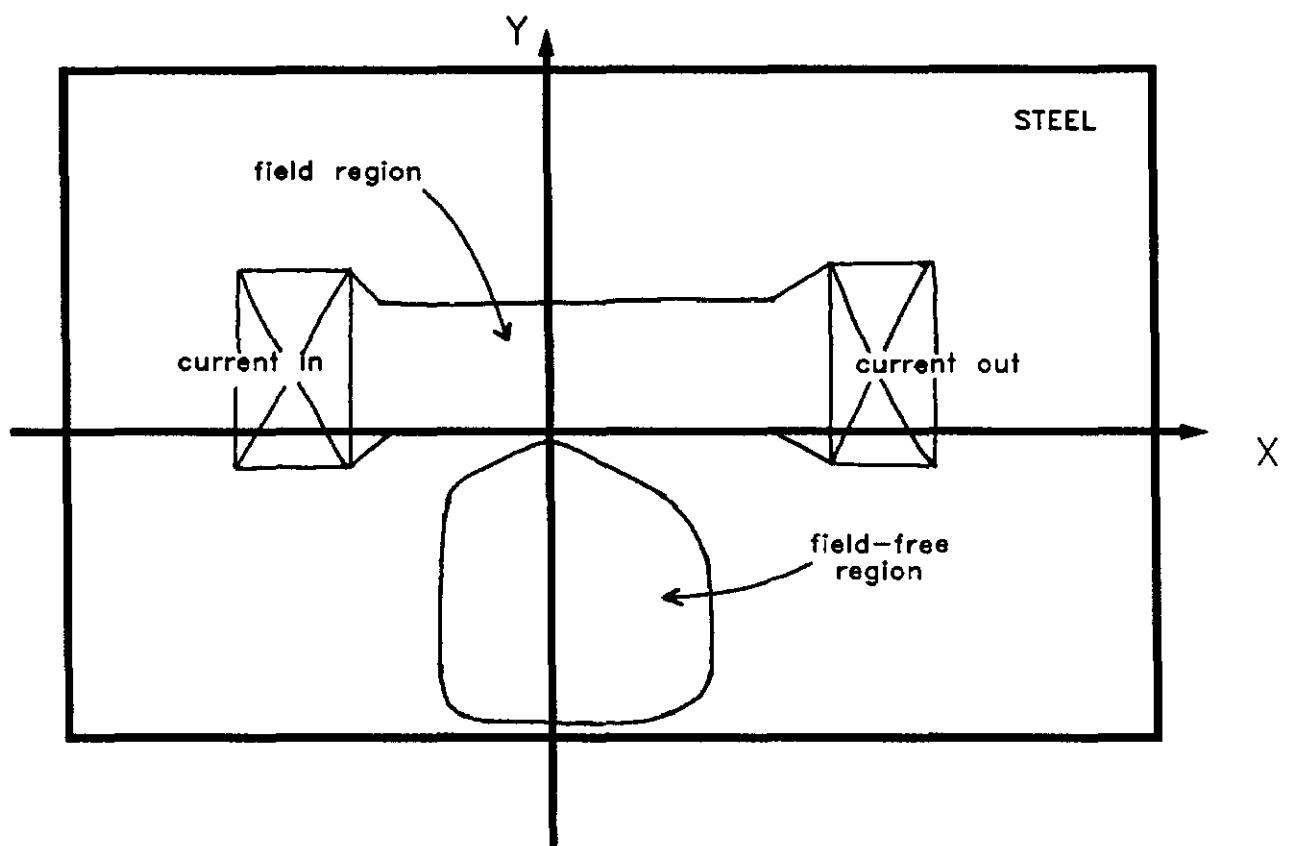
Figure AI-2

Injection Lambertson Magnet
Side View

Figure AI-3

Lambertson Field Region Calculation
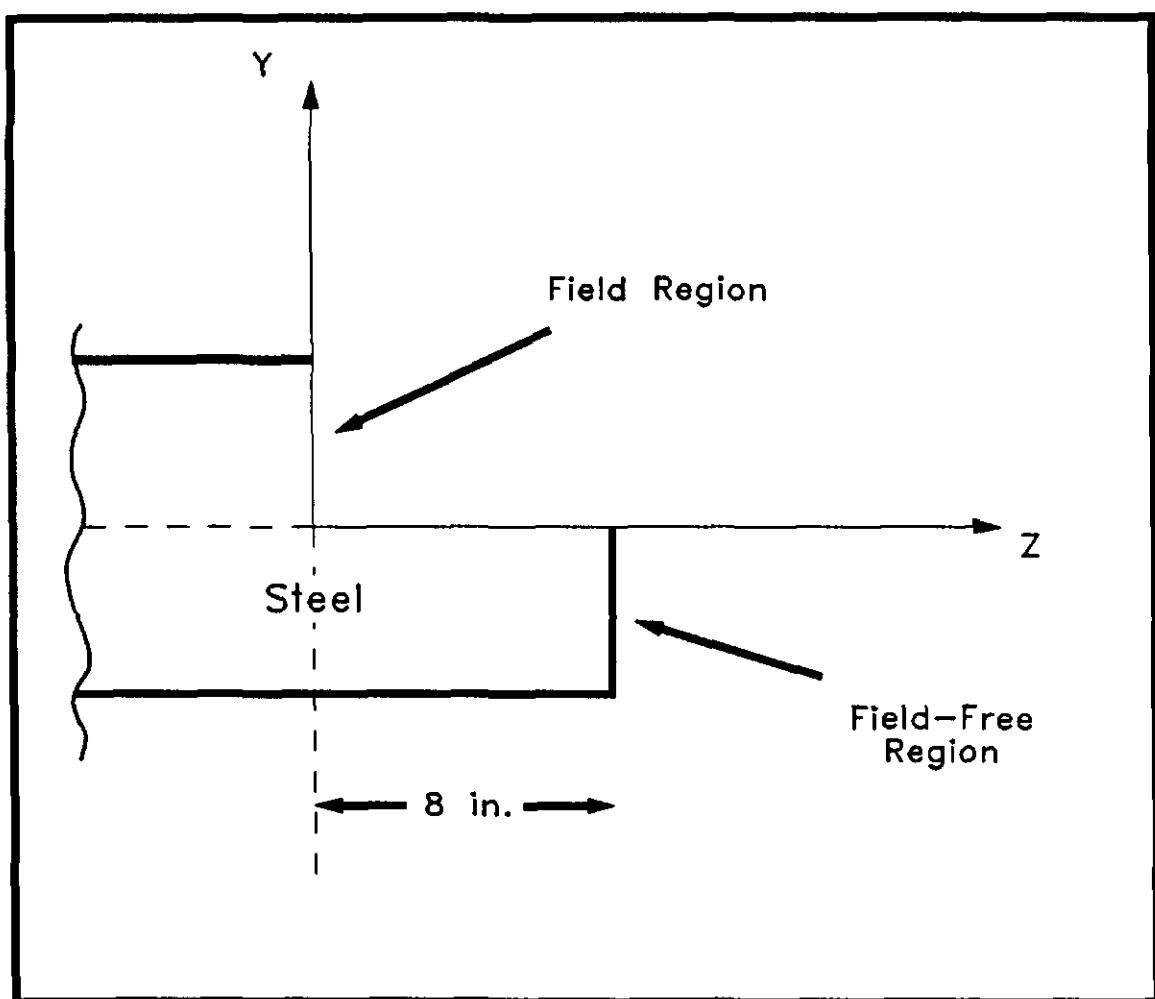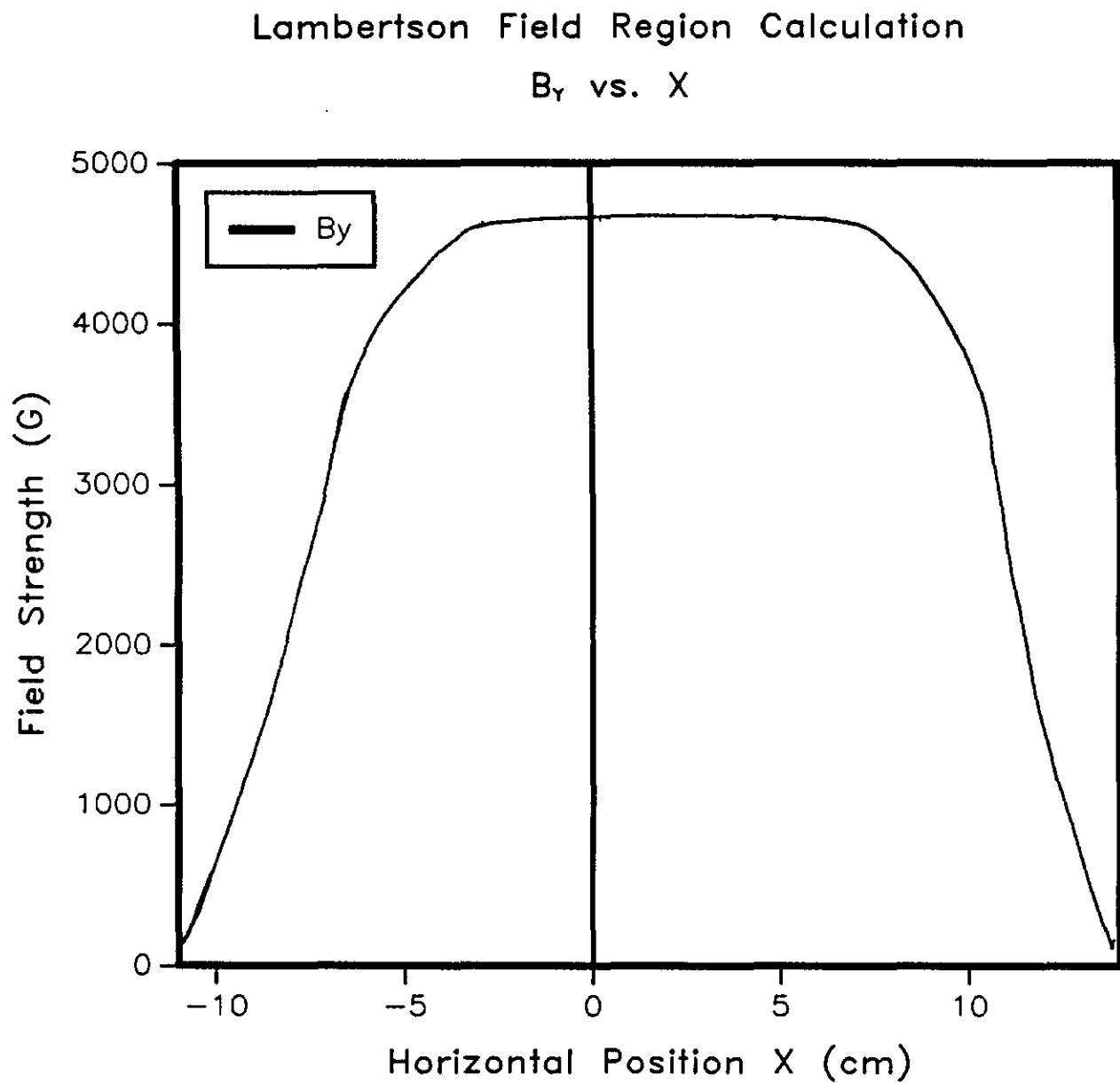
B_Y vs. X

Figure AI-4

Calculated B_X, B_Y vs. X
for Y = −1.5 cm
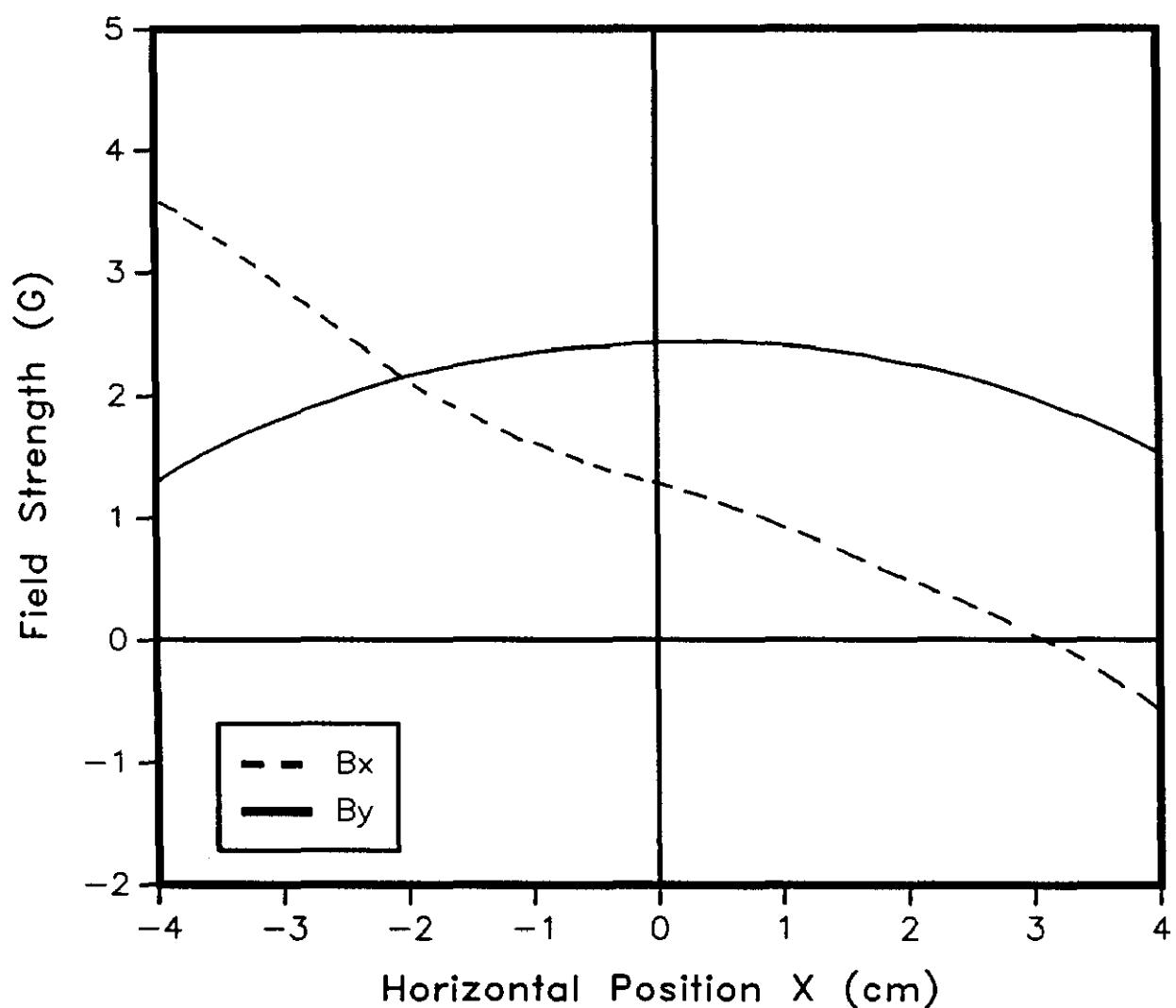
Figure AI-5

Figure AI-6

Calculated B_x, B_Y vs. Y

for X = 0.0 cm
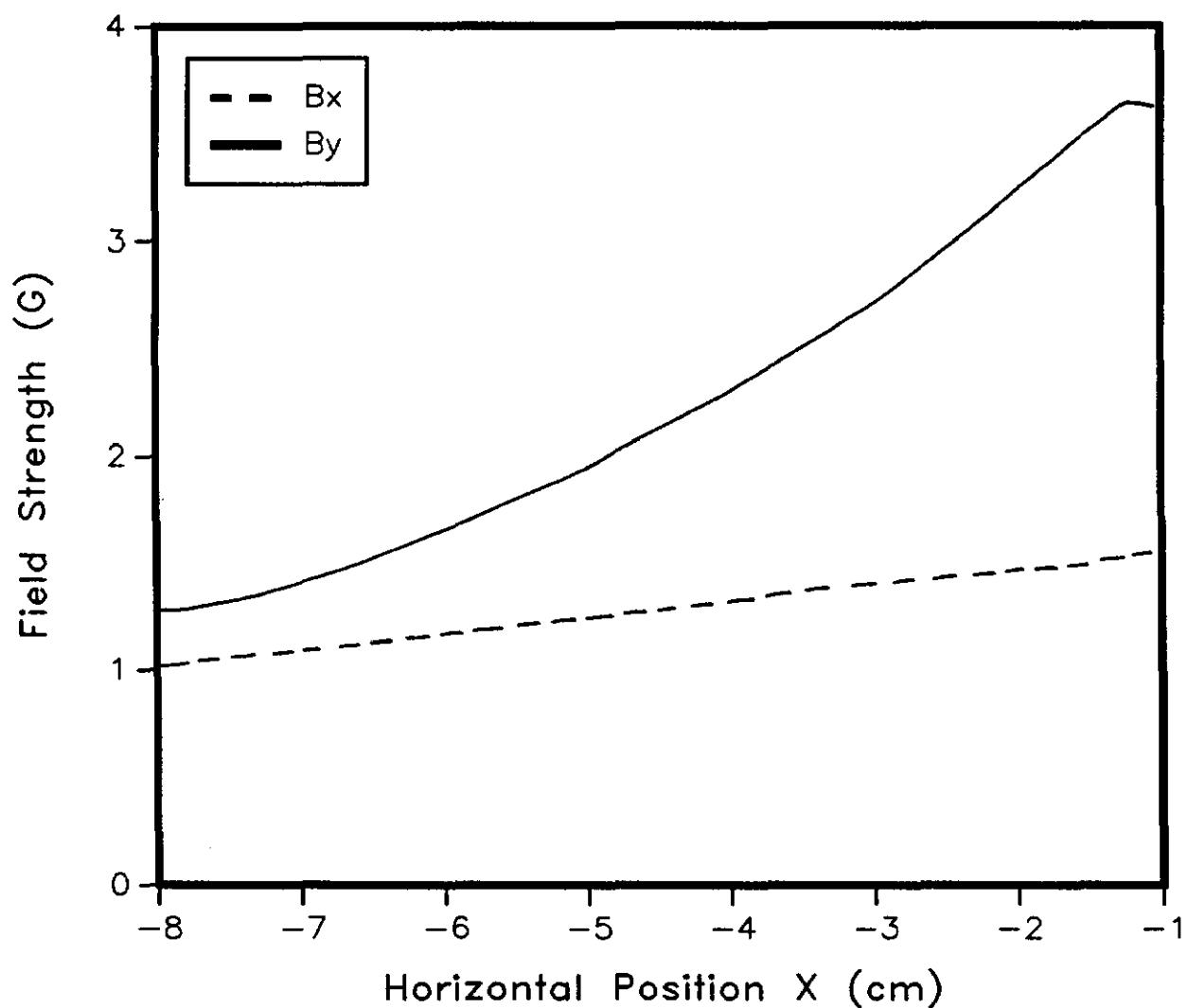
Figure AI-7

Vertical Field Strength vs. Current
(Field Region)
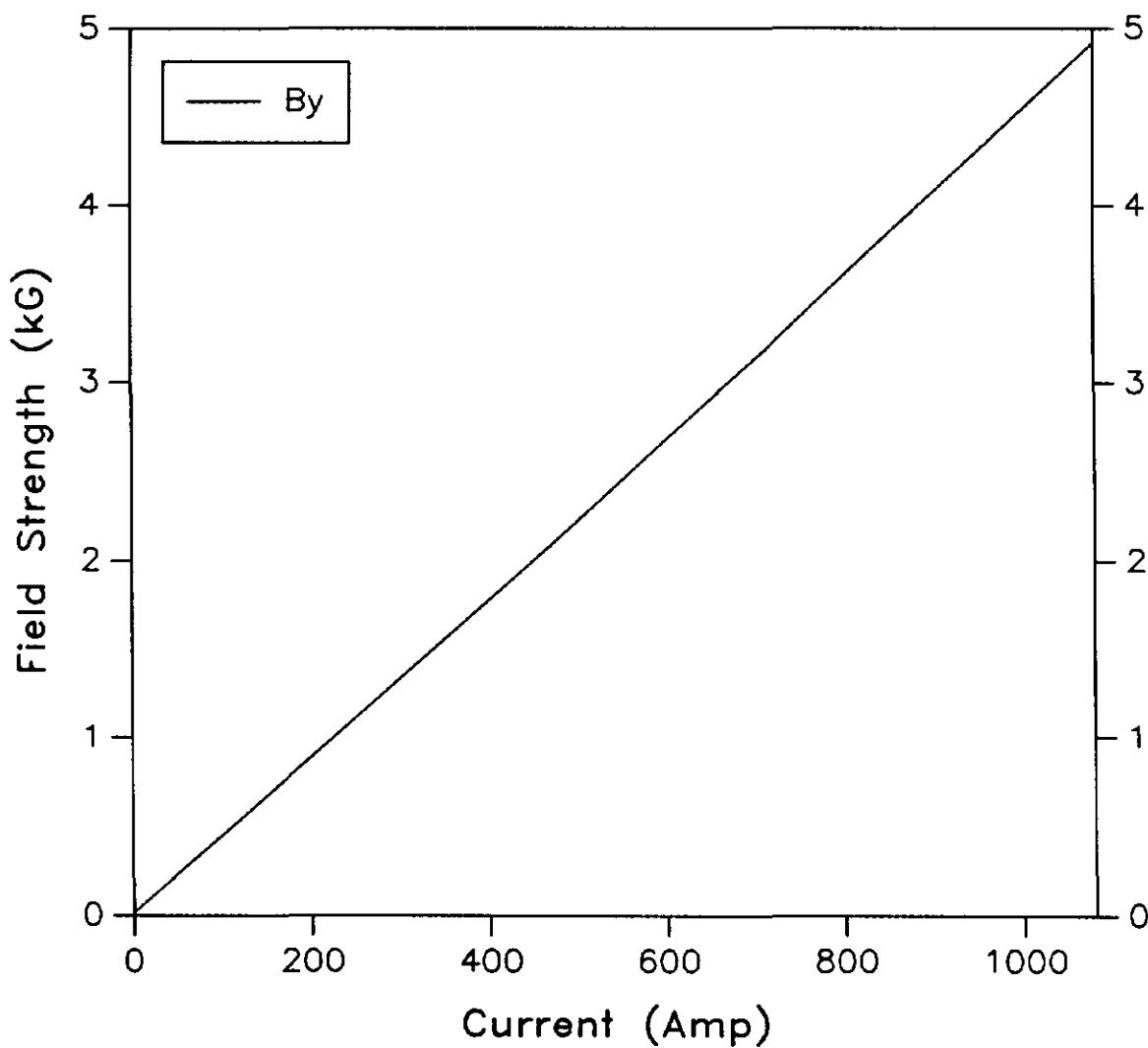
Figure AI-8

Vertical Field Strength vs. Horizontal Position
(Field-free Region; y = −1.5 cm)
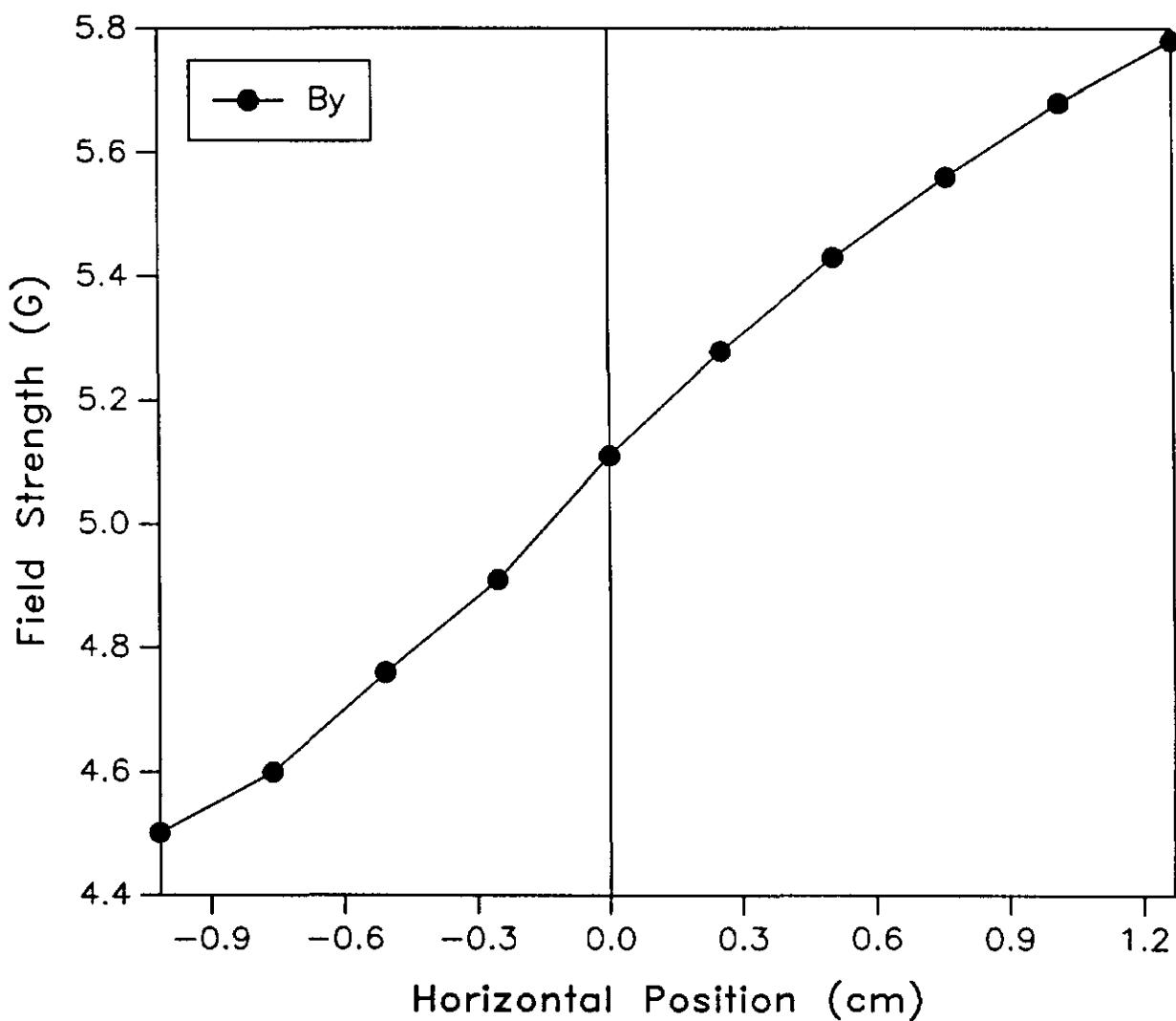
Figure AI-9

Horizontal Field Strength vs. Horizontal Position
(Field-free Region; y = −1.5 cm)
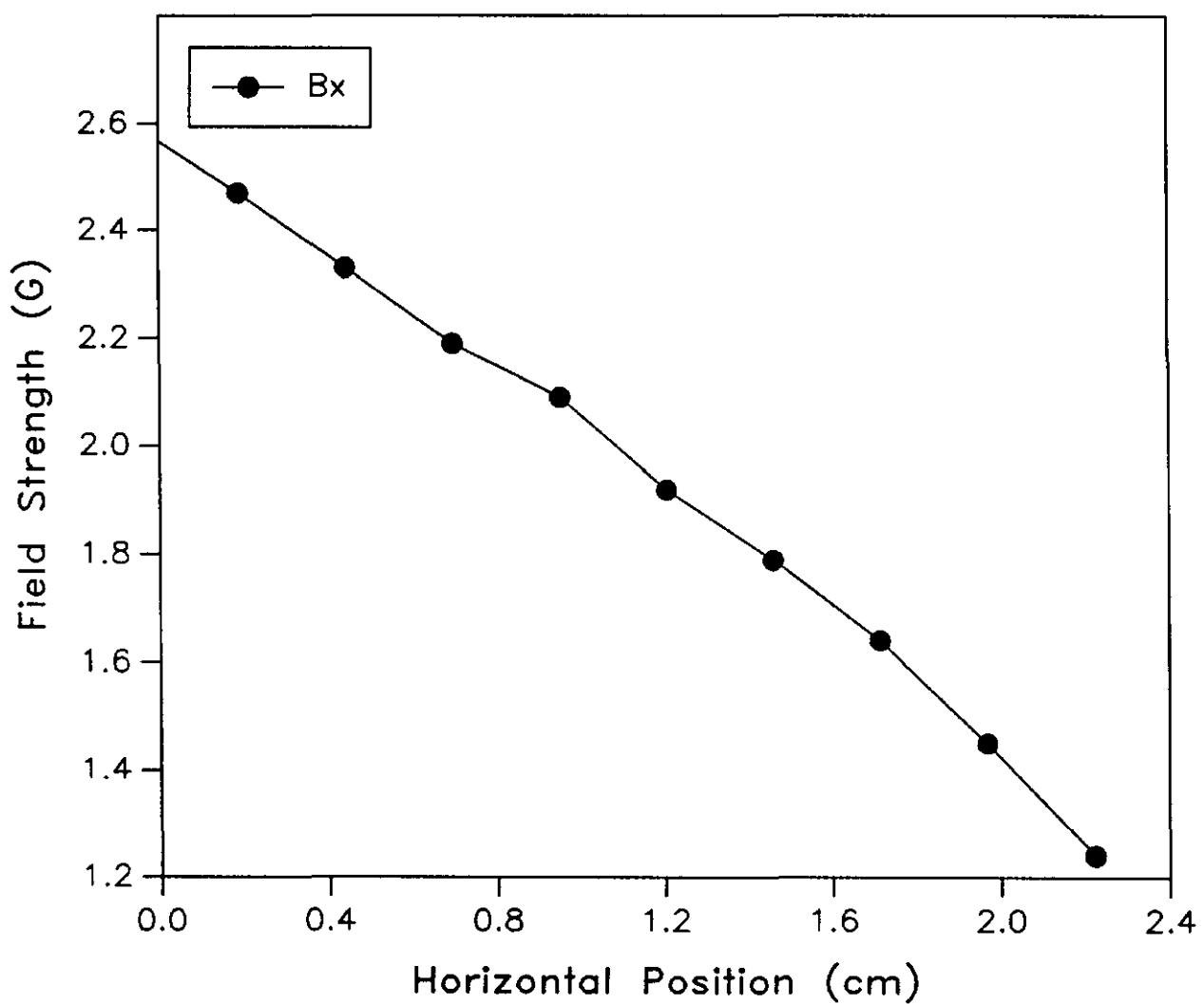
Figure AI-10

Vertical Field Strength vs. Horizontal Position
(Field-free Region; y = −4.4 cm)

Figure AI-11

Horizontal Field Strength vs. Horizontal Position
(Field-free Region; y = -4.4 cm)

Figure AI-12

Vertical Field Strength vs. Vertical Position
(Field-free Region; x = 0.0 cm)

Figure AI-13

Horizontal Field Strength vs. Vertical Position
(Field−free Region; x = 0.0 cm)
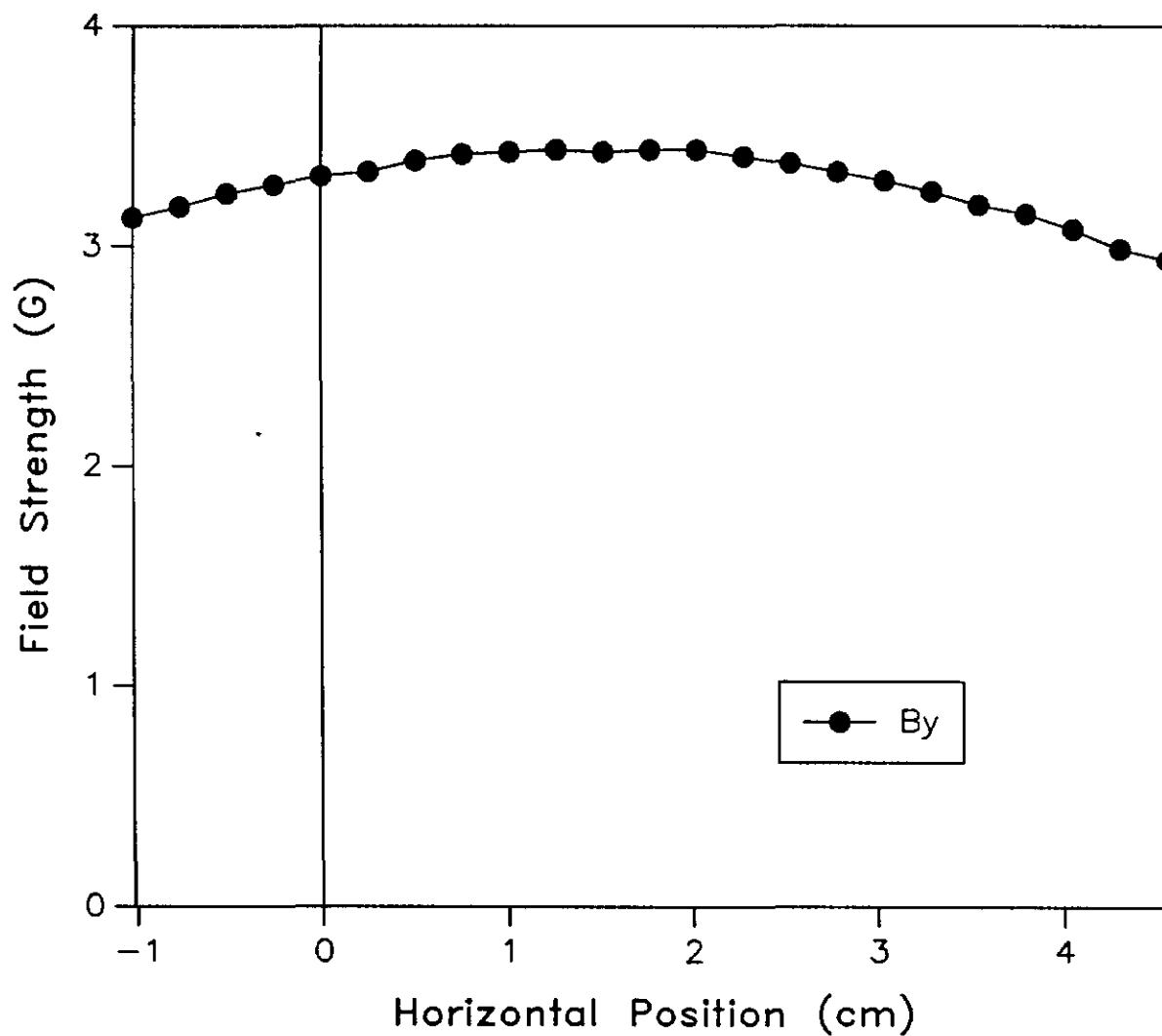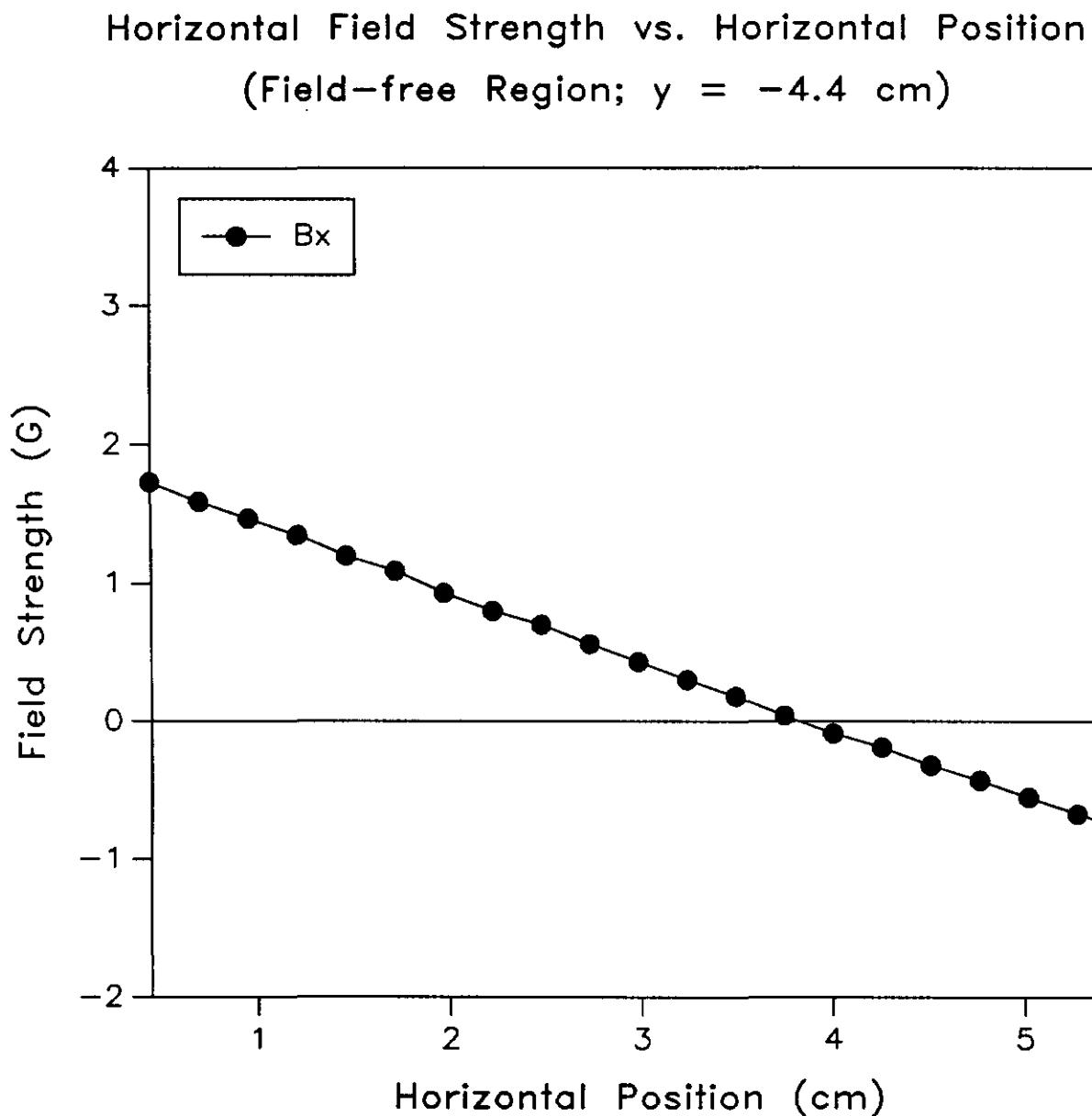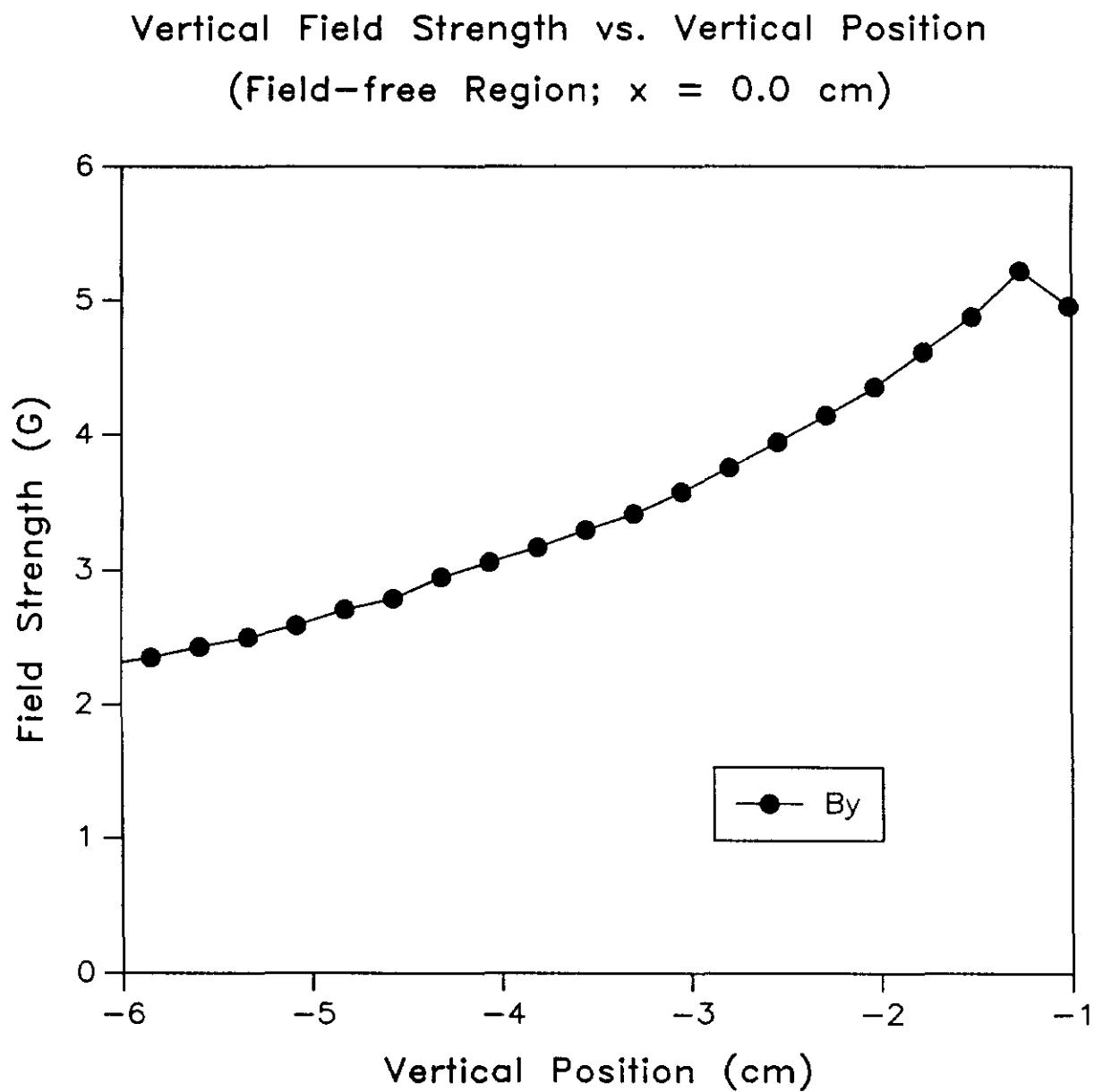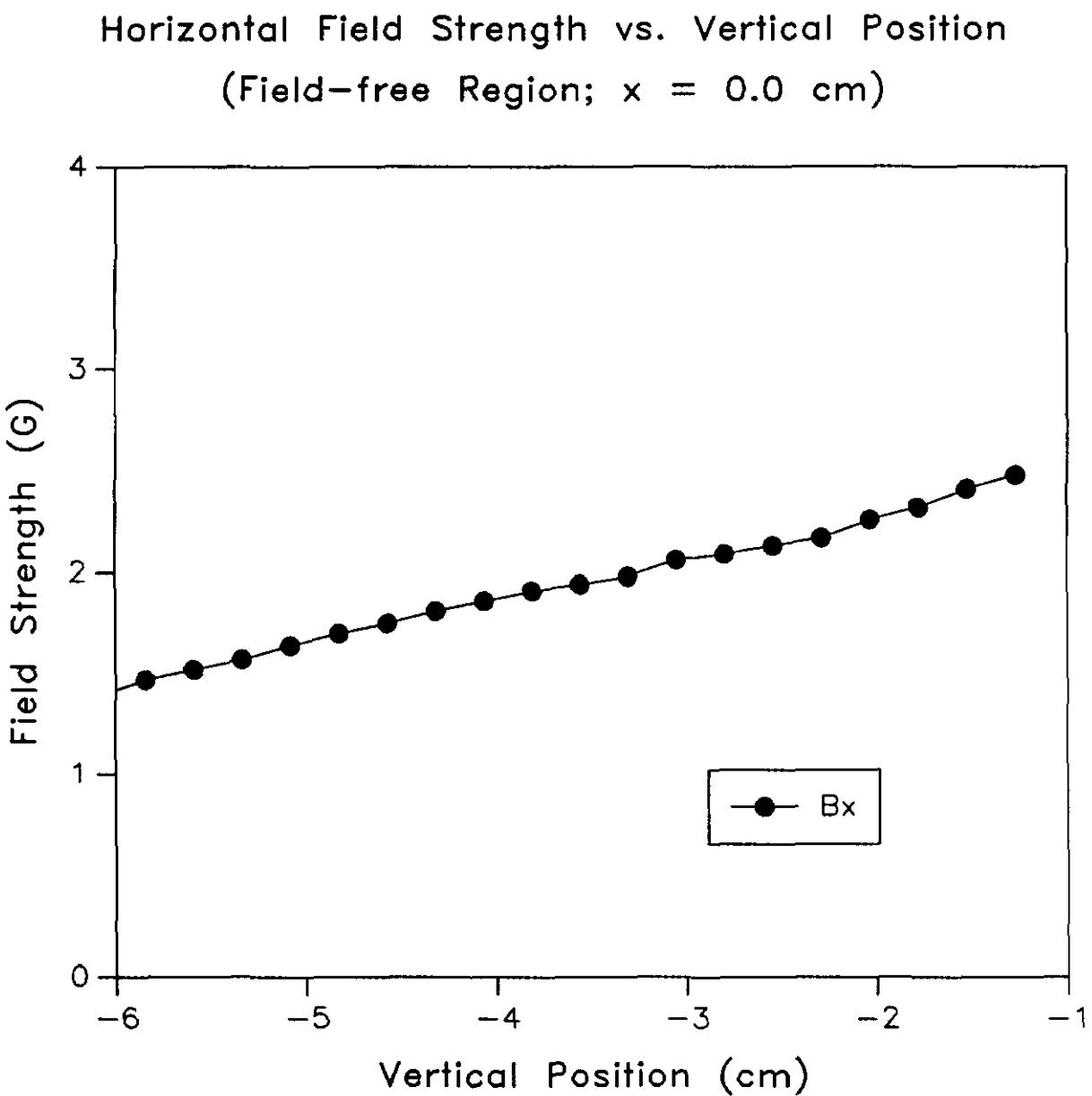
Figure AI-14

## Vertical Component of End Field
## for Main Ring Injection Lambertson
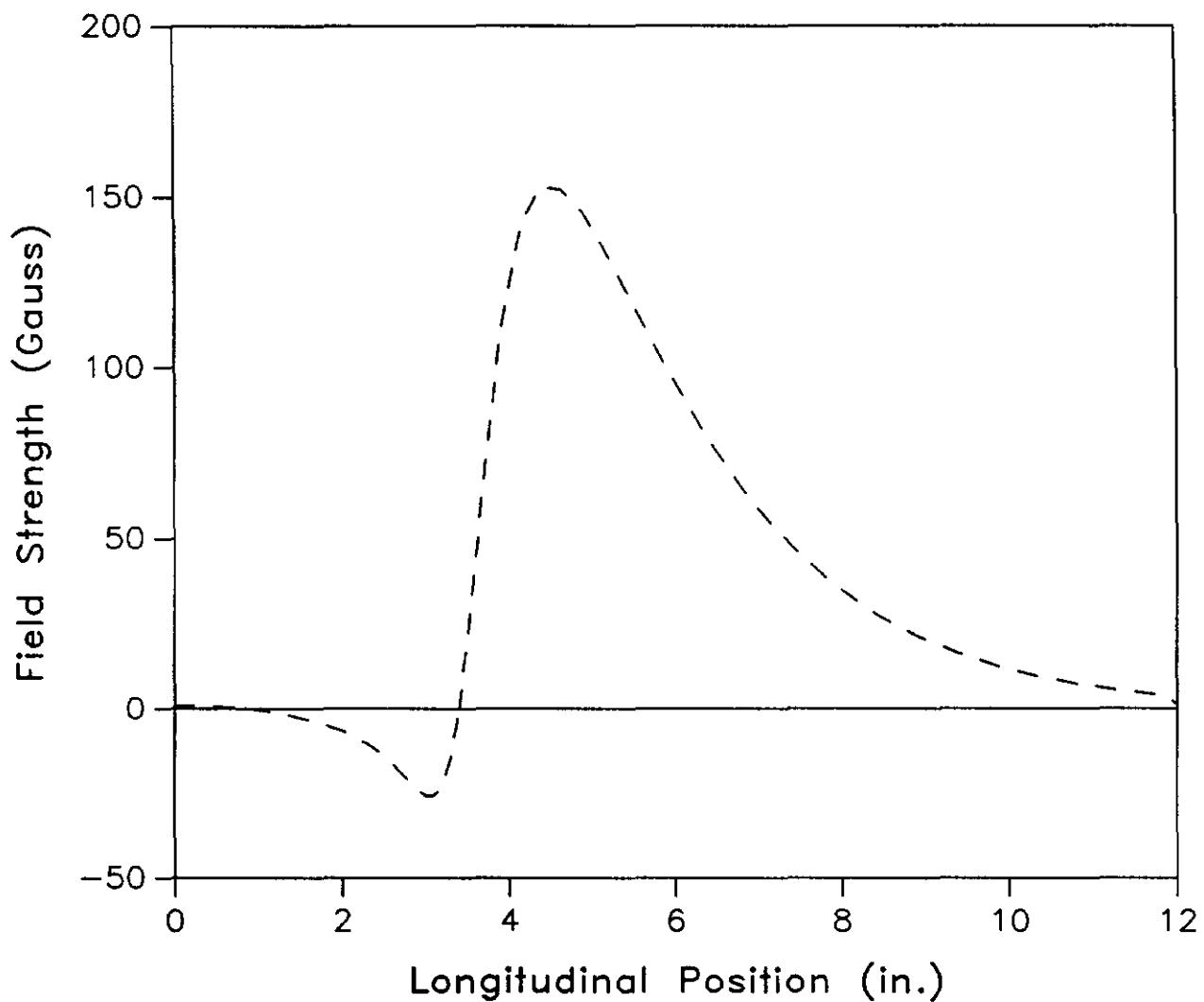
Figure AI-15

Vertical Component of End Field
for Main Ring Injection Lambertson
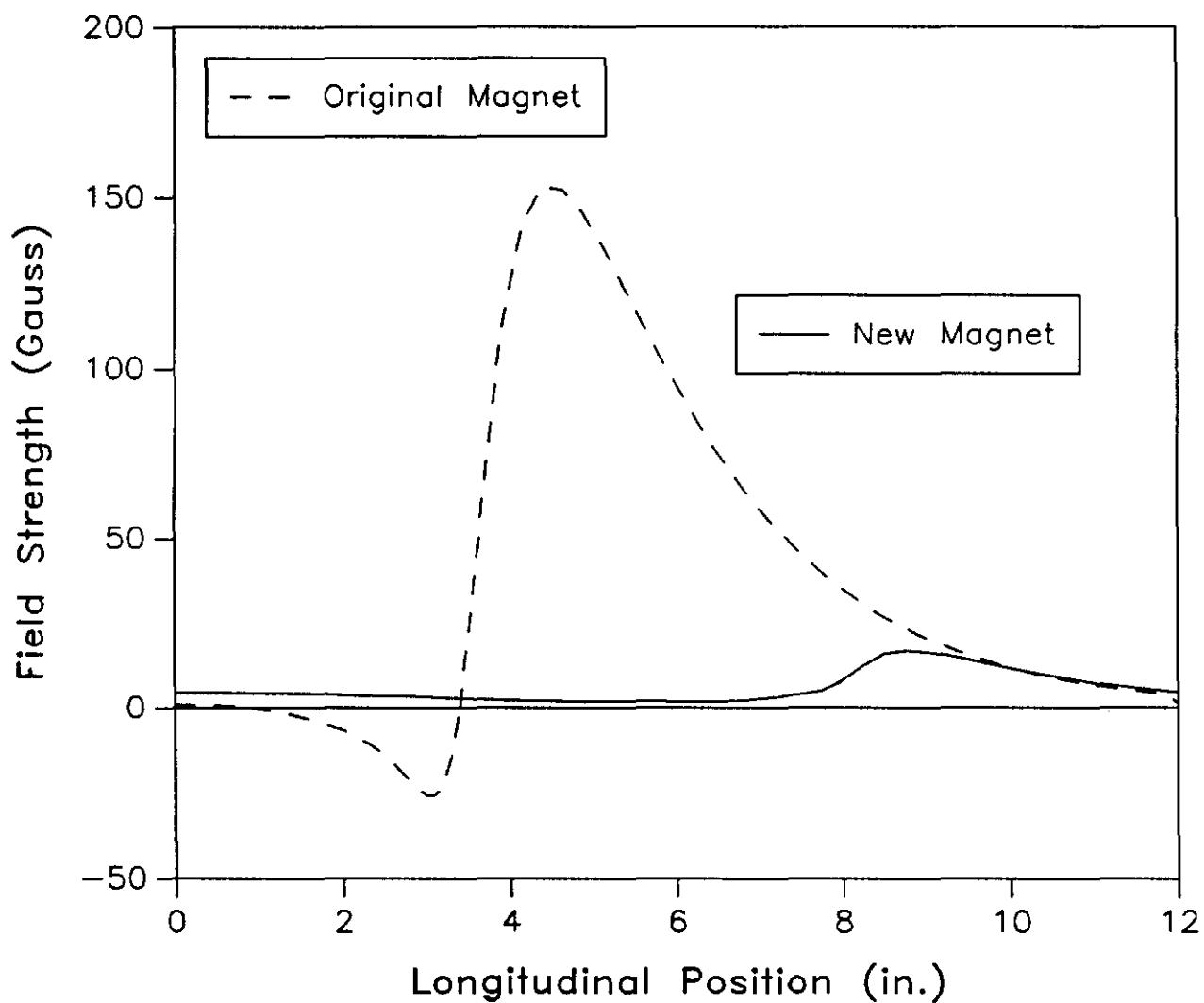
AII. Effects on Circulating Beam of a Ramped Bending Magnet with

    Large Sextupole Error

This section will discuss the effects of the original vertical orbit bump magnets on the Main Ring circulating beam observed during the commissioning of the new 8 GeV Line. The original magnets were discussed in Chapter VI and Figure VI-1 shows the horizontal field strength as a function of vertical position through the gap of these magnets. This figure is reproduced in Figure AII-1. As can be seen, the field is strongly quadratic in appearance and so may be expressed in the form

$$B_x = B_0(1 - ky^2)$$

where $B_0 = 2940$ G and $k = .0057$ cm^{-2}. These original magnets were not water cooled and were ramped up to nominal excitation just prior to the transfer of beam to the Main Ring from the Booster then ramped down to zero current roughly .5 sec after the transfer took place when acceleration began. Once the fields in these magnets had been computed, the center two magnets of the four-bump were displaced vertically by 2.5 cm (the height of the orbit bump) so that the beam would pass through the center of each magnet during injection. (See Figure AII-2.) However, during the period of time when the magnets would ramp down, the beam would pass through the highly nonlinear regions of the magnets, although these fields were simultaneously decreasing, and a tune shift would develop.

The amount of tune shift expected during this process is given by

$$\Delta \nu = \beta q/4\pi = \beta B'l/(4\pi B\rho)$$

$$= \quad (\beta/4\pi)\,(B'/B)\,(1/\rho) \quad = \quad (\beta/4\pi)\,(\Delta B'/B)\,\theta$$

$$= \quad \left(\frac{\beta}{4\pi}\right)\left(\frac{2ky}{1-ky^2}\right)\left(\frac{h-y}{L}\right) \quad ,$$

where L is the distance between the first two vertical bend

centers (and the last two vertical bend centers) as depicted in

Figure AII-2, h is the amount by which the middle two magnets are

displaced vertically with respect to the outer two, and y is the

absolute vertical displacement of the beam from the centers of

the middle magnets. When the magnets are at nominal current, y =

0 and $\Delta\nu$ = 0. When the magnets are off, y = h and again $\Delta\nu$ = 0.

While the magnets ramp down, $\Delta\nu$ will reach a maximum given by

$d\Delta\nu/dy$ = 0. This maximum occurs at y = y_{max} where

$$y_{max} \quad = \quad \frac{1 - \sqrt{1 - kh^2}}{kh}$$

which, for small kh^2 reduces to $y_{max} = (h/2)(1 - kh^2/8)$.

The maximum tune shift which should be observed during the time

the magnets are ramping down is thus

$$\Delta\nu_{max} \sim (\beta/L)(kh^2)/8\pi \quad \text{(for small } kh^2\text{)}.$$

Inserting numbers into the above expression, specifically

L = 4.57 m, k = .00557 cm^{-2}, h = 2.5 cm, and at the second magnet

β_x = 51 m, β_y = 110 m while at the third magnet β_x = 64 m and β_y

= 84 m, the expected maximum tune shifts are

$$\Delta\nu_x = -.03, \quad \Delta\nu_y = +.06 \quad .$$

By firing a fast kicker magnet while beam is circulating

within the Main Ring a coherent betatron oscillation may be

induced, the oscillation may be recorded with the beam position

monitors, and the data may be fast Fourier analyzed to provide

betatron oscillation frequencies. Such a study was performed on September 25, 1986 during which the beam was kicked at various times during the ramp of the orbit bump magnets. The tunes which were observed as a function of orbit bump magnet current are shown in Figure AII-3. As can be seen the observations of $\Delta \nu_x$ = -.02 and $\Delta \nu_y$ = .03 are in reasonable agreement with the predicted values. As mentioned in Chapter VI, these four magnets have since been replaced by magnets with much more uniform fields. The change in tune with magnet current is unobservable.

Figure AII-1

Original Vertical Orbit Bump Magnet
## Horizontal Field Component vs. Vertical Position
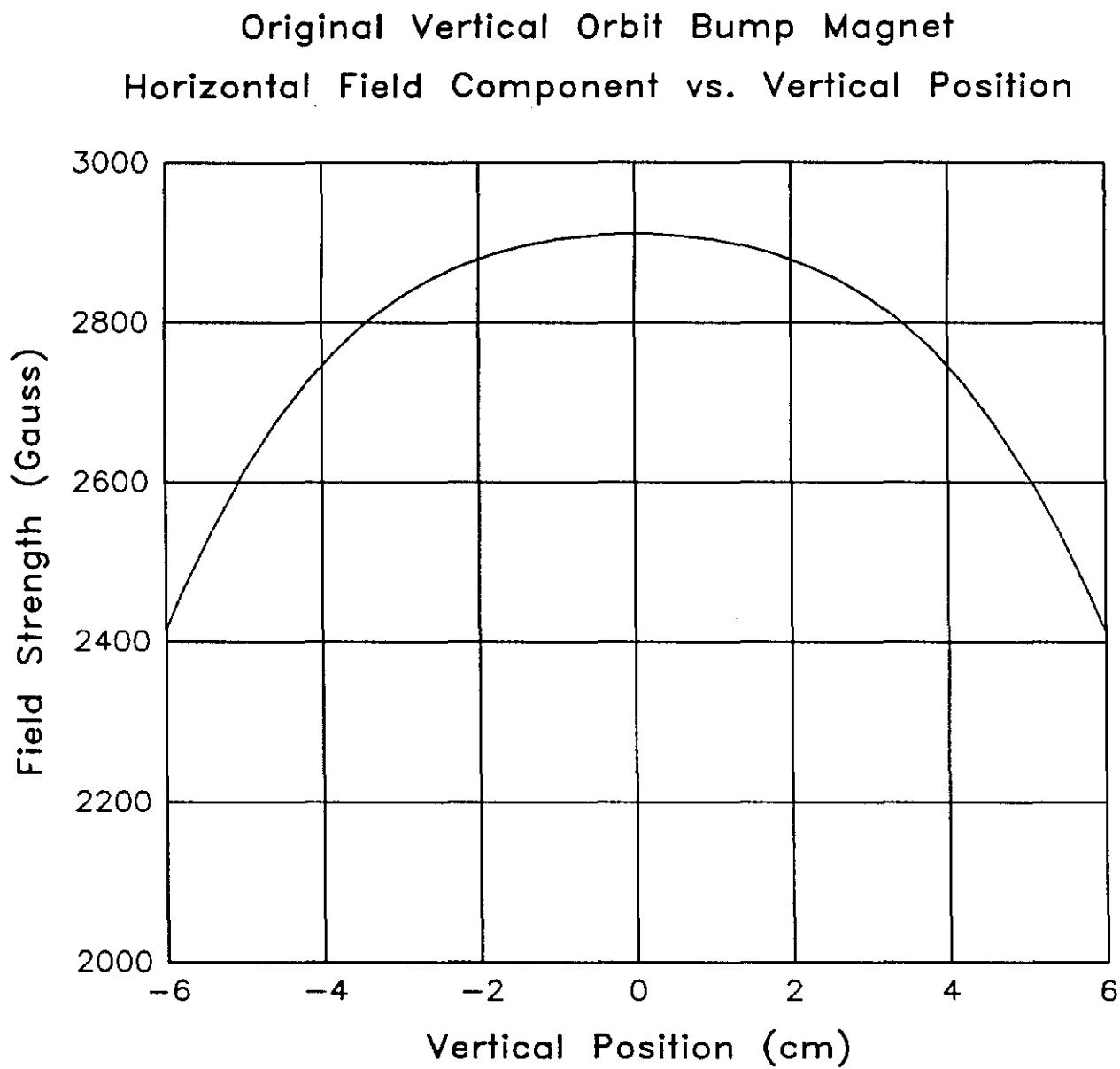
## Displacements of Original
## Vertical Orbit Bump Magnets
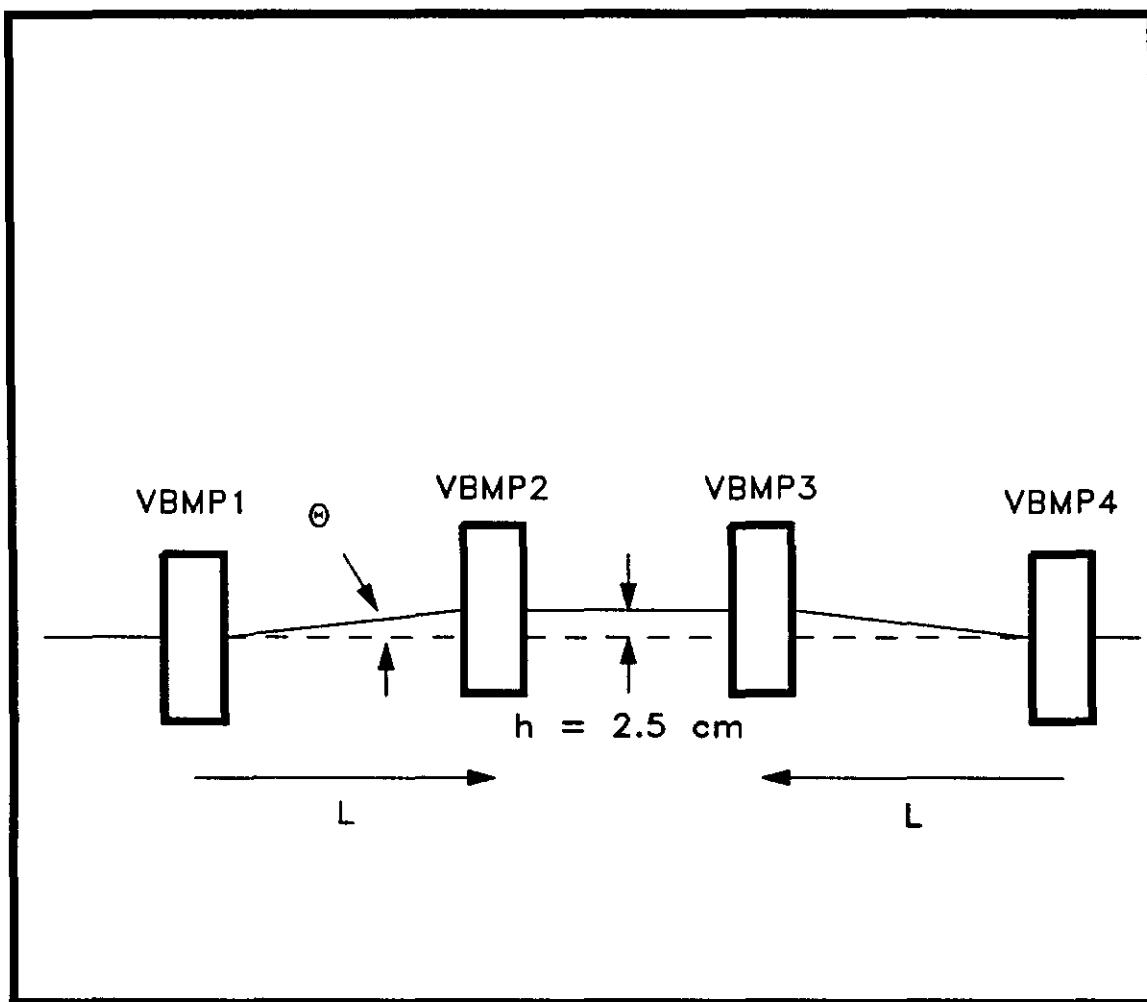
Figure AII-3

Measured Variation of Tune with Orbit Displacement
(I = Magnet Current)
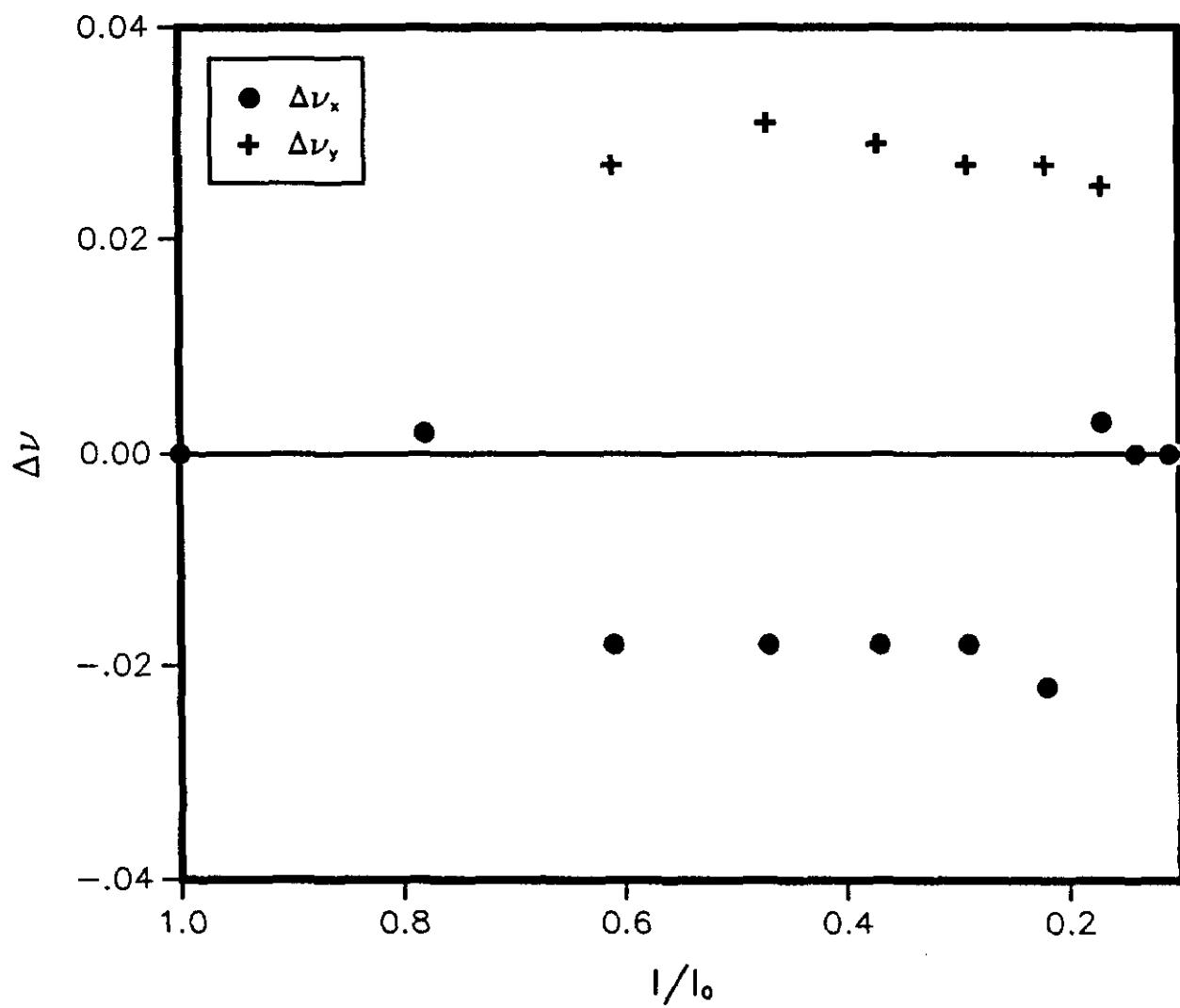
References

1. Holsinger, R. F., <u>POISSON Group User's Guide</u>; February, 1981; Field Effects, Inc., Carlisle, Massachusetts.

VITA

Michael James Syphers ██████████████████████

████████████ ████████ ████████████████████████████████████ ██████████████████████████ enrolled in Indiana University from which he graduated in August 1979. During the school year of 1979-1980 he taught physics at Batavia High School in Batavia, Illinois and the following summer began employment with the Fermi National Accelerator Laboratory as a member of the Accelerator Division Operations Group. During the next five years, he studied graduate physics at De Paul University on a part-time basis, earning the M.S. degree in physics in June 1984. Since the spring of 1985, he has held the position of engineering physicist at Fermilab and in September 1985 entered the Graduate School of the University of Illinois at Chicago.